creative commons
COMMONS DEED

저작자표시 2.0 대한민국

이용자는 아래의 조건을 따르는 경우에 한하여 자유롭게

- 이 저작물을 복제, 배포, 전송, 전시, 공연 및 방송할 수 있습니다.
- 이차적 저작물을 작성할 수 있습니다.
- 이 저작물을 영리 목적으로 이용할 수 있습니다.

다음과 같은 조건을 따라야 합니다:

저작자표시. 귀하는 원저작자를 표시하여야 합니다.

- 귀하는, 이 저작물의 재이용이나 배포의 경우, 이 저작물에 적용된 이용허락조건을 명확하게 나타내어야 합니다.
- 저작권자로부터 별도의 허가를 받으면 이러한 조건들은 적용되지 않습니다.

저작권법에 따른 이용자의 권리는 위의 내용에 의하여 영향을 받지 않습니다.

이것은 이용허락규약(Legal Code)을 이해하기 쉽게 요약한 것입니다.

Disclaimer

dCollection

공학석사 학위논문

Experimental Study on Release of Plastic Particles from Coastal Sediments into Water Body

해안 유사에서 수체로의 플라스틱 입자 방출에 관한 실험적 연구

2022년 08월

서울대학교 대학원

건설환경공학부

황 동 욱

Experimental Study on Release of Plastic Particles from Coastal Sediments into Water Body

해안 유사에서 수체로의 플라스틱 입자 방출에 관한 실험적 연구

지도 교수 박 용 성

이 논문을 공학석사 학위논문으로 제출함

2022년 06월

서울대학교 대학원

건설환경공학부

황 동 욱

황동욱의 공학석사 학위논문을 인준함

2022년 08월

위 원 장 _____ (인)

부위원장 _____ (인)

위 원 _____ (인)

Abstract

The increasing global plastic production and indiscreet use of these products lead to aggravation of plastic pollution which is regarded as the main destroyer of the marine ecosystem. Millions of tons of them are dumped into the oceans, and they can now be found in every ocean in the world. As it shows the seriousness of environmental pollution, serval related studies are currently underway. However, most of them are for studying the real condition of the pollution in the marine environments, and there are few studies on transport of plastics in near-shores and coastal areas. Nevertheless, physical basis of plastic behavior therein has to be studied to resolve the problems, because they experience interactions with various factors, such as waves, winds, sands, human activities, etc. in coastal regions. Accordingly, this study focused on investigation of release of the plastic particles from coastal sediments into fluids by carrying out a set of experiments.

To reach the purpose, an oscillating water tunnel was newly designed and built at Seoul National University that is a kind of u-tubed closed conduit. An actuator drives a bidirectional piston that can generate an oscillatory motion instantaneously. The generated flow is uniform in the x-direction with no vertical velocity component, and it can have a high Reynolds number. Moreover, it can generate sediment transport with a detachable sediment basin in the middle of the bottom part of the tunnel. Thus, the experimental cases consist of different 14 flow conditions and 3 plastic particle sizes.

As a result, bedform change played an important role in the release of the particles. Consequently, the threshold value for sediment transport and release could be estimated by expressing the Reynolds number and the sand mobility number. In

this study condition, it was as $Re_{cr} = 5.5 \times 10^4$ and $\psi_{cr} = 7.25$. As the bedform changes above the critical value, particles in sediments will be released into water body. Also, the flow with the larger Reynolds number results in more releases. The effect of the particle size on the release was studied as well. It showed that the smaller plastics have a higher probability of release than the larger ones. In conclusion, this study can contribute to solving marine plastic pollution by offering an understanding of the relation between the flows, the sediments, and the plastics.

Keywords : Experimental study, Plastic pollution, Release of plastic particles, Sediment transport, Oscillating water tunnel

Student Number : 2020-26707

Table of Contents

Abstract i
Table of Contents iii
List of Tables v
List of Figures vi

Chapter 1. Introduction 1
1.1. Motivation 1
1.2. Objectives 2

Chapter 2. Research Background 6
2.1. Plastic pollution in marine environments 6
2.1.1. General pollution caused by plastics 6
2.2. Transport of plastics 16

Chapter 3. Methodology 18
3.1. Experimental equipment 18
3.1.1. Oscillating water tunnel 18
3.1.2. Particle image velocimetry, PIV 26
3.2. Experimental conditions & set-up 30
3.2.1. Sediments and plastic particles 30
3.2.2. Experimental conditions 38
3.2.3. Experimental procedure 39

Chapter 4. Results and Discussions 43
4.1. Sediment transport & ripples 43
4.1. Release of plastic particles 64

Chapter 5. Conclusion 76

Bibliography 80

APPENDIX A: Bedform change over time 85
APPENDIX B: Digitized two-dimensional bedform over time 111
APPENDIX C: Length between ripples on reference depths over time 119
APPENDIX D: Two-dimensional area of ripple under

reference depths over time.....127

국문 초록.....135

List of Tables

Table 1. The 10 top countries ranked by the amount of plastic waste that entered the ocean (Jambeck et al., 2015)..... 12

Table 2. Conditions for each experimental case..... 39

Table 3. The occurrence probability of the release of plastic particles from sediments to fluids..... 79

List of Figures

Figure 1. Definition of 'release' of plastic particles 2

Figure 2. Flow chart of this study 5

Figure 3. Production of conventional synthetic plastics (UNEP, 2017; GESAMP, 2015) 7

Figure 4. Timeline for plastic pollution 9

Figure 5. Annual global plastic production from 1950 to 2020 (PlasticsEurope, 2021) 10

Figure 6. Estimated global mass of mismanaged plastic waste generated in 2010 (Jambeck et al., 2015) 11

Figure 7. Plastic loads for the top 10 ranked catchments in the world (MMPW: mismanaged plastic waste; MP: microplastic) (Schmidt et al., 2017) 12

Figure 8. Distribution of plastic debris on the surface of the ocean (Cozar et al., 2014) 13

Figure 9. Global plastic debris concentrations (Hurley et al., 2018) 15

Figure 10. The average number of plastic waste from 2008 to 2020 on Korean beaches (해양수산부 & 해양환경공단, 2020) 15

Figure 11. Transport of plastic wastes in coastal area (Brennan et al., 2018) 17

Figure 12. Drawing of the designed oscillating water tunnel 19

Figure 13. Appearance of the constructed SOWT 19

Figure 14. Relation between the Reynolds number and the relative roughness under field conditions and in laboratory studies (*Figure 1.1.3* in Nielsen (1992)) 21

Figure 15. Flow motions with wave-induced velocity, $u \propto t$ ((a): under fields (Nielsen, 1992); (b): the oscillating water tunnel) 25

Figure 16. Measuring devices for PIV system ((a): Continuous laser; (b):

Highspeed camera) **26**

Figure 17. Appearance of installed PIV devices onto the oscillating water tunnel **27**

Figure 18. Overview of the workflow for PIV analysis in PIVlab (Thielicke & Stamhuis, 2014) **30**

Figure 19. Cumulative curve for grain size distribution **33**

Figure 20. Grain size distribution with weight **33**

Figure 21. Gravel : Mud : Sand ratio **34**

Figure 22. Sand : Clay : Silt ratio **34**

Figure 23. Classification of sections in a sediment basin **36**

Figure 24. Set-up of plastic particles in a section **37**

Figure 25. Set-up of plastic particles on each depth **37**

Figure 26. Notations for properties of ripples **41**

Figure 27. General experimental procedure **42**

Figure 28. Progress of bedform change during an hour **45**

Figure 29. Comparison between the original (a) and the distortion correction image (b) **47**

Figure 30. Definitions of λ, η, σ, and α **49**

Figure 31. Digitized two-dimensional bedform over the time **50**

Figure 32. Numerical integration for cumulative area of formed ripples **51**

Figure 33. The number of the formed ripples for all cases **52**

Figure 34. The ripple lengths λ for all cases **52**

Figure 35. Comparison between models and data for ripple length (Nielsen, 1981) **55**

Figure 36. Comparison between models and data for ripple height (Nielsen, 1981) 56

Figure 37. Interval length between the ripples for all cases ((a): On the surface; (b): On $z = -5\ mm$; (c): On $z = -10mm$; (d): $z = -15mm$; (e): $z = -20mm$) 59

Figure 38. Interval length in cases of R05a, R05b, and R05c 60

Figure 39. Cumulative ripple area for all cases ((a): Above surface; (b): Below surface; (c): Below $z = -5$ mm; (d): Below $z = -10$ mm; (e): Below $z = -15$ mm; (f): Below $z = -20$ mm) 62

Figure 40. Cumulative ripple area in cases of R05a, R05b, and R05c .. 63

Figure 41. Number of released plastic particles with Reynolds number 67

Figure 42. Number of released plastic particles with mobility number 67

Figure 43. Number of released plastic particles with flow velocity 68

Figure 44. Number of released plastic particles with the square of flow velocity 68

Figure 45. Number of released plastic particles with the Froude number 69

Figure 46. Criterion of erosion and deposition with mean velocity and grain size (*Figure 2.4* in Yang et al. (2007)) 71

Figure 47. Critical velocity with grain size (*Figure 2.5* in Yang et al. (2007)) 71

Figure 48. The number of released particles with their sizes 73

Figure 49. Definition of plastics in the ocean by size (GESAMP, 2015) 74

Figure 50. Relation between the ripple size and the release ((a): with $\zeta -$; (b): with $\zeta +$; (c): with $H = \zeta - + \zeta +$) 75

Chapter 1. Introduction

1.1. Motivation

As the use of plastics in the world has rapidly increased since the 1900s, plastic wastes are found to be prevalent around the world (G20, 2017; GESAMP, 2015). Consequently, it has raised awareness about the perils of plastic litter, and the pollution has come to the fore as a major environmental issue. An estimated 4 to 13 million tons of plastic waste generated on land entered the marine environment in 2010 which is an amount equal to almost one-third of annual plastic production (Geyer et al., 2017). About 85% of the amount of waste discharged into the ocean is plastics (탁성제, 2020). Thus, it is certain that we must make a greater effort to discover some fundamental solutions to resolve the problem.

As mentioned above, numerous plastic wastes are released into the marine environment every year. Accordingly, a lot of research related to plastic pollution is being carried out, but it mostly focused on the abundance of plastic waste in the marine environment. However, little is known about plastic particle behavior in coastal areas. Most plastics discharged into the ocean are transported to nearby shores and experience physical changes in the regions, such as arrival, departure, deposition, and fragmentation (Brennan et al., 2018). The process includes complex mechanisms interacting the plastics with waves, winds, solar, sediments, human activities, etc. Thus, understanding the mechanism and observation of the plastic behavior in coastal areas should be important to resolve the marine pollution. Especially, waves and sediments affect the transport of plastics. Furthermore, much

plastic debris is found in coastal sediments. They can depart to the ocean, and then, the small particles make it difficult to deal with. Therefore, the behavior of plastic particles in coastal areas has to be studied.

In accordance with the motivation, this study focused on understanding the mechanism of release of plastic particles in sediments into the fluid. The resultant objectives are explained in *Section 1.2.*, and the detailed research background with regard to coastal plastics will be referred to in *Chapter 2*. Also, before this study, the 'release' was specifically defined as a phenomenon which plastic particles are got out of the sediments into water body by turbulent motion as shown in Figure 1. In addition, this study did not consider the processes of coagulation, absorption, and desorption of the particles, and a prior condition of the study is that the plastics are buried in sediments for some reasons.

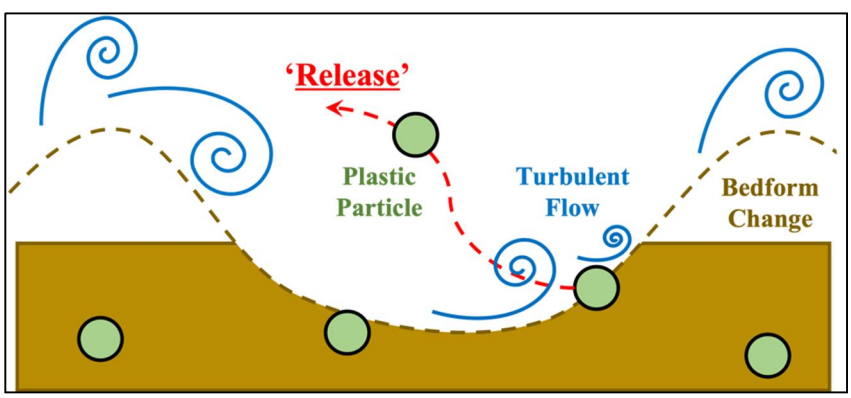

Figure 1. Definition of 'release' of plastic particles

1.2. Objectives

The purpose of this study is mainly to understand the progress of release of the plastic particles in coastal sediments. So, the research aims to carry out experiments to investigate the

characteristics of the release.

In order to succeed completely in the purpose, the following objectives were planned. Firstly, a new type of oscillating water tunnel was designed and constructed to generate oscillatory flow. The flow is the most suitable and common for coastal research. The tunnel has a detachable sediment basin to fill sand and plastics. It can make generation of sediment transport and transport of plastics possible. Moreover, utilizing particle image velocimetry (PIV) enables to obtain the overall properties of fluid motion and to visualize the flow easily. The optical measuring technology was constructed onto the oscillating water tunnel. The oscillatory flow generated by the tunnel was recorded during the experiments, and the flow velocity and period were acquired. The acquired data were used to improve the performance of the tunnel and to plan the experimental conditions with the flow Reynolds numbers.

Next is the main objective of this. It is to observe the release of plastic particles through experimental cases. The experiment was conducted with various two parameters, properties of the oscillatory flow such as flow velocity and period and plastic particle sizes. It was carried out to investigate the interaction between the release of plastics and the two parameters.

In summary, this researcher realized the seriousness of marine pollution created by lots of plastic litter. They are regarded as the main destroyer of the marine and coastal ecosystem. Thus, this study aims to lay the groundwork for providing some clues in resolving the pollution. To achieve this purpose successfully, the objectives of this study were planned, and they can be found in a flow chart of this study as shown in Figure 2.

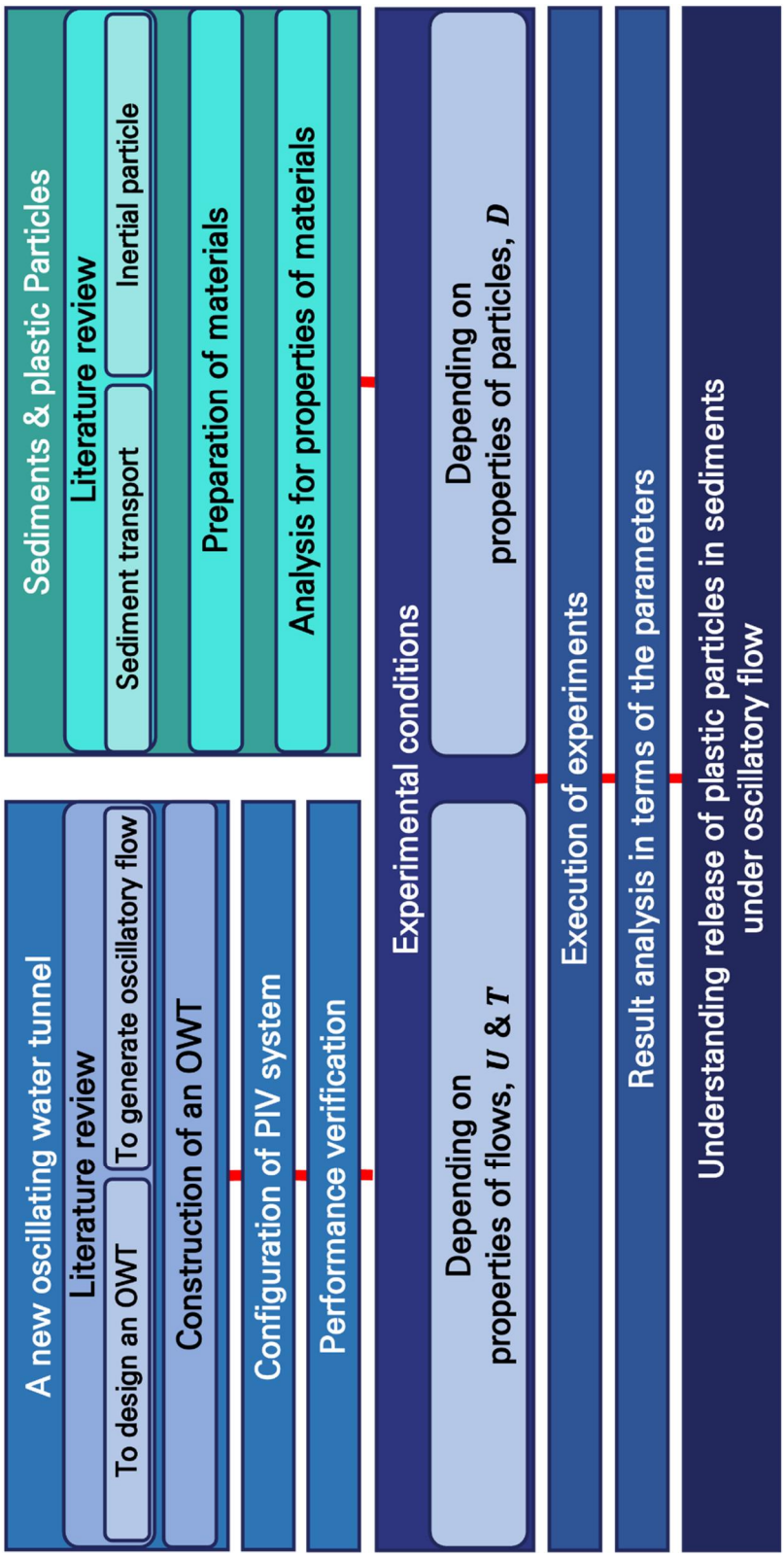

Figure 2. Flow chart of this study

Chapter 2. Research Background

2.1. Plastic pollution in marine environments

2.1.1. General pollution caused by plastics

A literature review was conducted to analyze the severity of the plastic pollution problem in marine environments and to identify the research trends. First of all, plastic is an easily processable material, a type of synthetic polymer (진정일, 2013). Its intrinsic properties have led to their ubiquitous use in various fields, and it is hard to imagine an area of life that has not been profoundly impacted by plastics (Gibb, 2019). Our lives scarcely pass a moment away from plastics. Of course, much has been done in recent years to get away from that, but our dependency on it is so great that the efforts appear relatively insignificant.

Plastic can be classified into thermos-plastic and thermosetting-plastic according to its molecular structure, formable, and moldability. Thermos-plastic can be easily deformed by heating, and it accounts for over 90% of global plastic production (UNEP, 2017). It consists of polyethylene terephthalate (PET), polyethylene (PE), polypropylene (PP), polystyrene (PS), polyvinyl chloride (PVC), polycarbonate (PC), etc. Also, it is composed of chains of carbon-based units, and the carbon can be obtained from fossil fuels or biomass (UNEP, 2017). The thermoset plastic cannot be re-molded. The production of plastics is shown in Figure 3.

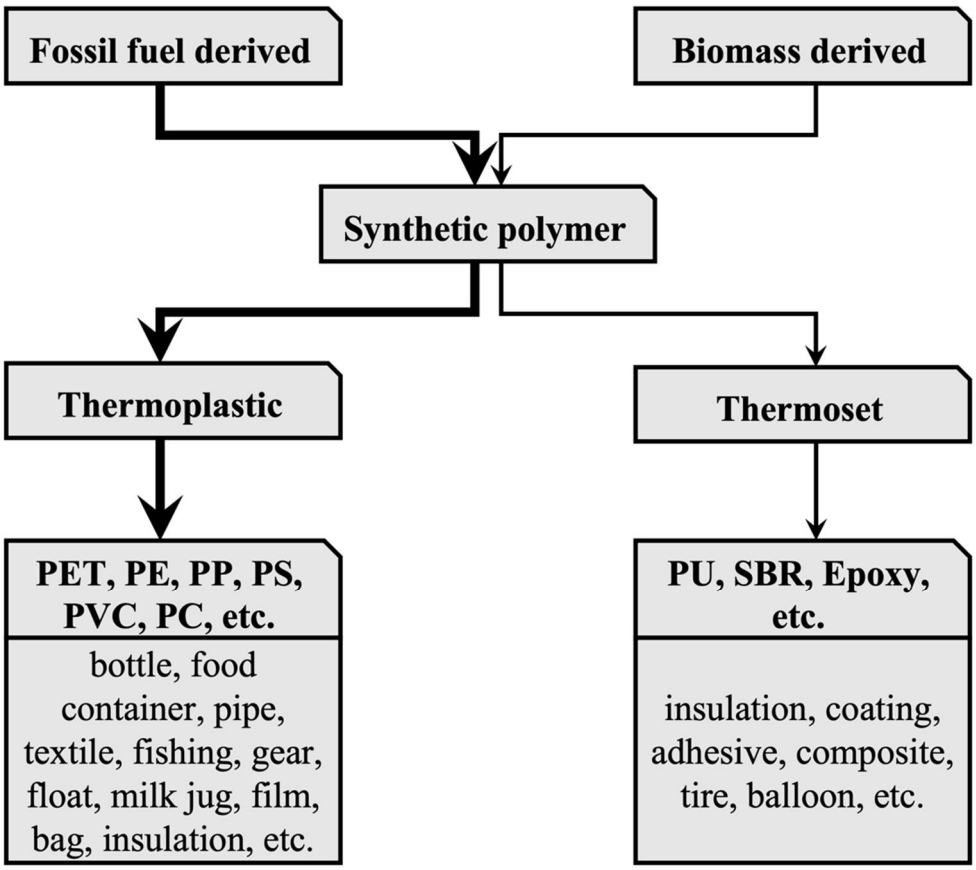

Figure 3. Production of conventional synthetic plastics (UNEP, 2017; GESAMP, 2015)

During the industrial revolution, plastic pollution was mentioned and seriously addressed starting in the 1900s, due to its abundance and its long decomposition time in nature. The discarded plastic products can be transformed for various reasons, and the little pieces are flowing into the ocean and destroying the marine ecosystem. In the early 1970s, plastic debris floating in the ocean was first reported (Carpenter et al., 1972; Carpenter & Smith, 1972). However, at that time, the dangers of that were not known, then for years, people turned a blind eye to them. Thompson et al. (2004) raised concern about the plastic particles' seriousness based on their description of their distribution in the seawater. After the research, many studies related to plastic particles in marine environments have been done, and the number rose steeply.

Moreover, international organizations and experts found the studies noteworthy. Considering the seriousness of the situation, the National Oceanic and Atmospheric Administration (NOAA) developed officially policies and guidelines associated with marine litter in 2005. Also, they held the first international conference on marine debris in 2008 to discuss the problem and to grope towards a solution. In 2012, the Group of Experts on the Scientific Aspects of Marine Environmental Protection (GESAMP) WG40 was established to assess marine debris. Since the late 2000s, the international communities, such as UNEP, UNEA, UNESCO, etc., placed the problem on the major international environmental agenda, and they have been urging governments and companies to regulate and lower the pollution. Figure 4 gives a concise illustration of the history of the pollution.

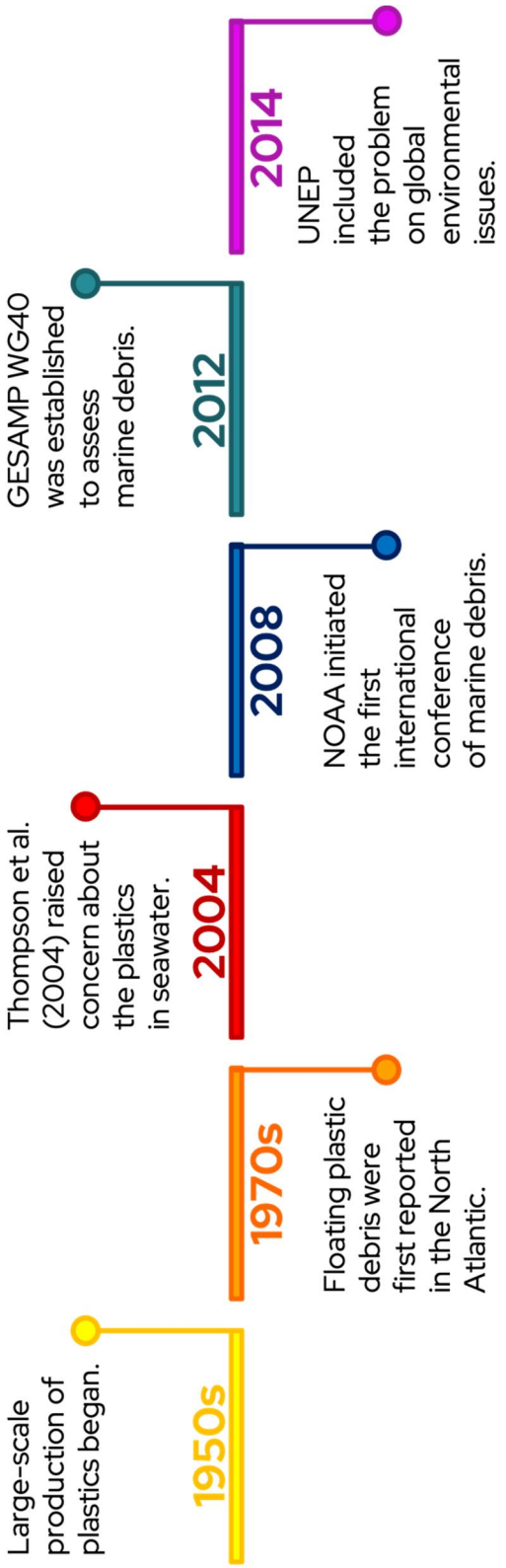

Figure 4. Timeline for plastic pollution

Despite plastics having a history of less than a century, the amounts of production and consumption are no longer insignificant. Besides, these amounts are expected to keep rising. Figure 5 shows that plastic production worldwide was steadily increasing since 1950. The number reached almost 370 million tons by 2020, an 80 % rise between 2002 and 2020 (PlasticsEurope, 2021). According to Geyer et al. (2017), approximately 8300 million tons of plastic had been produced by 2017, but less than 10 % had been recycled. In 2010, about 4.8 to 12.7 million tons of plastic waste from 192 coastal counties entered the ocean, which is equal to 1.7 % ~ 4.6 % of the total plastic waste (Jambeck et al., 2015). Around 80 % of the plastic debris in the ocean comes from land, according to many researchers. A recent study by Boucher & Friot (2017) even found that 98 percent of primary microplastics originate from the land. Also, rivers can act as a major transport pathway for plastic litter, the 10 top-ranked rivers transport 88 % ~ 95 % of the world plastics load into the sea (Schmidt et al., 2017). Thus, it is evident that a great deal of plastic waste is entering the ocean, which can be hazardous to marine life and humans.

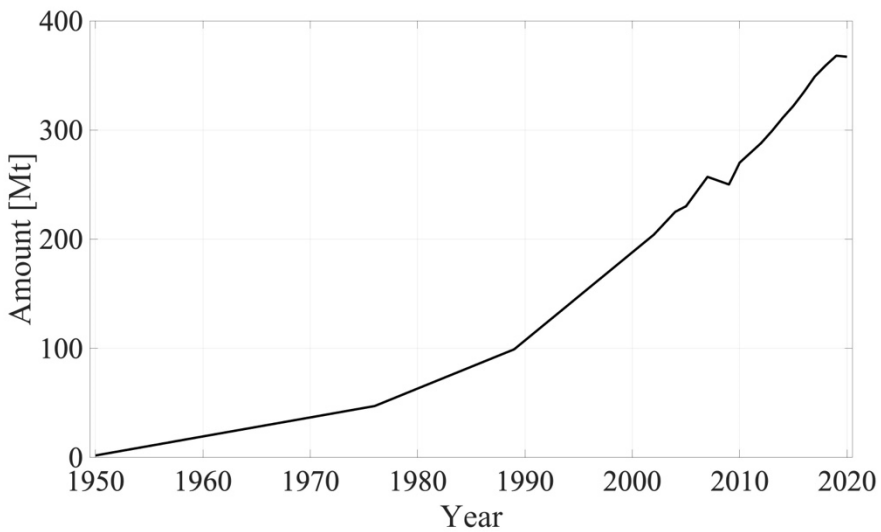

Figure 5. Annual global plastic production from 1950 to 2020 (PlasticsEurope,

2021)

Many researchers and organizations have tried to examine the distribution of plastics in marine environments. Jambeck et al. (2015) reported that 8 of the 10 top-ranked countries were in the Asia region, including China, which is the biggest emitter of plastic wastes into the sea in 2010, as shown in Figure 6 and Table 1. Based on Figure 7, Schmidt et al. (2017) reported that the Yangtze River in China is carrying the largest amount of plastics in the world, and most of them are transported to the Yellow Sea. Besides, the plastics entering the sea from the river are about nine times as many as from the Indus River, which ranks in the top two rivers. Moreover, Figure 8 shows the concentration of the plastic particles on the surface of the ocean, and it illustrates that plastic debris is accumulated in the convergence zone of each of the five large subtropical gyres (Cozar et al., 2014). Also, in the global ocean, the North Pacific Ocean has the largest amount of plastics, which is related to the most densely populated coasts in the world. It is the same result as a publication by Shim et al. (2018).

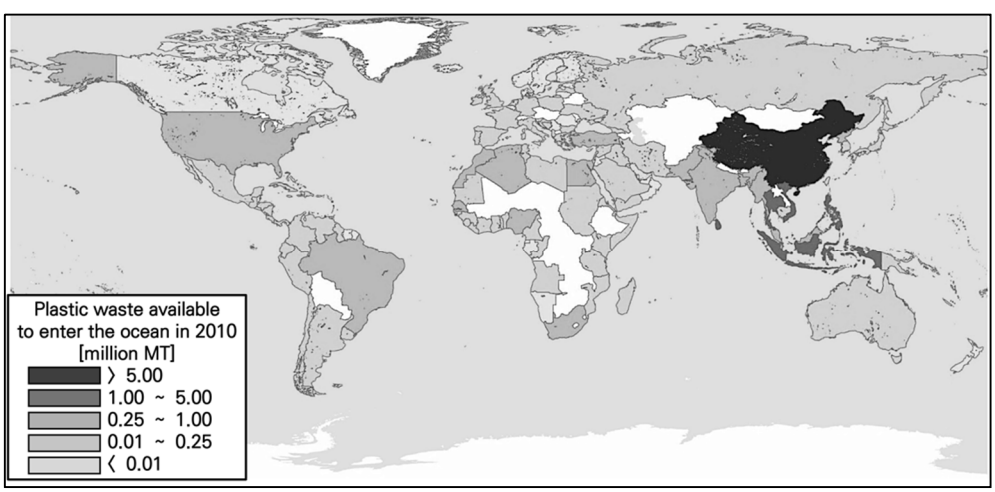

Figure 6. Estimated global mass of mismanaged plastic waste generated in

2010 (Jambeck et al., 2015)

Table 1. The 10 top countries ranked by the amount of plastic waste that entered the ocean (Jambeck et al., 2015)

Rank	Country	Mismanaged plastic waste [Mt/yr]	Plastic marine debris [Mt/yr]
1	China	8.82	1.32-3.53
2	Indonesia	3.22	0.48-1.29
3	Philippines	1.88	0.28-0.75
4	Vietnam	1.83	0.28-0.73
5	Sri Lanka	1.59	0.24-0.64
6	Thailand	1.03	0.15-0.41
7	Egypt	0.97	0.15-0.39
8	Malaysia	0.94	0.14-0.37
9	Nigeria	0.85	0.13-0.34
10	Bangladesh	0.79	0.12-0.31

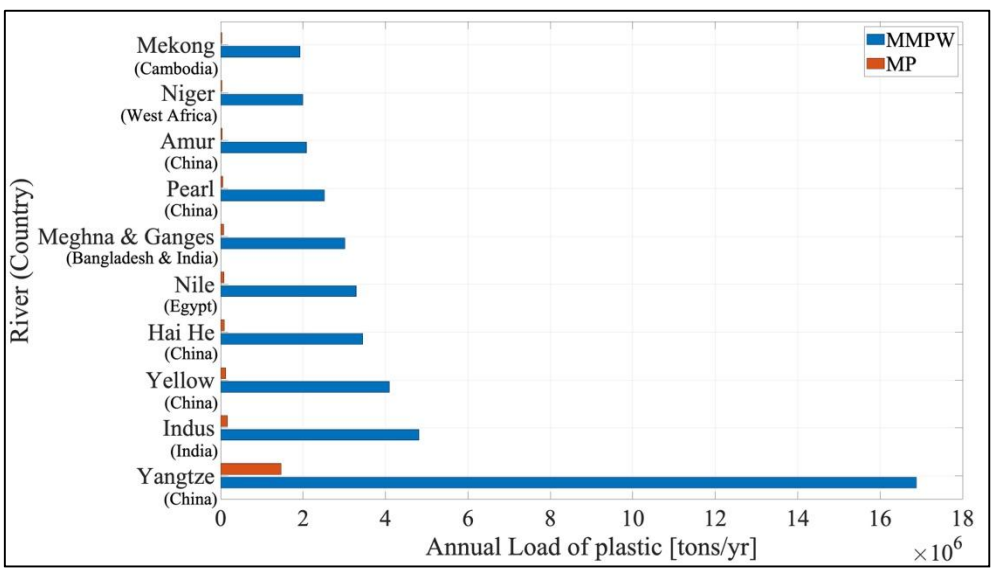

Figure 7. Plastic loads for the top 10 ranked catchments in the world (MMPW: mismanaged plastic waste; MP: microplastic) (Schmidt et al., 2017)

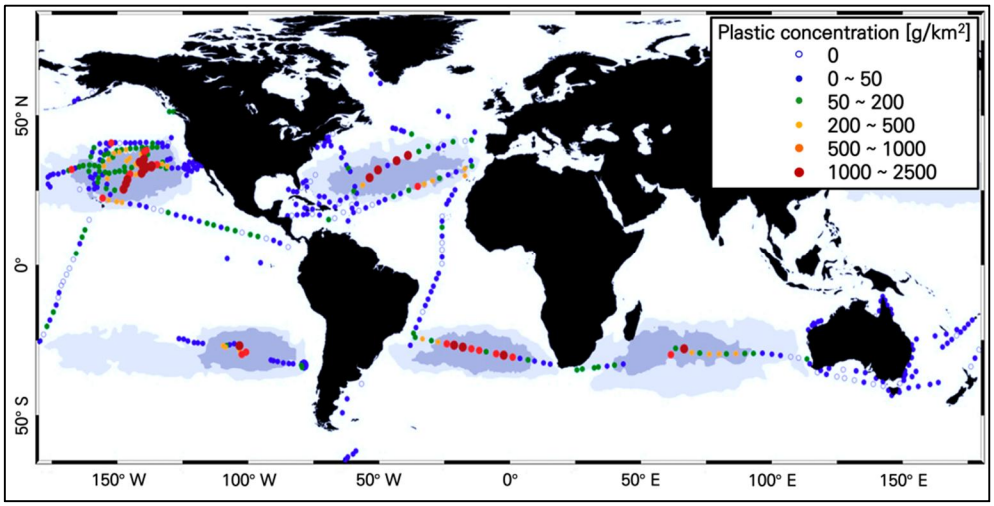

Figure 8. Distribution of plastic debris on the surface of the ocean (Cozar et al., 2014)

As such, the plastics can be found from the poles to the equator and seabeds (Barnes, 2005; Barnes et al., 2009; Shim et al., 2018; Thompson et al., 2009), and particularly, its high abundances have been recorded in the Asian countries. As for the South Korean coasts, if the amount of plastic debris is compared globally, it has the highest level of global seawater contamination (Shim & Thomposon, 2015). The Incheon-Kyyonggi beaches and the Nakong River estuary were ranked the second and third highest concentration regions of plastic particles among 30 sites around the world by Hurley et al. (2018) (Figure 9). The government-backed Korea Marine Environment Corporation (KOEM) has been monitoring the abundance of plastic wastes in 40 coastal areas since 2008. According to a report by 해양수산부 & 해양환경공단 (2020), the southern and eastern beaches have more plastic waste than the western beaches (Figure 10), and the Daebo Beach in Pohang and the Guomongdol Beach in Geoje were the most polluted in 2020. Additionally, the most common type of plastic found was hard and formed plastics, and the majority of

foreign coastal wastes came from China. There can, however, be no judgment assigned to who is responsible. A study by 남정호 (2004) found that foreign marine wastes have been found on Korean beaches, and wastes originating from Korea have also been discovered in Japan, Australia, and the United States. 천권필 (2021) investigated the transport of plastic from the Nakdong River estuary, and it showed that it can move to North Korea. Furthermore, some wastes can transport to the North Pacific Ocean along currents. As a result, it shows the importance of close cooperation between countries in resolving this issue, and understanding the transport of plastics is important.

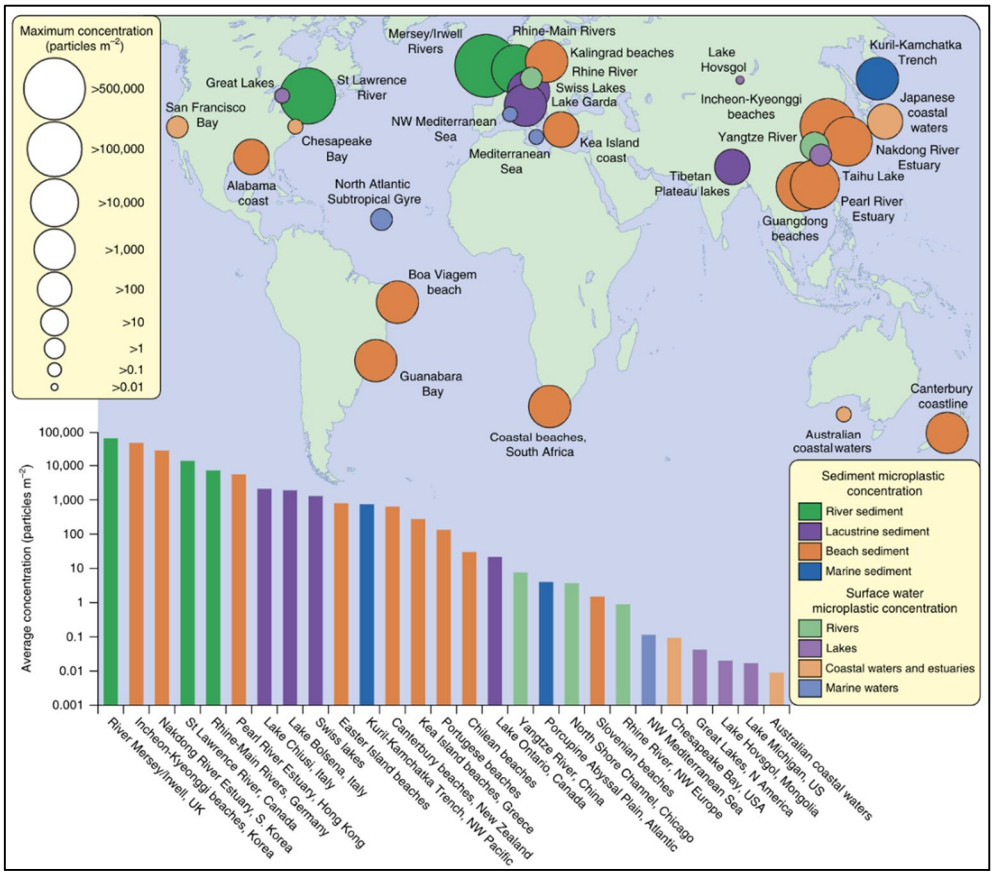

Figure 9. Global plastic debris concentrations (Hurley et al., 2018)

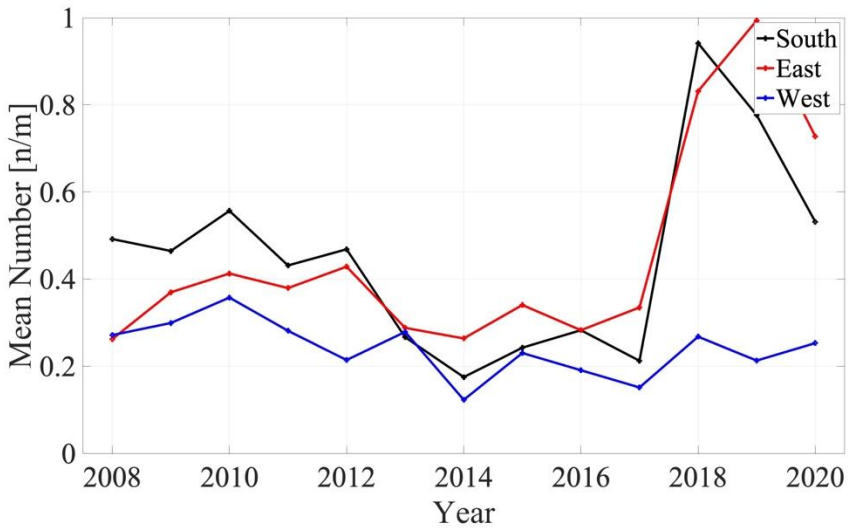

Figure 10. The average number of plastic waste from 2008 to 2020

on Korean beaches (해양수산부 & 해양환경공단, 2020)

2.2. Transport of plastics

The increasing threat requires understanding how plastics are moving and where they accumulate, and why these places differ from others that do not accumulate much marine debris (Critchell & Lambrechts, 2016). Since coastal regions and shores are subject to many dynamic actions, plastic debris can undergo some physical changes and it can affect both arrival and departure. It is essential to understand and estimate both to know how plastic accumulates, travels, and interacts with spatial, social, and temporal factors (Brennan et al., 2018; Willis et al., 2017) (Figure 11). In addition, Willis et al. (2017) found that the majority of debris that enters the marine environment washes toward the coast and is deposited locally. It represents that they spend a long time at the coast before leaving for the ocean (Turner et al., 2021). Especially, it was noted by Turner et al. (2021) that local and offshore plastic wastes are trapped within foredunes for years to decades, before being released by surges sufficient to effect scarping. Thus, dunal systems should act as significant reservoirs of plastics in the coastal zone. Nonetheless, most studies focus on surface sediments. However, Turra et al. (2014) reported that there are significant concentrations of plastic within beach sediments to depths of at least 2 meters, compared to the current beach surface. Therefore, plastic in coastal sediments has to be studied to understand the mechanism of arrival and departure of plastics.

As time passes on coasts, the waste fragments, and it continues to reduce in size. After then, the debris is washed out and floats into the ocean. Eriksen et al. (2014)

estimated that at least 5.25 trillion plastic particles weighing about 0.27 million tons are currently floating at sea. Furthermore, Chubarenko et al. (2016) showed that the drift speed for the floating polyethylene particles is four times larger than the current speed, and the floating foamed particles can be faster than the water under open-sea conditions. It means that the particles will travel about 250 kilometers in around 2 to 3 days if the wind speed is constant at 10 meters per second. Also, 천권필 (2021) found that a plastic buoy can travel almost 1000 kilometers in 20 days through a field survey. Several studies have demonstrated that plastics are widespread in the ocean (Hidalgo-Ruz et al., 2012), as well as their ability to travel long distances very quickly (Gregory, 1977, 1978).

Figure 11. Transport of plastic wastes in coastal area (Brennan et al., 2018)

Chapter 3. Methodology

3.1. Experimental equipment

3.1.1. Oscillating water tunnel

To generate an oscillatory boundary layer flow, an oscillating water tunnel was designed and newly built in the Seoul National University, as shown in Figure 12 and Figure 13, namely, SOWT. It is a u-shaped closed conduit with a bidirectional piston. It has a 4.5 meters long horizontal tube with a square cross-section of 0.27 meters side length. In addition, the tunnel has a unique feature that a detachable sediment basin can be equipped under its center, and is made entirely of transparent acrylic so that it can observe the sediment transport phenomenon effectively. Also, observation of plastics released from sediments is made simpler and more convenient. This study set the depth and length of the basin at 0.1 meters and 1 meter, respectively.

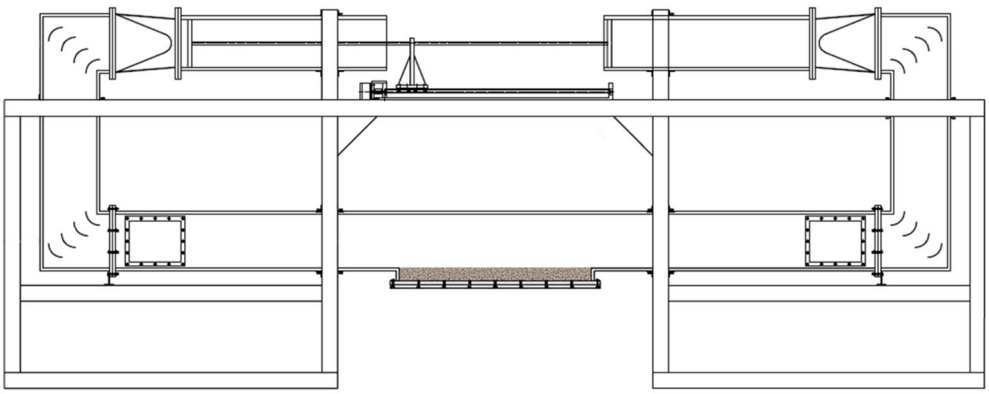

Figure 12. Drawing of the designed oscillating water tunnel

Figure 13. Appearance of the constructed SOWT

The reason why an oscillating water tunnel was chosen as the main equipment of the experiment is simple. Many types of facilities have been used to carry out experimental studies related to coastal engineering and sediment transport. For example, there are wave flumes, wave basins, oscillating water tunnels, etc. Each type has its pros and cons. The tunnel was suggested firstly by Lundgren & Sorensen (1957). An actuator drives a piston, and it generates an oscillatory motion instantaneously. The flow generated by the motion is uniform all over the x-direction of the tunnel, and the vertical orbital motion needs no consideration. Consequently, it makes to consider the only horizontal velocity to investigate the movement of the particles on the near-bed, because the vertical velocity can be ignored. Also, the flow leads to the movement of sand grains. Furthermore, it can make higher order of Reynolds number flow with its smaller size than the others. Also, it is feasible generating turbulent flow. The horizontal test section of such tunnels can be several meters long so that the Reynolds number over 10^6 can be obtained (Nielsen, 1992). To obtain the high Reynolds number, it is inevitable that the size of the facility has to be very large before oscillating water tunnel was introduced. It may cause an increase in production costs. Also, researchers have to take the spatial problem into account. Generating a flow with a high Reynolds number is important to coastal engineers. Figure 14 clearly shows the difference in the relations between the Reynolds number and the relative roughness with respect to the different types of apparatus and the natural conditions. From that, the tunnel can make the highest Reynolds number and it is the closest to the field condition. As a result, the reason is that using an oscillating water tunnel is simpler and cheaper than the other facilities.

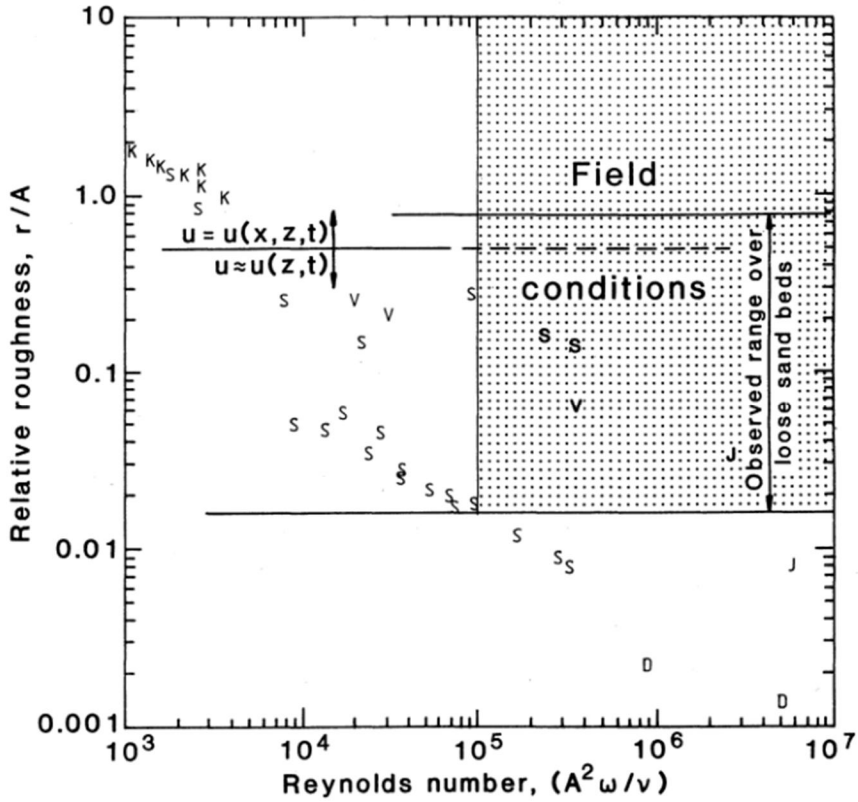

Figure 14. Relation between the Reynolds number and the relative roughness under field conditions and in laboratory studies (*Figure 1.1.3* in Nielsen (1992))

In general, the Reynolds number has been known as a dimensionless parameter with a ratio of inertia force to viscous force. It was firstly introduced by Osborne Reynolds in 1883 as follows:

$$Re = \frac{U\ L}{\nu}$$
$$\frac{inertia\ \ force}{viscous\ \ force} = O\left(\frac{U^2/L}{\nu\ \ U/L^2}\right) = O(Re) \tag{1}$$

where ν is the kinematic fluid viscosity (Reynolds, 1883). Also, the wave boundary layer Reynolds number that represents the laminar-to-turbulent transition in wave boundary layers can be expressed by:

$$Re = \frac{U_m\ \ A}{\nu} = \frac{A^2\ \ \omega}{\nu} \tag{2}$$

where U_m is the maximum value of the horizontal free stream velocity, and A is the amplitude of motion of water particles and equal to U_m/ω if the free stream velocity varies sinusoidally with time. ω is the radian frequency with T being the period. It has been commonly used in many research for the flow inside wave boundary layer in oscillatory motion or solitary motion, and oscillatory flow in a pipe. It can be found in Jensen et al. (1989), Sumer & Fuhrman (2020), Yuan & Madsen (2014), Yuan & Wang (2018), etc. Sometimes, the Reynolds number can also be used in conjunction with the conventional thickness of the Stokes boundary layer, δ, with regard to oscillating boundary layer flow. So, it is defined as (Scandura, 2007):

$$Re = \frac{U_m\ \sqrt{2\nu/\omega}}{\nu} = \frac{U_m\ \ \delta}{\nu} \tag{3}$$

Nonetheless, the following form was used in this study. As oscillating water tunnel does not have the concept of amplitude, the form is defined to view intuitively the extent of effect of the flow velocity

and period as follows:

$$Re = \frac{U^2 \ T}{2 \ \pi \ \nu} \tag{4}$$

However, it is essentially the same with Equation (2).

Through the newly built oscillating water tunnel, the oscillatory flow is generated and it was used in this study. Since hydrodynamics on natural wave fields in coastal zone has a very complicated mechanism, especially outside the boundary layer, the conditions and the calculations need to be simplified. Normally, the tides and rip currents and longshore currents could be considered quasi-steady flows, and the effects of the rotation of the earth are ignored (Nielsen, 1992). Then, it is the oscillatory flow that is a periodic motion of a point along a straight line called a simple harmonic motion (Bird & Chivers, 1993). It shows a monochromatic wave with the wave-induced velocity, $u_\infty(t)$ above the boundary layer expressed as:

$$u_\infty(t) = U_\infty \cos \omega t = U_\infty \cos \theta \tag{5}$$

where U_∞ is the amplitude of the velocity oscillation, t is the time, and θ is the phase angle. The $u_\infty(t)$ can be changed only near the bed in vertical z-direction, and variations in the horizontal x- and y- can be neglected (Nielsen, 1992). Moreover, the sediment transport will show the back-and-forth movement on the bottom due to the same movement of the oscillatory flow as coastal field condition. A periodic excitation force in the drag direction is generated due to the resulting time-dependent inertia and drag forces, and it should work more important than that in the lift direction in case of the oscillatory flow (Kaneko et al., 2014). Therefore, the oscillatory flow is suitable for this study in the characteristic of the apparatus and the sediment transport purpose. Figure 15 shows the comparison flow motions in

fields and the oscillating water tunnel.

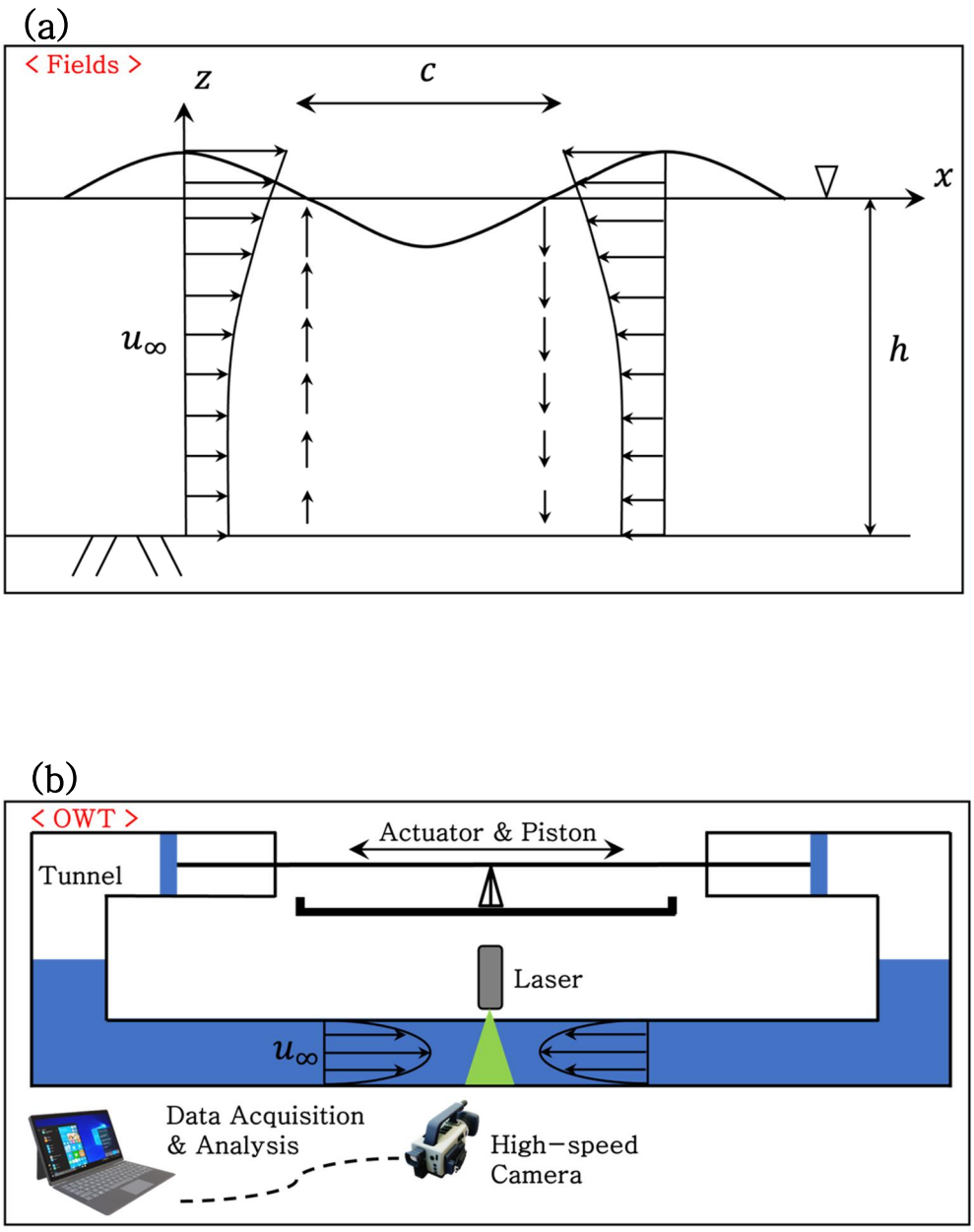

Figure 15. Flow motions with wave-induced velocity, $u_\infty(t)$ ((a): under fields (Nielsen, 1992); (b): the oscillating water tunnel)

3.1.2. Particle image velocimetry, PIV

Particle image velocimetry, PIV is an incoherent laser optical measuring technique for obtaining instantaneous fluid properties by producing the two-dimensional or three-dimensional vector fields in fluids. To construct generally the system, the apparatus consists of a laser with a lens to produce a laser sheet focused on the field of interest, a digital camera, and seeding particles that have to be geared to the properties of fluids reasonably.

Two- dimensional PIV system was constructed in the oscillating water tunnel to obtain the more accurate properties of the generated flow such as the flow velocities and periods. After several attempts to be considered accurate enough, the system was constructed properly as shown in Figure 17. The PIV equipment used here consists of a continuous wave laser of the Dantec Dynamics RayPower 5000 model to visualize the flows, a high-speed camera of Photron FASTCAM Mini UX100 model, and polyamide seeding particles (PSP) of Dantec Dynamics. The laser intensity is used at $5\ mW$. Setting intensity properly is important. If it is weak, the camera cannot pick up on the right amount of seeding particles to analyze. The poor quantity of the particle leads to the poor quality of the PIV analysis results, because each particle represents the flow data.

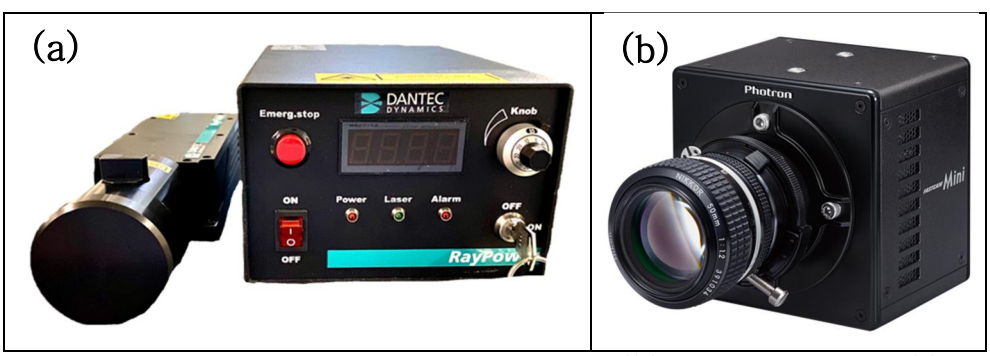

Figure 16. Measuring devices for PIV system ((a): Continuous laser; (b):

Highspeed camera)

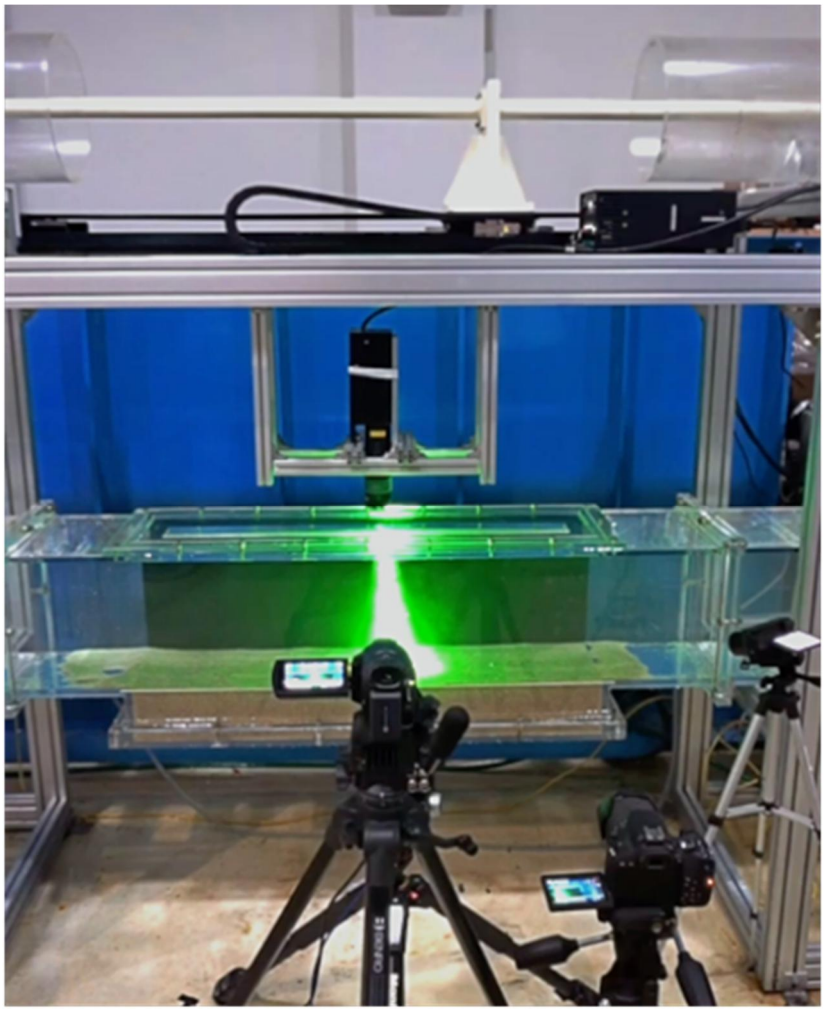

Figure 17. Appearance of installed PIV devices onto the oscillating water tunnel

Next, the prepared camera can shoot with framerates up to $4{,}000\ Hz$ in $1{,}280 \times 1{,}024$ pixels, but the experiments were taken with $500\ Hz$ or $1{,}000\ Hz$. Using appropriate framerate in research is mightily important as well. Any equipment can be limiting, even with high powers. Framerate refers to a ratio of the speed of photographing successive images. That is, it is the number of taken images per second. However, the framerate and the available recording time of the camera have mutual relations with each other. As the high framerate demands the high performance of the camera and it makes the camera overwork, the recording time will be shorter. On the contrary, the low framerate results in a long recording time, but the interval time between the sequential images is too long. Moreover, the flow properties such as the velocity and period should be taken into account when the framerate is adjusted. The lower the framerate, the higher the exposure of the camera. Then, the greater amount of the particles data will be taken in a frame because the camera can detect more of the light reflected off the particles. Due to the high exposure, the streamline can be easily taken in the condition of the too fast flow compared to the performance of the camera.

Another consideration is the choice of the proper seeding material for the successful acquisition of data. The accuracy of the velocity determination directly related to the success depends on the ability of the scattering particles to follow the instantaneous motion of the continuous phase (Melling, 1997). There exist many kinds of seeding particles. They have different colors, sizes, shapes, and materials. Among them, finding out the compromise between reducing the size to improve the ability of flow tracking and increasing that to improve their light scattering is a significant matter (Melling, 1997; Melling & Whitelaw, 1973). Also, the flow

tracking capability can be decided as well by the shapes and materials. The shape of the seeding particle has an influence on the flow resistance. Each material has different densities. The seeding particle with low density compared with the fluid density may show the buoyancy effects and low seeding concentration. In investigations with PIV in liquid flows condition, polyamide particles and hollow glass particles are commonly recommended and used the most. Both have spherical shapes and densities close to the water density. Of the two types, the former was chosen to use in this study by trial and error. Its density is closer to the fluid than the latter, and it has a broader range of sizes. Therefore, the used seeding particles are a mean particle size of $50\ \mu m$ and a mean density of 1.03 grams per cubic meter. The particles were diluted with water, and the diluent was mixed thoroughly and uniformly in the oscillatory flow before every experimental case.

The recorded video with the PIV system was analyzed using open-source software based on MATLAB, namely PIVlab (Thielicke & Stamhuis, 2014). It is a common and user-friendly digital particle image velocimetry analyzing tool. The workflow of the analysis is presented in Figure 18. After input of the recorded images, the process of pre-processing is to improve the measurement quality, but choosing the option depends on the quality of the images. To evaluate the pre-processed images, interrogation areas of an image pair are cross-correlated by defining the most probable particle displacement in the areas with the following statistical function:

$$C(m,n) = \sum_i \sum_j A(i,j)\ B(i-m, j-n) \tag{6}$$

where A and B are corresponding interrogation areas from images A and B (Thielicke & Stamhuis, 2014). There are three different analysis methods. The method of ensemble correlation is for a steady flow, the direct cross-correlation

(DCC) has disadvantages of high computational cost and low quality compared with the other methods. The FFT window deformation is a common method to analyze. It used interrogation areas of identical size with multiple passes and deforming windows. It is based on discrete Fourier transform correlation. After analysis, the empty data were not interpolated to preserve the original data. Thus, the vector fields with magnitudes of velocity were obtained.

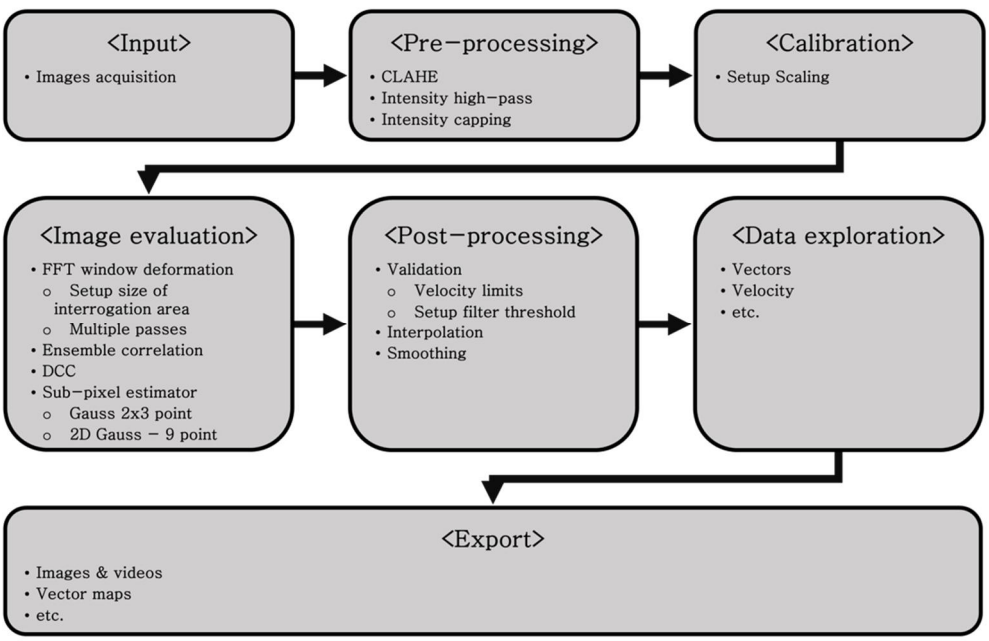

Figure 18. Overview of the workflow for PIV analysis in PIVlab (Thielicke & Stamhuis, 2014)

3.2. Experimental conditions & set-up

3.2.1. Sediments and plastic particles

Before conducting the experiments, the materials that are sediments and plastic particles were prepared. The sediments are the standard sand with uniform grain sizes, and the plastics are non-porous and spherical shape particles to simplify the

condition.

Firstly, the standard sand was prepared nonetheless, but the particle size analysis of the sand was performed by conducting sieving repeatedly after natural drying of the sand. Then, the sieved results of measuring the weight of sand by each grain size were used in the GRADISTAT Ver8.0 statistical processing software for sand grain size analysis (Blott & Pye, 2001). Using the program, the grain size distribution characteristics of the sand can be obtained. The cumulative mass retained and the weight of the sand is shown in Figure 19 and Figure 20. Among the different analysis methods, a method suggested by Folk & Ward (1957) was used. As a result, the mean size, the spread (sorting) of the sizes around the average, and the symmetry or preferential spread (skewness) to one side of the average of the sand are $0.198\ \phi$, $0.421\ \phi$, and 0.019, respectively. Also, the half of $95\ \%$ confidence interval of the average size is around 0.099. It was compared with the results of Rhew & Kang (2020) which investigated the coastal dunes in South Korea's 189 beaches. It shows 0.11 on the east coast, 0.08 on the west, 0.16 on the south, and 0.07 in total. The result of this study is within the range of the literature, and it appears the closest result to the Korean east coast. Moreover, the value of the sand grain size when the cumulative percentage reaches $50\ \%$, namely D_{50} or the median particle size stood at about $868.6\ \mu m$ which corresponds to the size of the coarse sand defined by the Udden-Wentworth grain size scale (Udden, 1914; Wentworth, 1922). The sediment can be found in sand:mud ratio and clay:silt ratio, as illustrated in Figure 21 and Figure 22. Kim & Song (2012) shows that D_{50} of sand in 35 coastal areas in Gangwon-do is $[355\ \mu m,\ 1{,}290\ \mu m]$ and $782.7\ \mu m$ on average. Therefore, it means that the sediment used in this study is

sufficiently representative of coastal sediment.

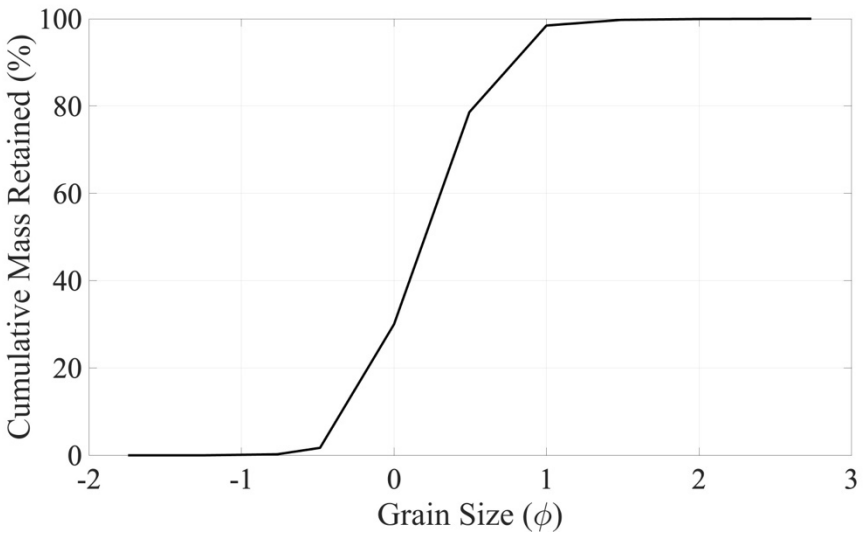

Figure 19. Cumulative curve for grain size distribution

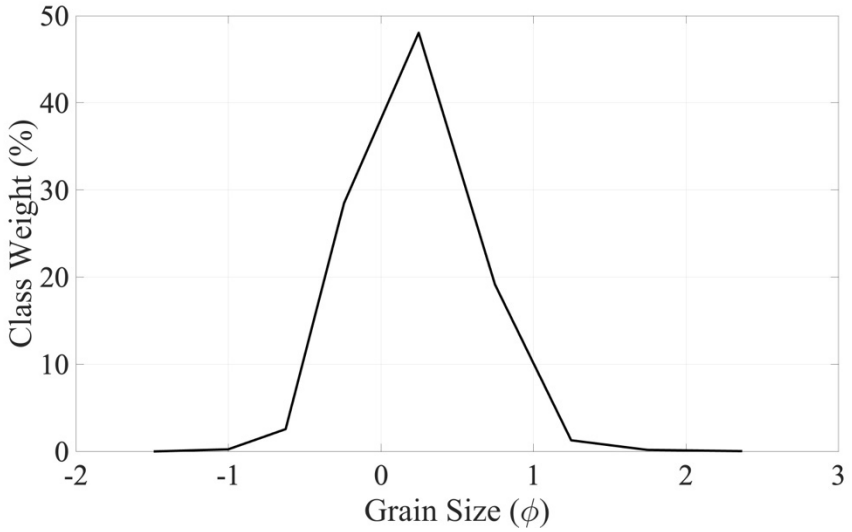

Figure 20. Grain size distribution with weight

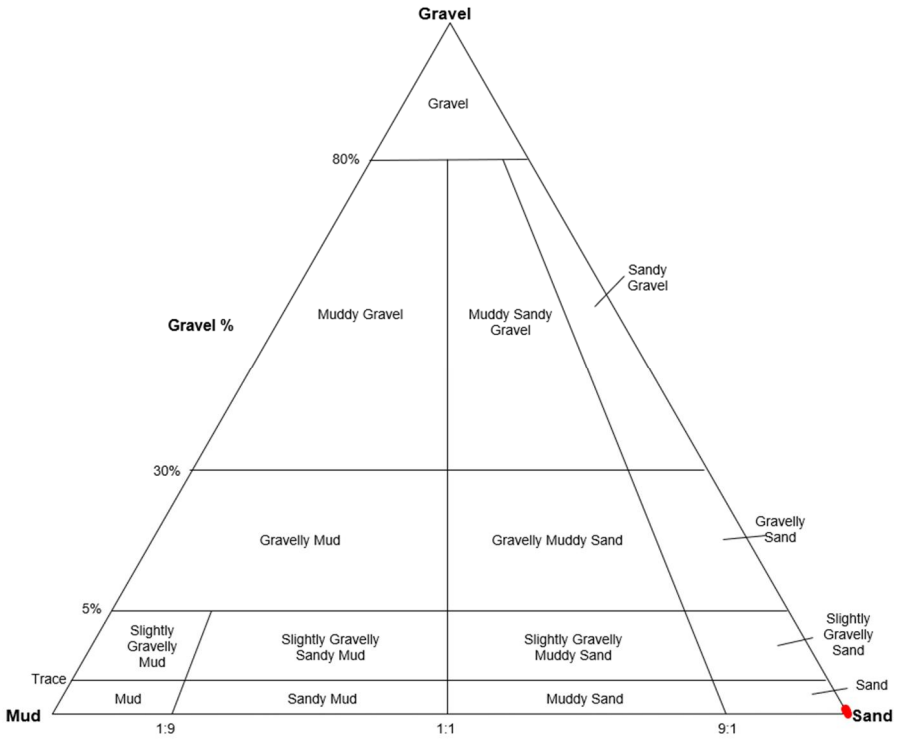

Figure 21. Gravel : Mud : Sand ratio

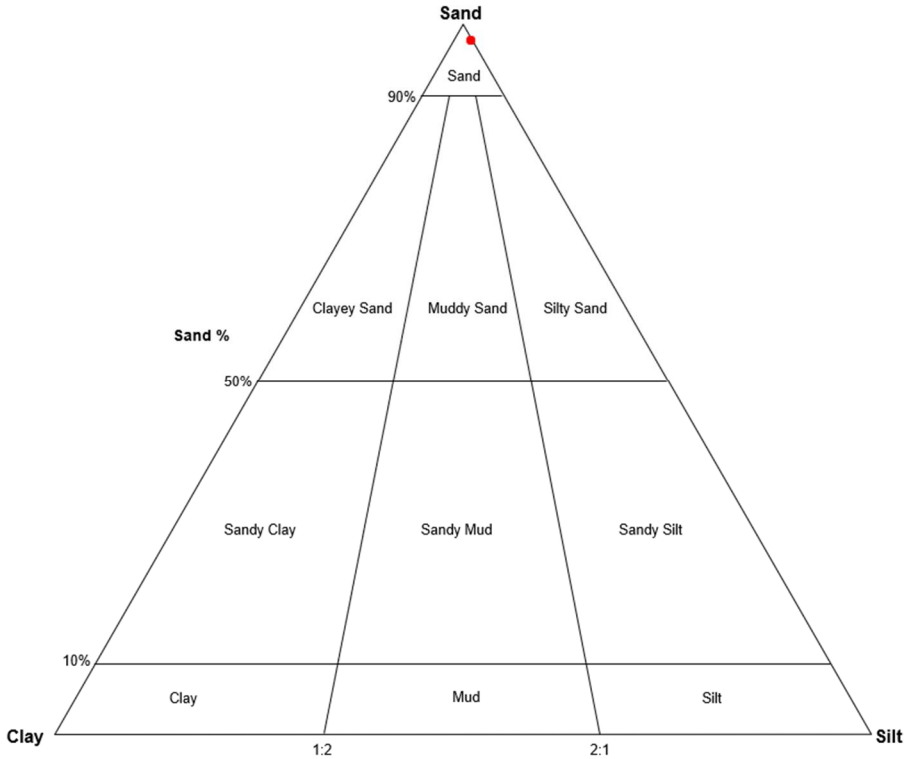

Figure 22. Sand : Clay : Silt ratio

The plastic particles are smoothly spherical. They have three different diameters of sizes, $3\ mm$, $6\ mm$, and $8\ mm$. To obtain the density exactly, random samples of the particles were extracted, and measured their sizes and weights repeatably. As a result, the mean density was estimated at around $0.95 \pm 0.04\ g/cm^3$. It is close to the density of a fluid.

Before each experimental case, the sediment basin in the oscillating water tunnel was filled with sand and plastics. Especially, the plastic particles were set into the sediments with certain rules. First of all, the sediment in the basin was flattened, and the inside air bubble was removed as much as possible. If not, the bubble will interrupt making a uniform laser sheet for PIV and releasing the plastics from the sediments to fluids. The reason why the sand bed was spread and flattened is because of the prior condition mentioned in *Section 1.1*. The initial condition is that all plastic particles have to be in sediment before the experiment and the bed is flat. So, all experiments were started with the same initial bed condition. After that, the basin was divided into 4 sections to consider the movement of plastics in sediments between the sections as shown in Figure 23. Each section has particles with different colors of plastic particles, but the same size in each experimental case. It will show whether the particles can move in the sediment or not. Also, each experimental case has a total of 440 pieces of the particles with different to investigate the effect of the size on their release. Moreover, the sediment basin was divided into 4 layers and the particles were set regularly on the layers to consider the difference in the release with sediment depth. There are 40 pieces of particles on the sediment surface ($z = 0\ m$), 144 pieces on $z = -0.02\ m$, 136 pieces on $z = -0.045\ m$, and 120 pieces on $z = -0.075\ m$. Figure 24 and Figure 25 explain the layers with depths and the

arrangement of particles in a section, respectively. After an experiment, the amounts of the released particles and the remained particles inside sediments were counted. However, the numbers of the particles placed in the first and fourth sections were excluded. The reason is the results of those sections are not reliable, because of the effect of both edges of the basin, which is one of the main causes of disturbing the flow.

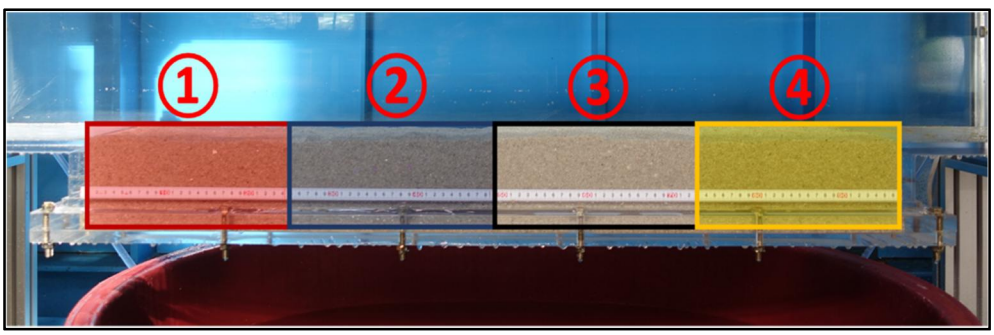

Figure 23. Classification of sections in a sediment basin

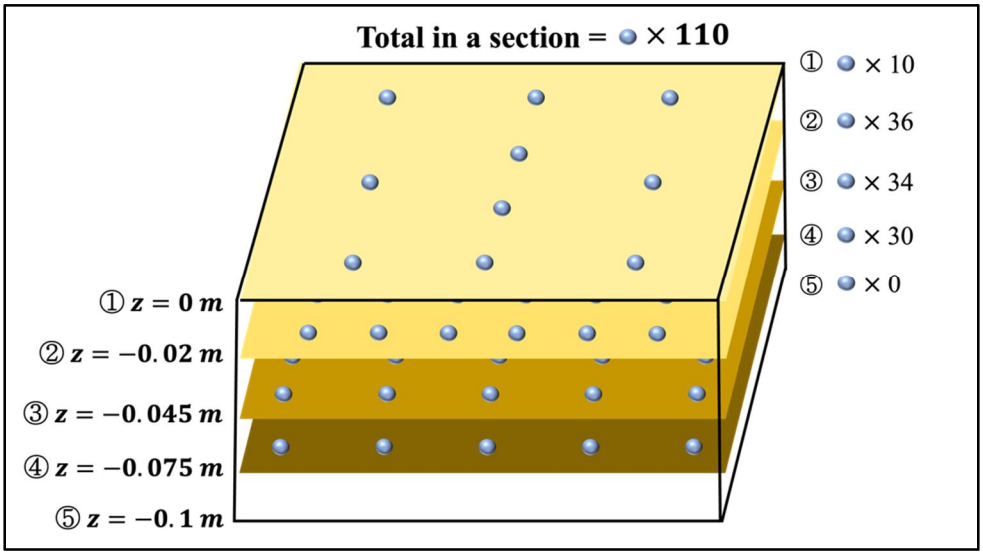

Figure 24. Set-up of plastic particles in a section

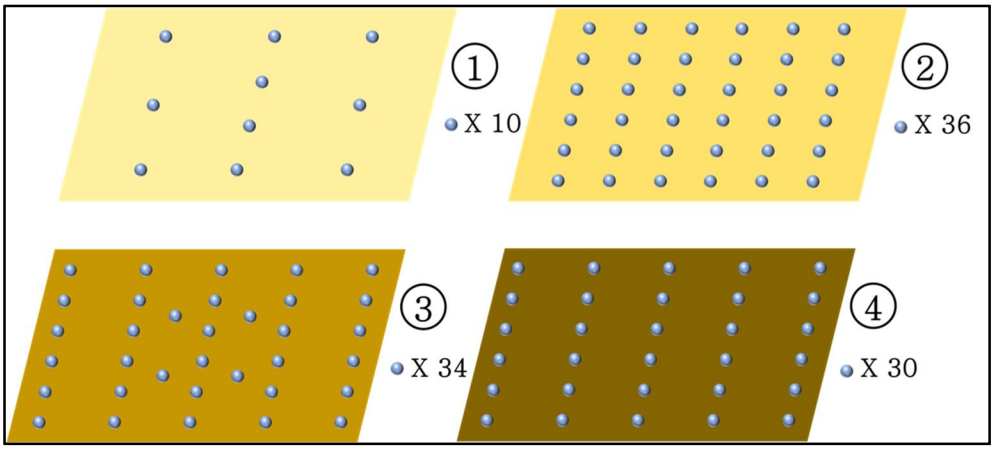

Figure 25. Set-up of plastic particles on each depth

3.2.2. Experimental conditions

In variations of the properties of the generated oscillatory flow such as the flow velocities and periods, and the sizes of the plastic particles, the experimental cases were planned into 42 cases. The flow conditions could be controlled by modulating the stroke length and input velocity for the actuator in the oscillating water tunnel. The accurate properties of the flow were obtained by analysis of PIV. From that, the Reynolds number for each case was estimated. Thus, all experimental cases are demonstrated with combination of the Reynolds numbers and the sizes of plastics in Table 2.

Each experimental case was conducted for one hour. It could be mostly described as a time to make quasi-steady bedform generally. Furthermore, in case of taking longer time than one hour, it would entail the sediment in the basin is spilled too much out the basin. The reason is there is no inflow of sand from outside of the basin, unlike the natural environment. Therefore, the experimental duration was set up for one hour after several tries.

Table 2. Conditions for each experimental case

Cases	Reynolds numbers	Particle diameters [mm]
R1a	3.7×10^4	3
R1b		6
R1c		8
R2a	3.79×10^4	3
R2b		6
R2c		8
R3a	4.557×10^4	3
R3b		6
R3c		8
R4a	5.417×10^4	3
R4b		6
R4c		8
R5a	5.597×10^4	3
R5b		6
R5c		8
R6a	5.717×10^4	3
R6b		6
R6c		8
R7a	5.928×10^4	3
R7b		6
R7c		8
R8a	5.932×10^4	3
R8b		6
R8c		8
R9a	5.945×10^4	3
R9b		6
R9c		8
R10a	6.88×10^4	3
R10b		6
R10c		8
R11a	6.984×10^4	3
R11b		6
R11c		8
R12a	7.561×10^4	3
R12b		6
R12c		8
R13a	7.58×10^4	3
R13b		6
R13c		8
R14a	7.666×10^4	3
R14b		6
R14c		8

3.2.3. Experimental procedure

With the intended conditions, the experiments were conducted following a

procedure. First of all, the sediments in the basin need to be leveled, and the air inside the sediment has to be removed. Next, the plastic particles are situated as set out in *Section 3.2.1*. The size of the particles is varied depending on the experimental case as shown in Table 2. After filling the tunnel with water and diluent of seeding particles, the actuator for generating the flow and PIV system need to be set. If so be that it is completed so far, all preparations for an experiment are done.

During the experiment, the flow is recorded by utilizing the PIV system. After one hour after starting an experiment, the size of the ripples formed by sediment transport was measured. The properties are notated as shown in Figure 26. The number of released particles is counted by the color of the plastics. The color indicates where the particles come from the section. Moreover, the number of the remaining particles in the sediment is quantified by each basin depth, as well. Now, it is the overall procedure of an experiment. Figure 27 shows the general procedure.

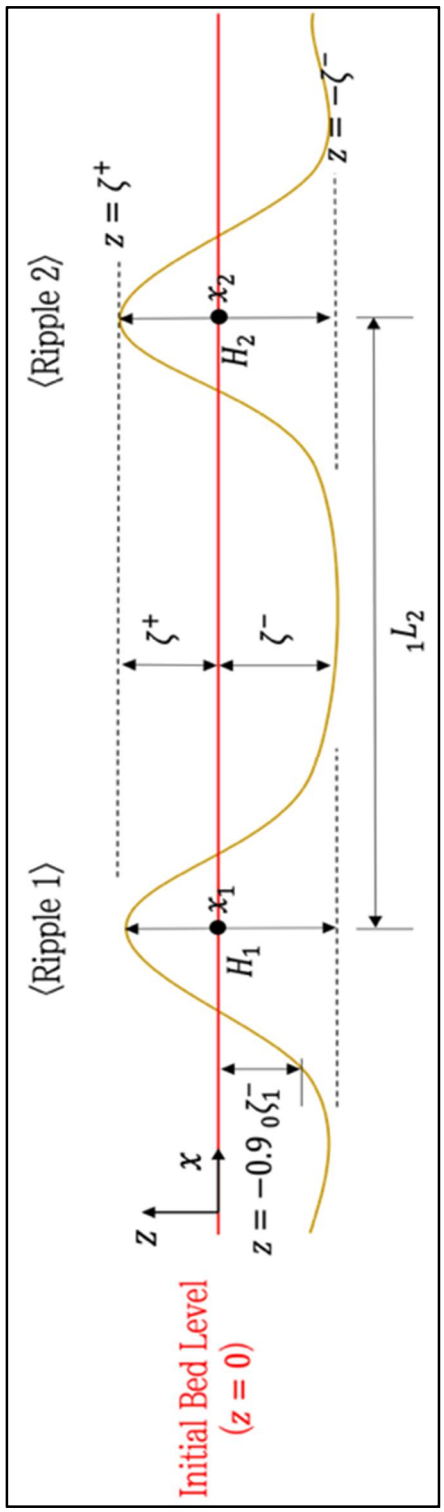

Figure 26. Notations for properties of ripples

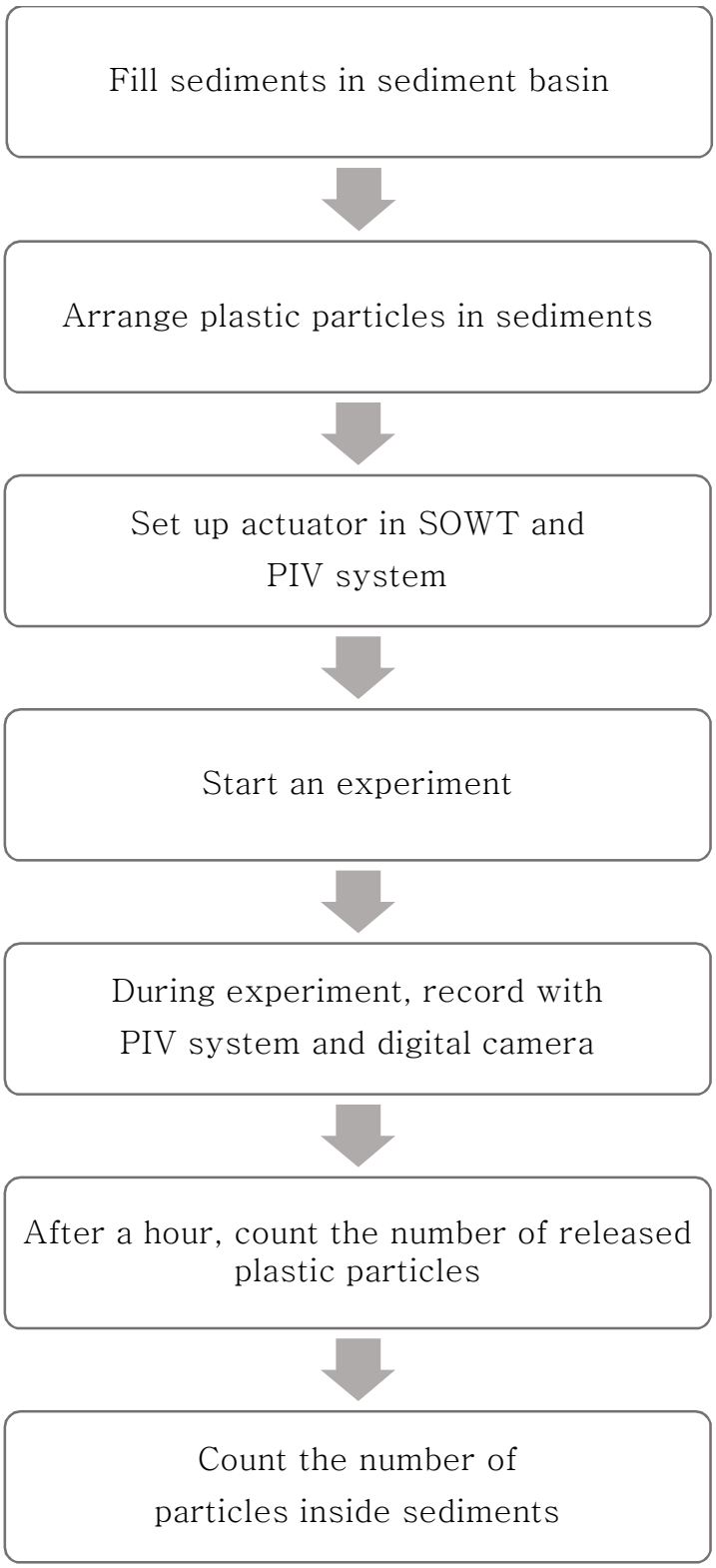

Figure 27. General experimental procedure

Chapter 4. Results and Discussions

4.1. Sediment transport & ripples

All experimental cases specified in Table 2 were conducted. Even though the release of the plastic particle was influenced by various factors, the results show that the bedform change is the first step to release. First of all, not only slight movement of the sand grain was observed in the conducted Reynolds number range of $[3.70 \times 10^4,\ 5.5 \times 10^4]$, but the oscillation was also unable to be turned into the appreciable bedform change in the flow conditions and the experimental duration. Consequently, the release of the plastics was not detected in the cases referred to from $R1a$ to $R4c$. The corresponding Reynold number flows cannot transfer sufficient energy to disturb and move the sand grain into the sediments. In other words, the disturbing force is much smaller than the stabilizing force due to gravitation, and then, there is still no room for moving the plastics in the sediment. Here, a flow threshold value for bedform change can be set to the Reynolds number of about 5.5×10^4 in this experimental condition. In relation to the flow threshold, Ribberink & Al-Salem (1994) and van der Werf et al. (2007) observed the sediment transport in oscillatory flow. Their thresholds are Reynolds numbers of almost 4.3×10^4 and 6.7×10^4, respectively, in their conditions. They are similar to one of this study, but the three studies have different conditions such as the sand grain size.

From the observation of the experiments, other interesting finds could be found. One is that ripples have quasi-steady form by around 15~20 minutes from starting of an experiment. This could be seen in all experiments, except the cases in which

the sediment transport did not occur in $Re\sim[3.70\times10^4,\ 5.5\times10^4]$. Figure 28 shows the progress of the bedform change over one hour, and the fact that the bed has almost steady shape at about 15 minutes can be known. After the formation, the ripples slowly moved to both ends of the basin until the end of the experiment. It resulted in a gradual increase in ripple length, and the formed ripples near the edges escape the basin. Another is that the depth of the ripples formed eventually in 60 minutes was no more than about $40\ \ mm$ from the initial surface level, $z=0\ \ m$. As a result, the condition for the release of plastic particles in the natural coastal areas can be predicted somewhat with the time for ripple formation and the maximum depth of ripple under the flow condition with $Re\sim[5.5\times10^4,\ 7.7\times10^4]$ and the grain size of $D_{50}\sim868.6\ \ \mu m$. Therefore, these results might be used and contributed to research and work on the abundance and distribution of plastic litter.

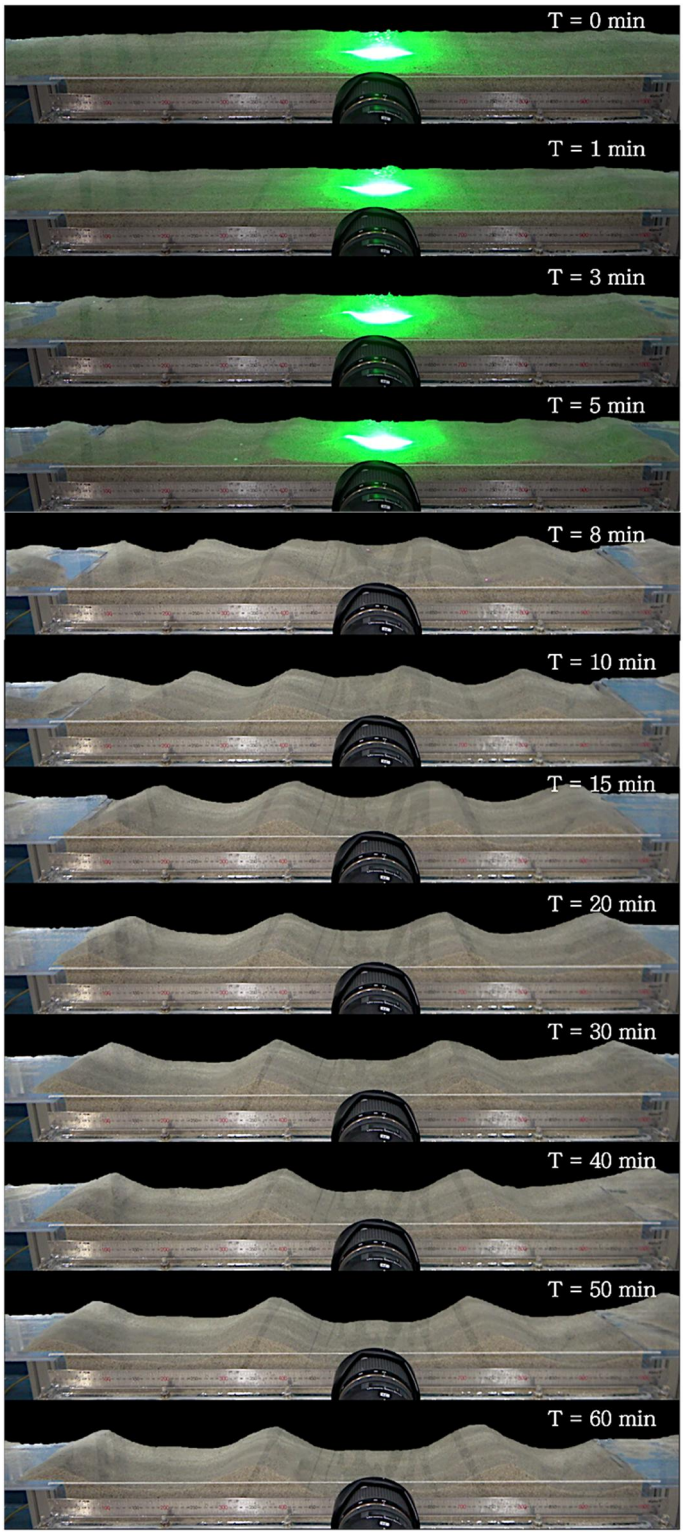

Figure 28. Progress of bedform change during an hour

To understand the properties of the ripples in more detail, the video data recorded like Figure 28 was digitized. The first step is correcting the distortion of the video shoot by a digital camera. The outermost acrylic plane of the tunnel would be the norm plane to convert into two-dimensional data. By setting the origin of coordinates with lengths on the $x-$ and $y-$ axis, the distortion was rectified. The leftmost endpoint of the sediment basin at the level of $z = 0$ was defined as the origin point $(x = 0,\ z = 0)$. The two lengths were input by the length scales of the tunnel because the scales cannot be changed and they are the most accurate among the other length scales. By calculating the distortion coefficient (k_c), focal length, coefficient of skewness from the boundary condition set with the coordinate, the images resolved the distortion can be obtained. The images did not vary much from the original as shown in Figure 29. The reason might be that there is not much distortion at the beginning, and the corrected area in the image is small. The corrected images were used to extract the boundary of the bedform.

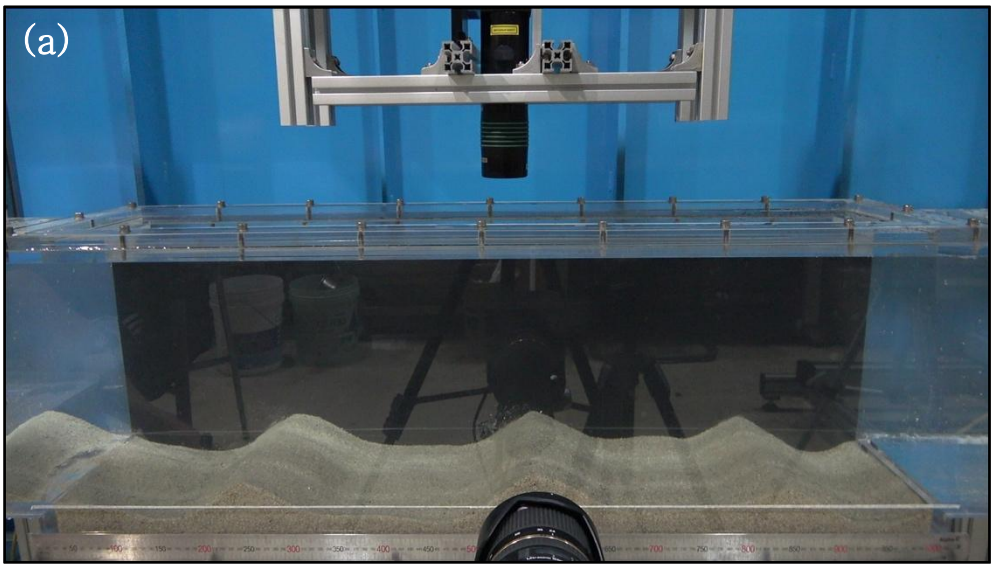

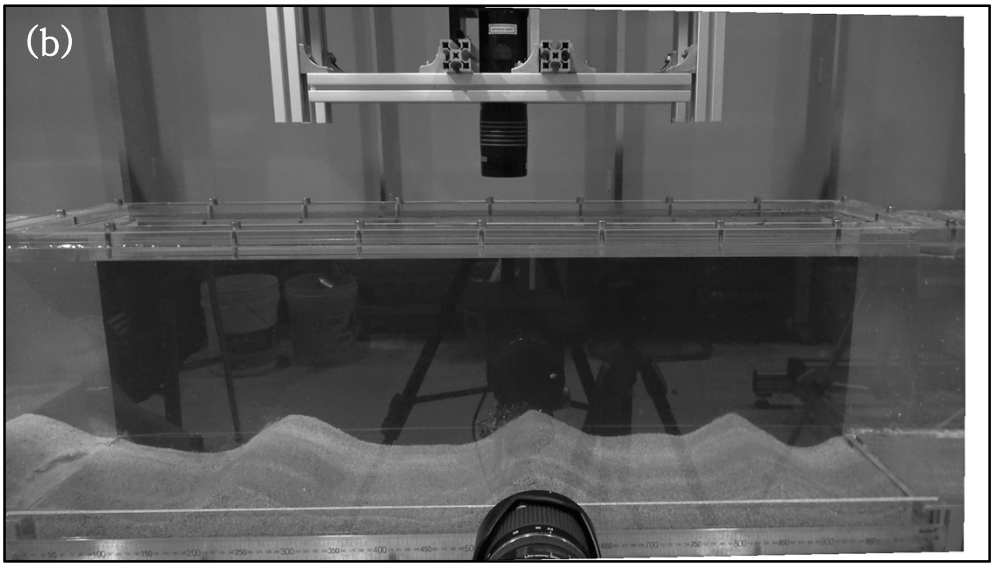

Figure 29. Comparison between the original (a) and the distortion correction image (b)

Now, the boundary of the bedform was extracted and it was made with the two-dimensional coordinate system. Figure 31 shows the results. With the results, the ripple length (λ) and the number of the eventually formed ripples in 60 minutes were obtained. Moreover, to investigate how deep the ripples reach over time, the ripple-ripple interval length (σ) and cumulative area on the seven basin layers ($z = 0\ m,\ z = -0.005\ m,\ z = -0.01\ m,\ z = -0.015\ m,\ z = -0.02\ m,\ z = -0.045\ m,\ z = -0.075\ m$) were calculated (Figure 30). The cumulative area was calculated by doing numerical integration as shown in Figure 32. As a result, the number of the formed ripples is illustrated in Figure 33. Two to four ripples were formed, and there are three ripples on average. Also, as the Reynolds number of the flow increases, the number decrease within a meter of the horizontal basin length. The reason can be found in the ripple length illustrated in Figure 34. An increase in the Reynolds number leads to a larger ripple length.

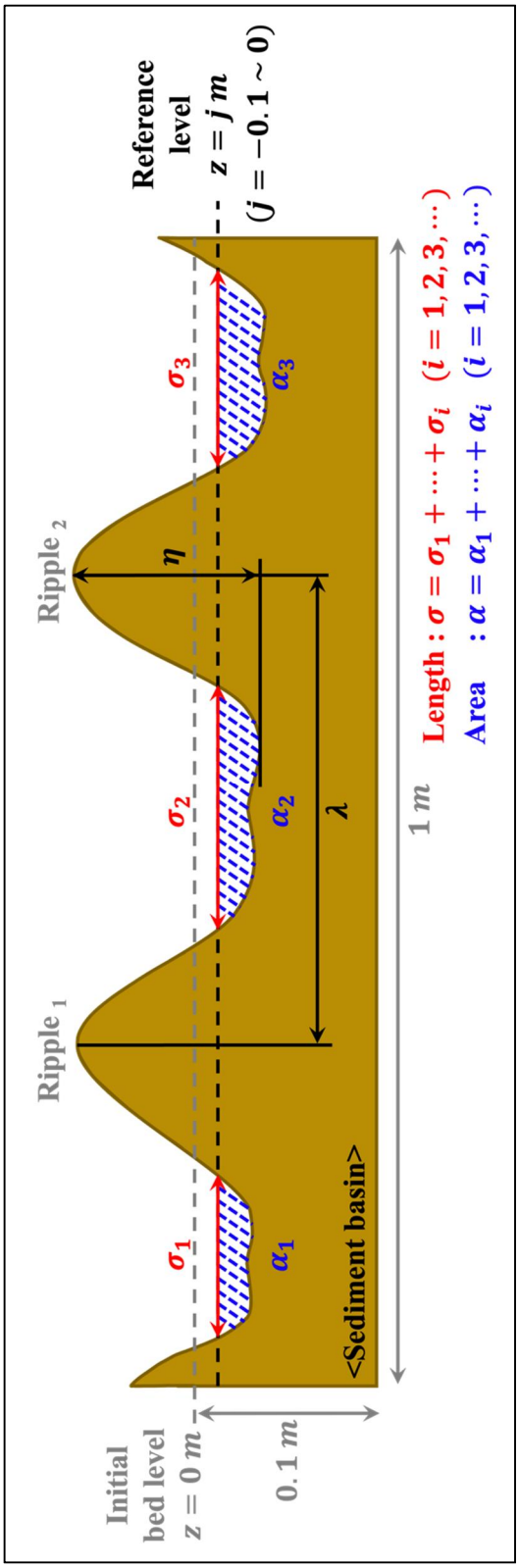

Figure 30. Definitions of λ, η, σ, and α

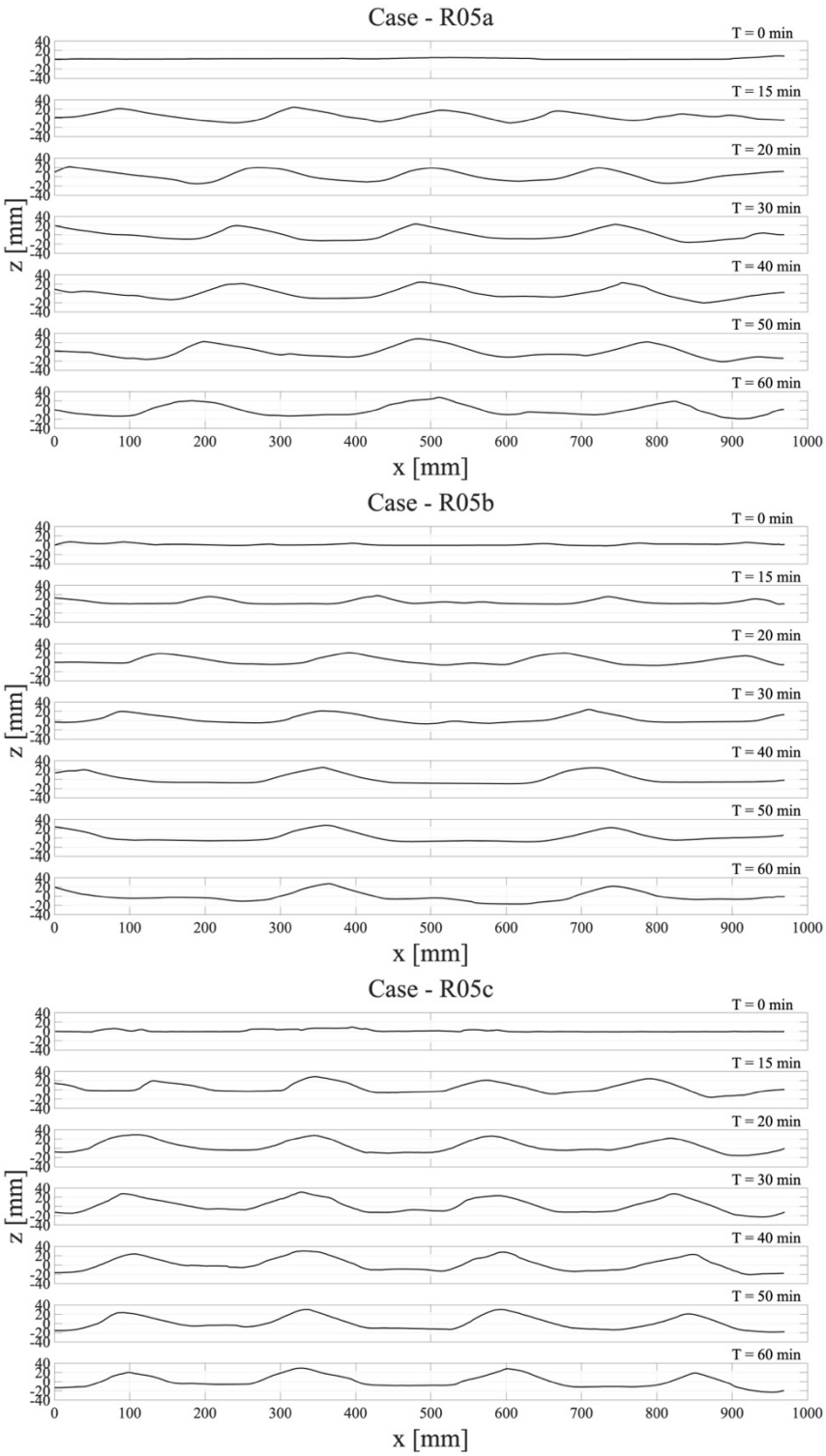

Figure 31. Digitized two-dimensional bedform over the time

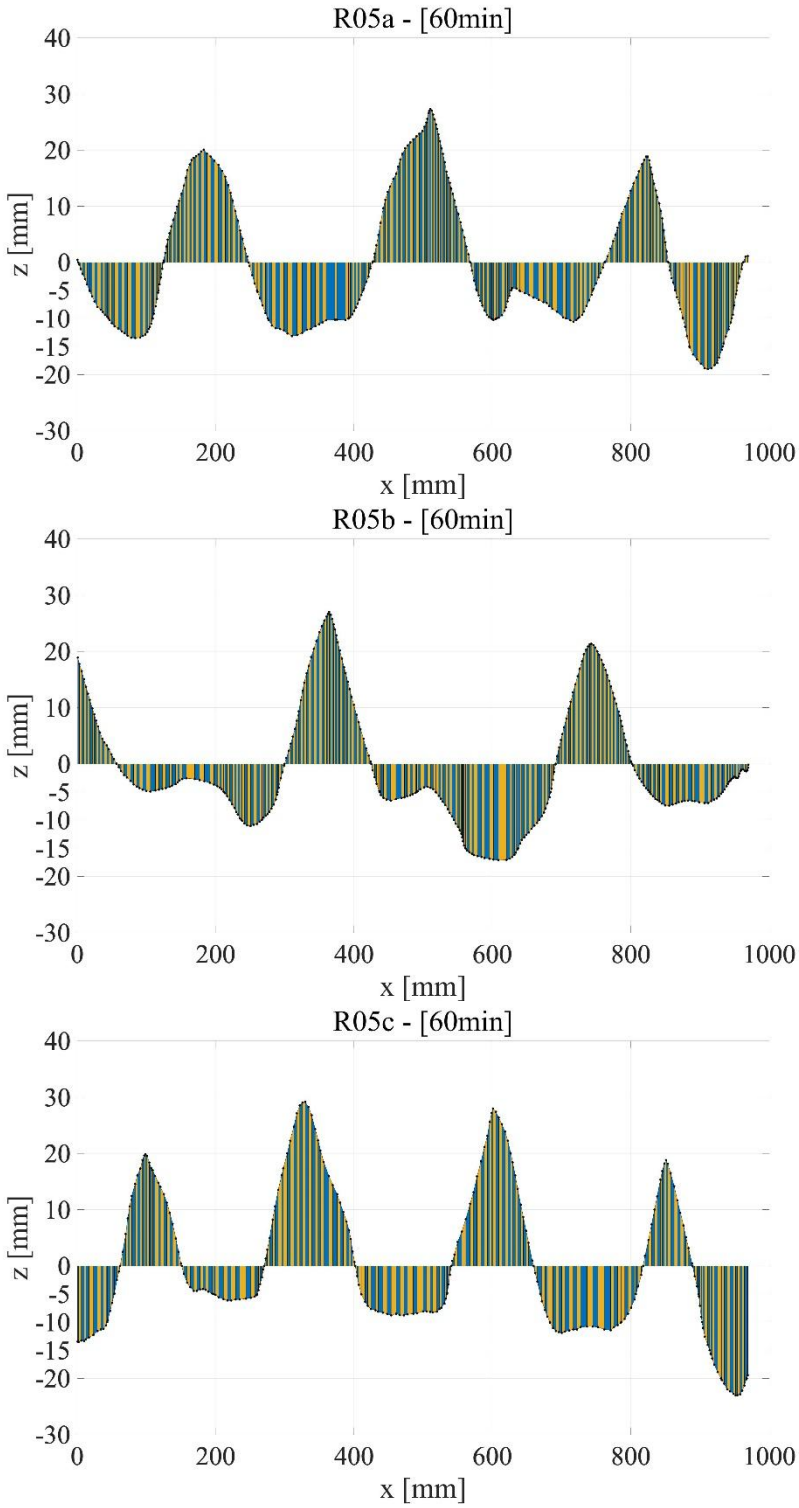

Figure 32. Numerical integration for cumulative area of formed ripples

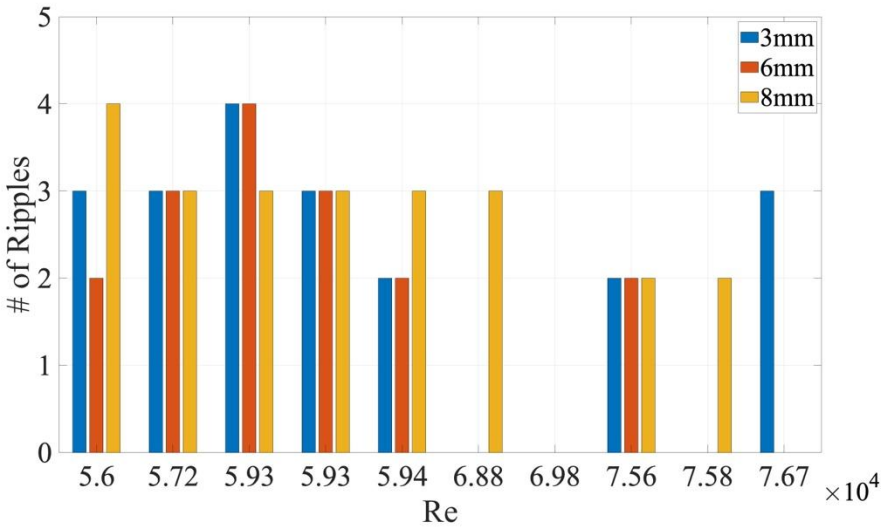

Figure 33. The number of the formed ripples for all cases

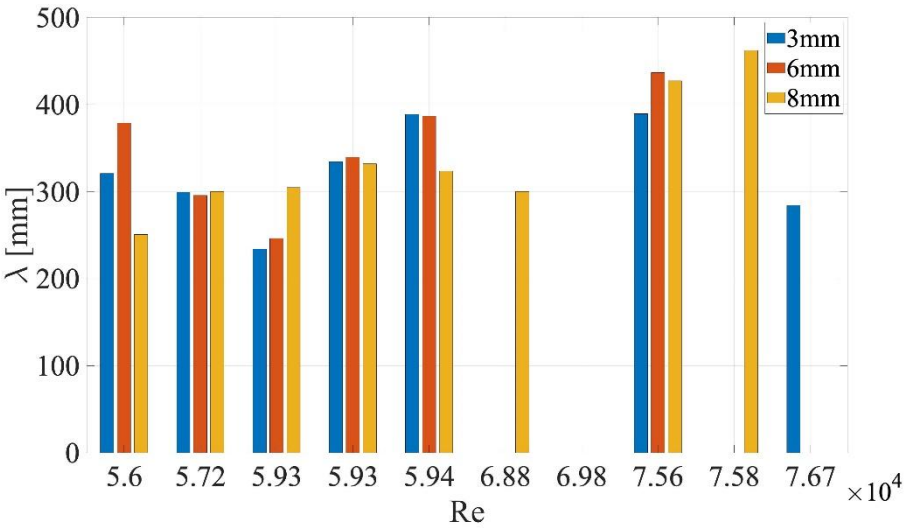

Figure 34. The ripple lengths (λ) for all cases

Understanding and predicting the length and height of ripple are important things that should be considered certainly by coastal engineers, for example, in the case to construct some coastal structures. So, some models for them have been suggested and developed consistently. Among a lot of models, a representative model was suggested by Nelson et al. (2013) and Soulsby & Whitehouse (2005) as follows:

$$\frac{\lambda}{U_0/\omega} = \frac{1}{a_1 + b_1 \frac{U_0}{\omega\ d}\left[1 - e^{-\left(c_1 \frac{U_0}{\omega\ d}\right)^{d_1}}\right]} \tag{7}$$

where U_0 is free stream velocity, and d is D_{50} representing grain size. Nelson et al. (2013) suggested $a_1 = 0.72$, $b_1 = 2 \times 10^{-3}$, $c_1 = 1.57 \times 10^{-4}$, and $d_1 = 1.15$, and Soulsby & Whitehouse (2005) used $a_1 = 1$, $b_1 = 1.87 \times 10^{-3}$, $c_1 = 2 \times 10^{-4}$, and $d_1 = 1.5$. Both models show the changing ripple length in the flow velocity, period, and grain size. Similarly, Nielsen (1981) introduced a model with the function of sediment mobility number (ψ). The mobility number is commonly used to represent the extent of forces on the sediment, indicating the forces by fluid and gravitation. It can be expressed as follows:

$$\psi = \frac{U_0^2}{(s-1)\ g\ d} \tag{8}$$

where s is the specific density of sediment and it is assumed to be around 2.65, and g is the gravitational acceleration. It denotes the ratio between the total disturbing force on a sand particle at the bed and stabilizing force of sediment (Nielsen, 1992). It is simple, and all necessary parameters to calculate it can be obtained clearly from the experiments without any preconditions or assumptions. With this number, the model for the length of ripples observed in the field is:

$$\frac{\lambda}{U_0/\omega} = \exp\left(\frac{693 - 0.37\ln^8\psi}{1000 + 0.75\ln^7\psi}\right) \quad (9)$$

and

$$\frac{\lambda}{U_0/\omega} = 2.2 - 0.345\ \psi^{0.34} \quad (10)$$

for laboratory conditions with oscillatory flows. So, the models indicated in Equations (9) and (10) were compared with the results of this experiment. The result can be found in Figure 35. It shows that the experimental results do not make much difference from the above model and data from literature, and besides, it is similar to the others. From the graph, both for field and laboratory are almost the same pattern by around $\psi = 10$. After that, the ripple length in the field decreases more rapidly than that in the laboratory. However, the data from this study situates on about $\psi = [8,\ 10]$ where there are both data for the fields and experiments. Therefore, it can say that this experimental study was conducted well and it represents a study for coastal sediment transport since the results belong to both data for the coastal fields and experiments. Moreover, according to Equation (10), the ripple length is directly proportional to both the flow velocity (U) and period (T), but there is an inverse relationship between the length and the grain size (d). In other words, the length will be larger as the velocity or period increases. Contrastively, if the grain size grows up, there will be a shorter ripple length and the stabilizing force due to gravitation will increase.

The following equation is a model for ripple height suggested by Nielsen (1981) for the ripples generated in the laboratory with the mobility number.

$$\frac{\eta}{U_0/\omega} = 0.275 - 0.022\sqrt{\psi} \quad (11)$$

The model for the fields with $\psi > 10$ is as follows:

$$\frac{\eta}{U_0/\omega} = 21\ \psi^{-1.85} \tag{12}$$

The comparison with this study is described in Figure 36. Although this study was conducted with coarse sand and relatively gradual flow, and the mobility numbers are within a range of $[8,\ 10]$, the results are closer to the model for the field than for the laboratory. However, they are also close to the experimental data from the literature. The difference between ripple length and height is that the field model for ripple height has a linear correlation with the mobility number.

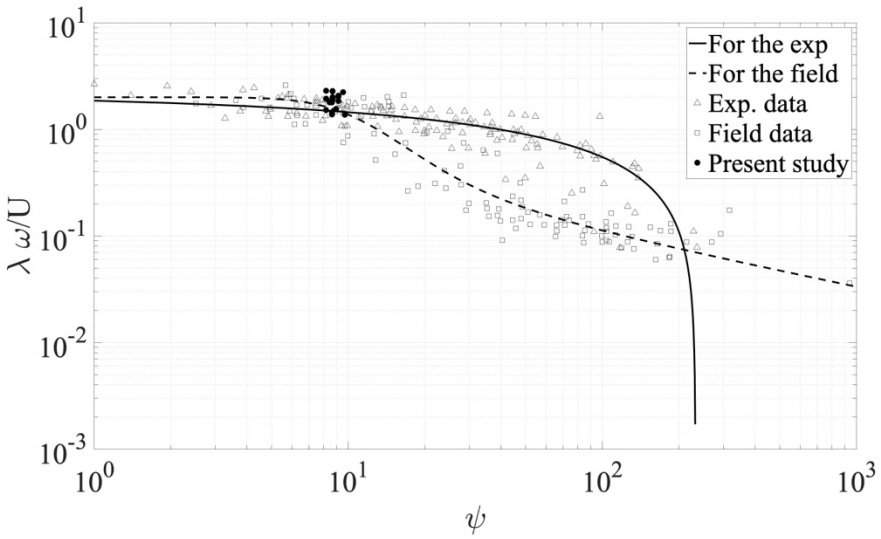

Figure 35. Comparison between models and data for ripple length (Nielsen, 1981)

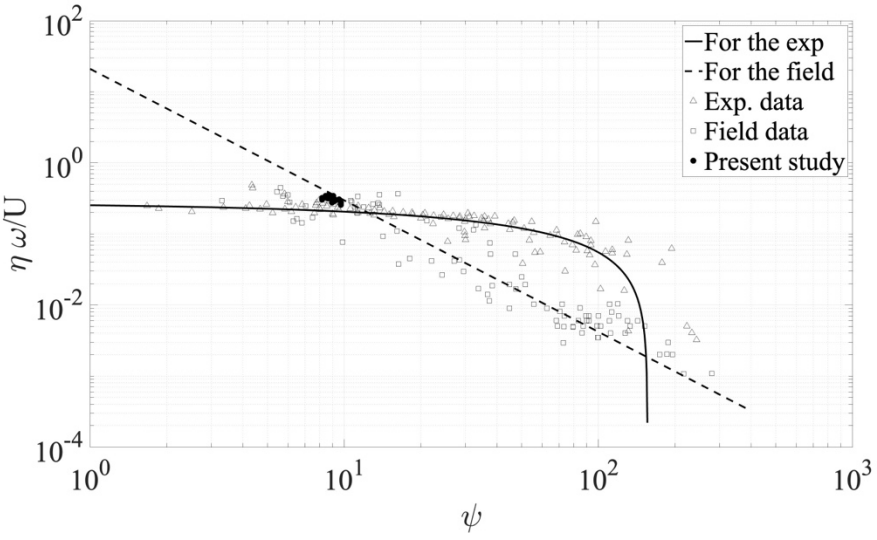

Figure 36. Comparison between models and data for ripple height (Nielsen, 1981)

With the laboratory model indicated in Equation (11), the height has a nonlinear relationship with the flow velocity, and it and the grain size are nonlinear inverse proportion. However, like the ripple length, the flow period is in direct proportion to the height.

Next, analyzing the interval length (σ) and the two-dimensional ripple area is important because the depth of the ripple should have an effect on the release of plastic particles. So, those from 20 minutes to 60 minutes after the start of the experiment were obtained. At that time, the bedform in $y-$direction was ignored. Figure 37 and Figure 38 show the interval length between the ripples at the different depths. Figure 39 and Figure 40 are plotted to describe the cumulative area. Both length and area, of course, are much smaller as the depth increases, and their values get larger in general with the higher Reynolds number. The large interval length is the same as the large ripple length, λ. So, as stated above, the relation between the Reynold number and the interval length would be the same relation between the Reynolds number and the ripple length. Also, the large area might mean a long ripple length or a big ripple depth. Therefore, since a higher Reynolds number makes the larger interval length and the ripple reach deeper over time, it will result in the release of plastics at a deeper depth.

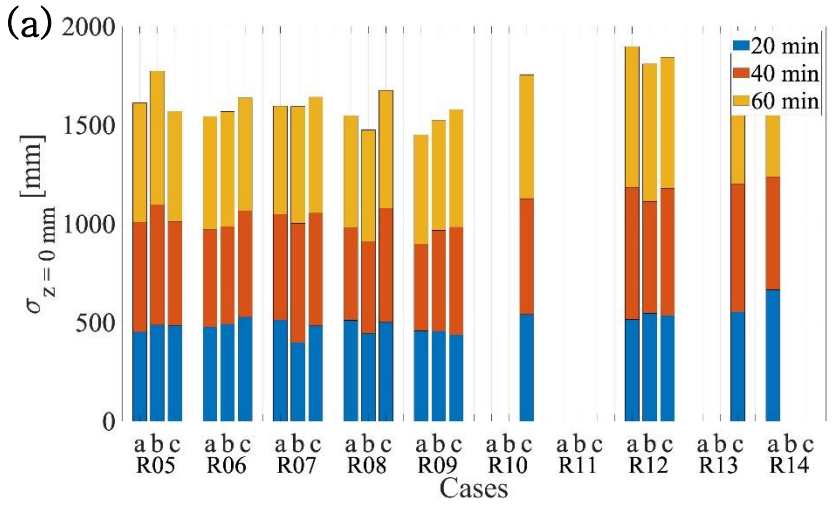
(a)
2000
1500
1000
500
0
σ z = 0 mm [mm]
20 min
40 min
60 min
a b c
R05
a b c
R06
a b c
R07
a b c
R08
a b c
R09
a b c
R10
a b c
R11
a b c
R12
a b c
R13
a b c
R14
Cases

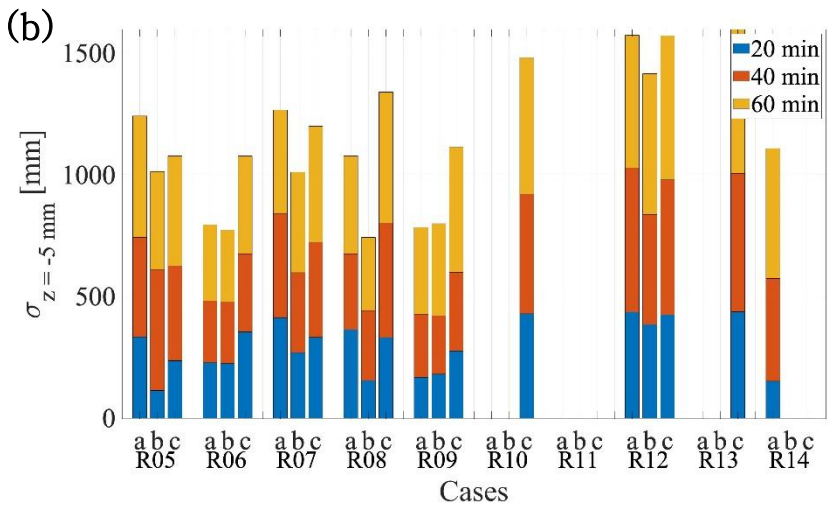
(b)
1500
1000
500
0
σ z = -5 mm [mm]
20 min
40 min
60 min
a b c
R05
a b c
R06
a b c
R07
a b c
R08
a b c
R09
a b c
R10
a b c
R11
a b c
R12
a b c
R13
a b c
R14
Cases

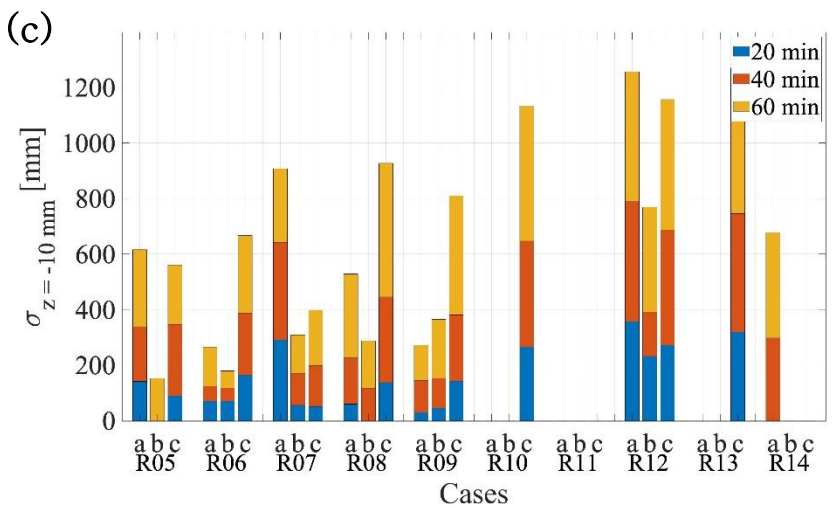
(c)
1200
1000
800
600
400
200
0
σ z = -10 mm [mm]
20 min
40 min
60 min
a b c
R05
a b c
R06
a b c
R07
a b c
R08
a b c
R09
a b c
R10
a b c
R11
a b c
R12
a b c
R13
a b c
R14
Cases

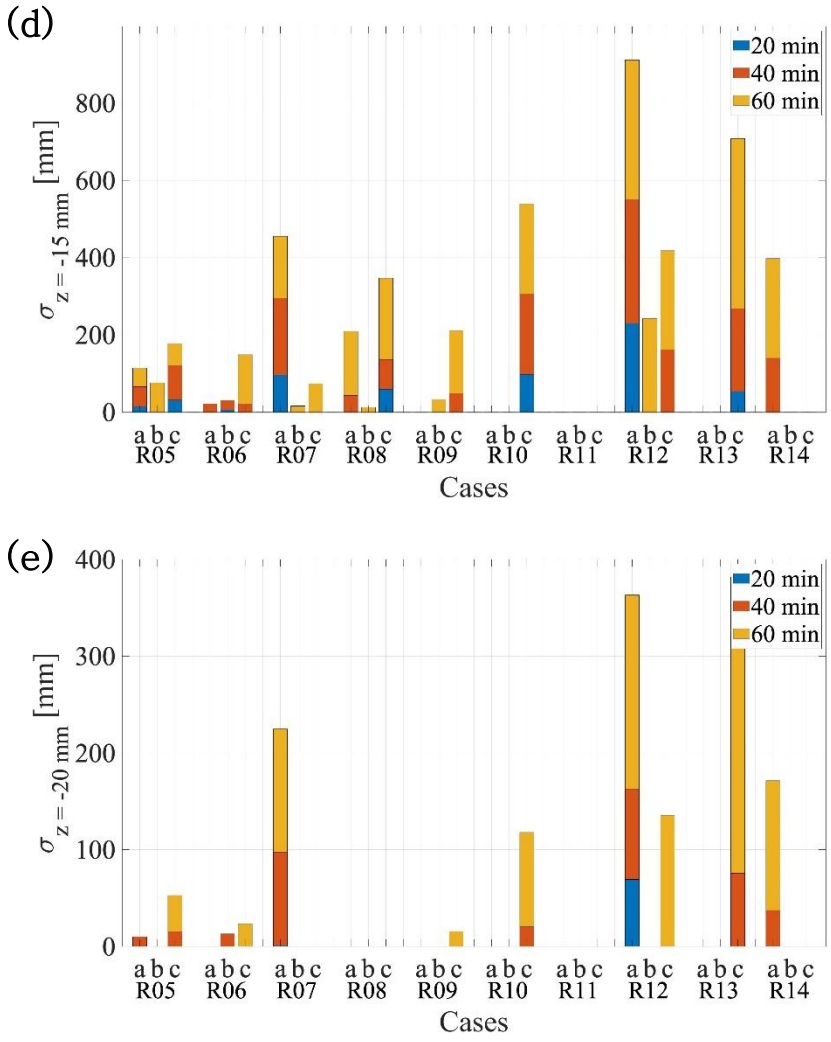

Figure 37. Interval length between the ripples for all cases ((a): On the surface; (b): On $z = -5\ mm$; (c): On $z = -10mm$; (d): $z = -15mm$; (e): $z = -20mm$)

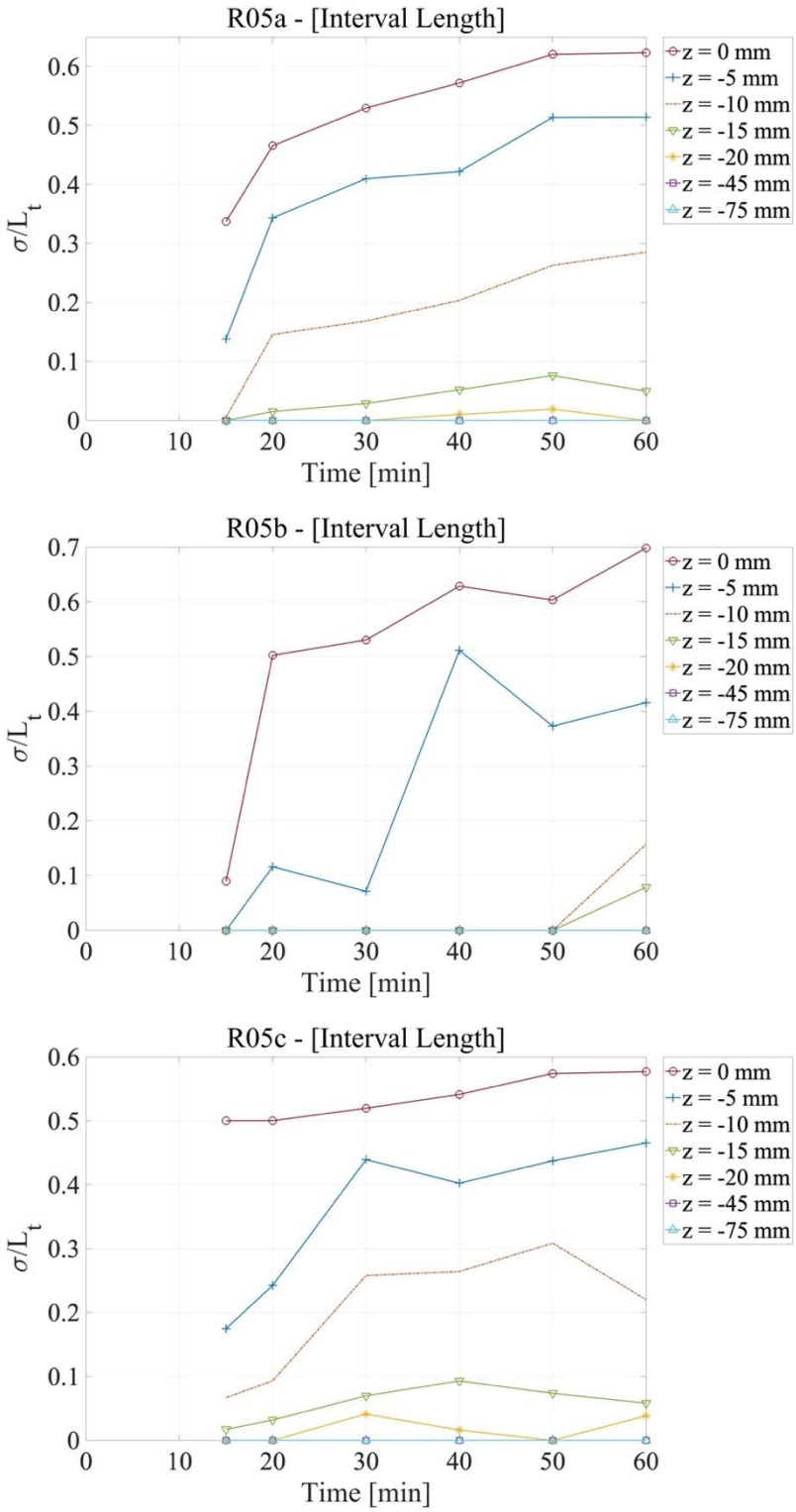

Figure 38. Interval length in cases of R05a, R05b, and R05c

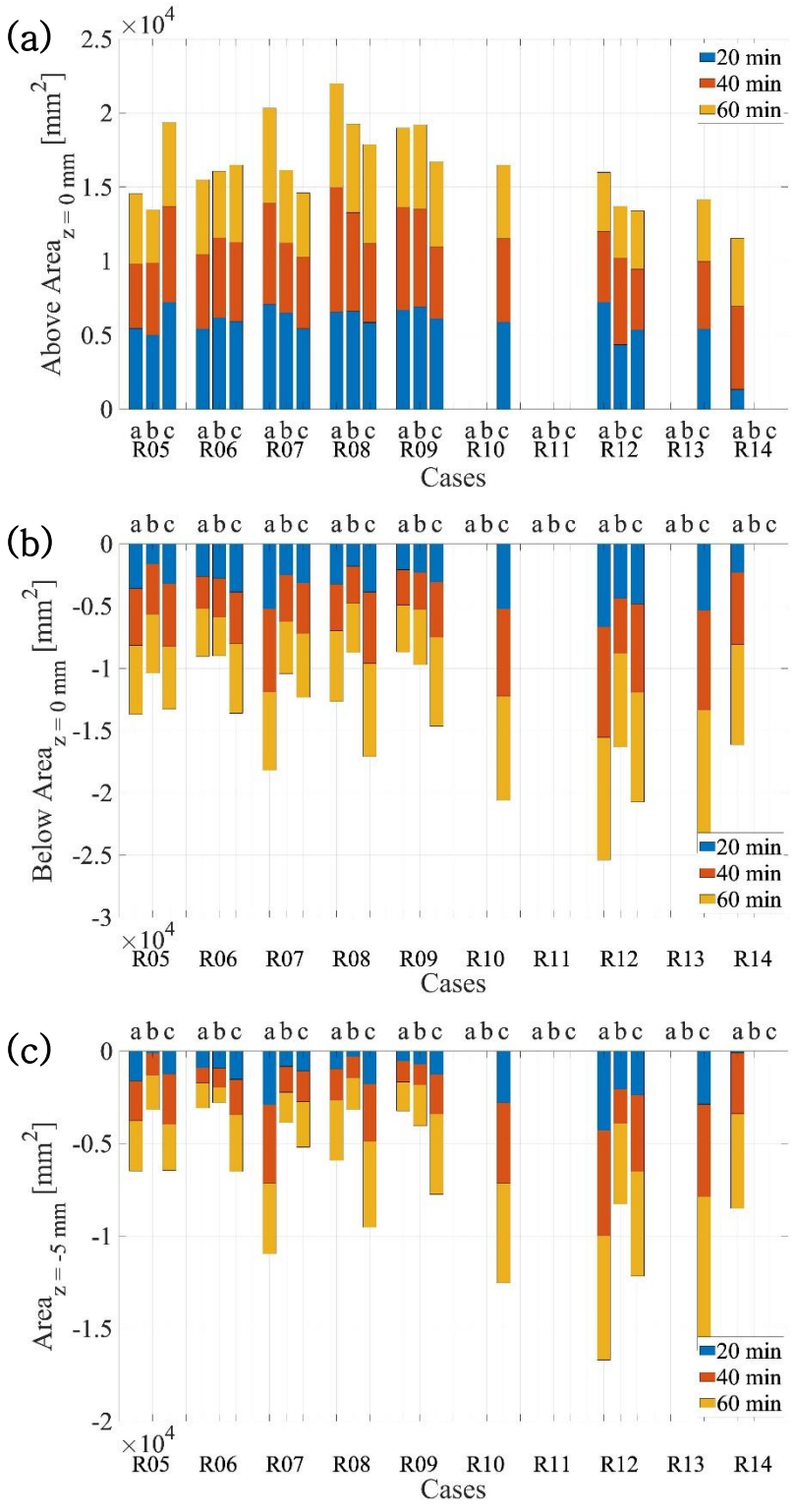
(a)
×10^4
2.5
2
1.5
1
0.5
0
Above Area z = 0 mm [mm^2]
20 min
40 min
60 min
a b c
R05
R06
R07
R08
R09
R10
R11
R12
R13
R14
Cases
(b)
0
-0.5
-1
-1.5
-2
-2.5
-3
Below Area z = 0 mm [mm^2]
(c)
Area z = -5 mm [mm^2]

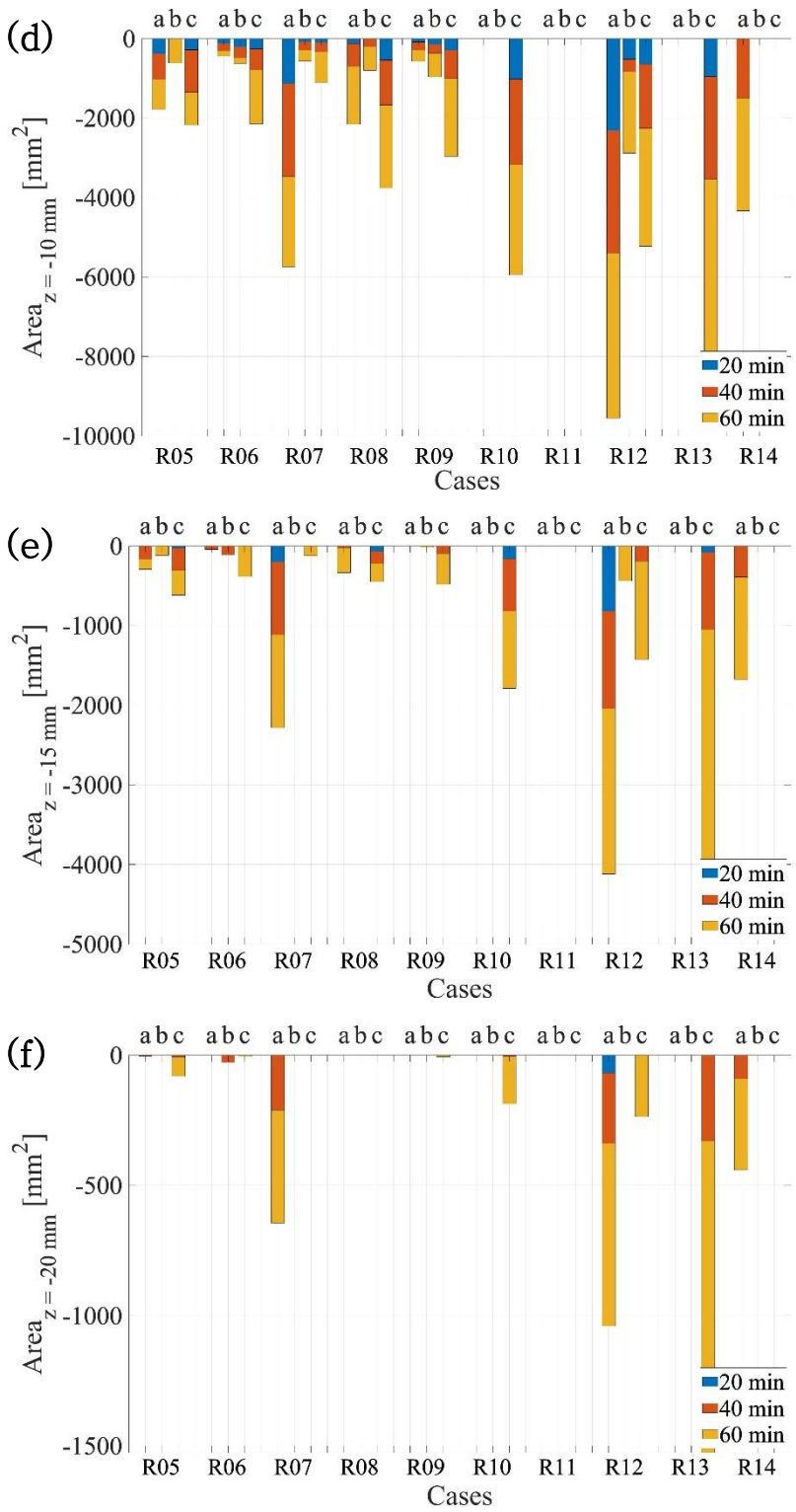

Figure 39. Cumulative ripple area for all cases ((a): Above surface; (b): Below surface; (c): Below z=-5 mm; (d): Below z=-10 mm; (e): Below z=-15 mm; (f): Below z=-20 mm)

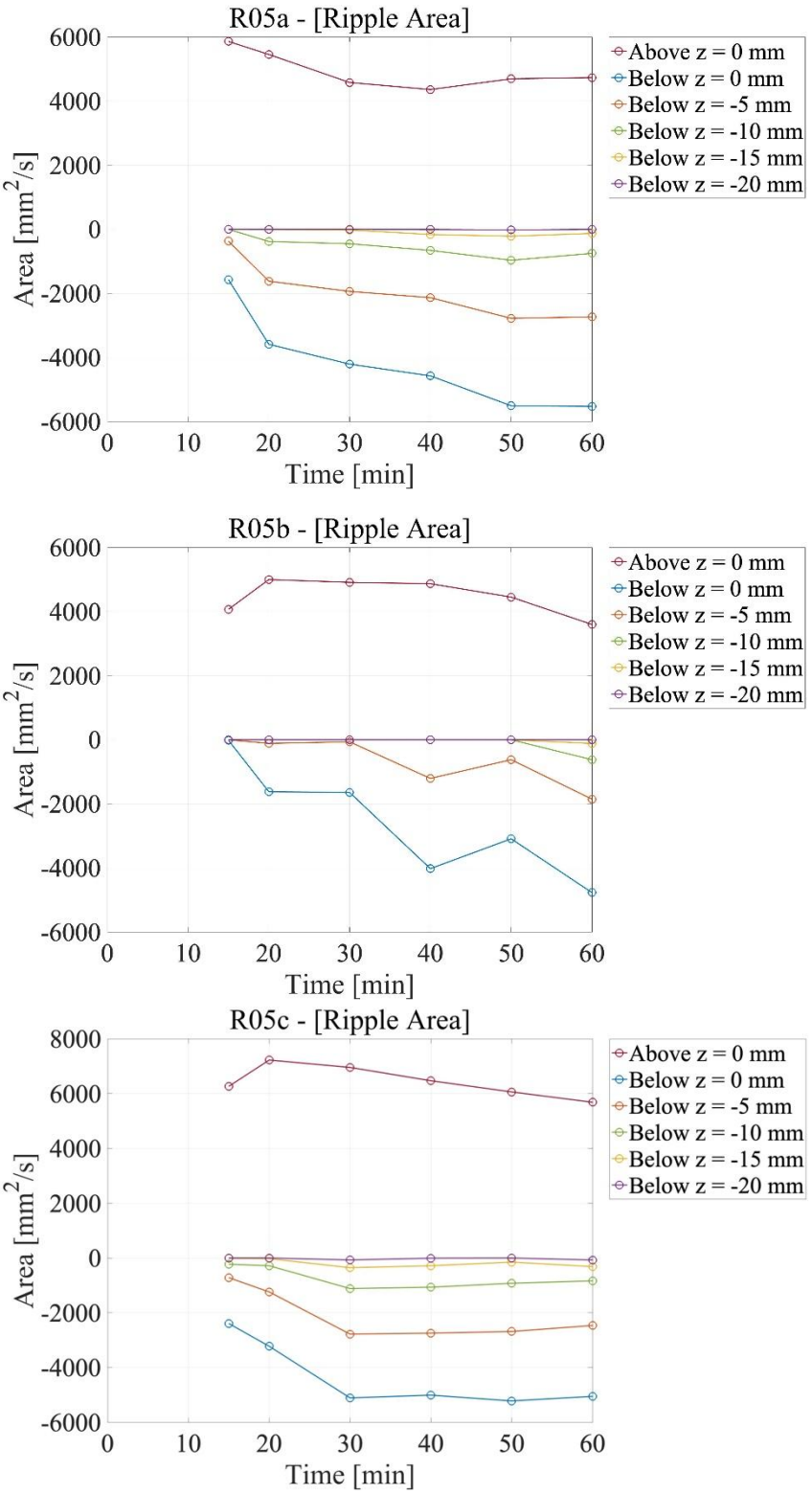

Figure 40. Cumulative ripple area in cases of R05a, R05b, and R05c

4.1. Release of plastic particles

From the above, the critical Reynolds number for ripple formation was found. However, the Reynolds number is for considering the properties of the flow only, without that of the sediment. Some numbers can consider both. One of them is the mobility number (ψ) that has already been mentioned above, indicated in Equation (8). This experimental study was conducted with the mobility number of about from 3.7 to 9.7. As the release of plastics does not occur within no bedform change, the threshold of the mobility number can be defined from how much the plastic particles were discharged from sediment to fluids over the number. With this method, the relation between the Reynolds number and the number of released plastics is plotted in Figure 41. The defined threshold Reynold number can be found again. Figure 42 is for the mobility number. The threshold of that for sediment transport is about $\psi \approx 7.25$. Moreover, Equations (4) and (8) have the square of the flow velocity (U^2) in their numerators, that is, both of Reynolds number and the mobility are proportional to it. Similar to the mobility number, the Shields parameter is a parameter representing the extent of movement of sand grain caused by fluid force with the properties of the sediment. It can be expressed as follows (Nielsen, 1992; Shields, 1936a, 1936b):

$$\theta = \frac{\tau}{\rho\ (s-1)\ g\ d} = \frac{u_*^2}{(s-1)\ g\ d} \tag{13}$$

where ρ is the density of water, τ is the bed shear stress, and u_* is the shear stress velocity. The shear stress can be obtained in steady flow as follows:

$$\tau = \rho\ g\ D\ I \tag{14}$$

where D is the flow depth, and I is the hydraulic gradient. Also, the shear stress

velocity can be expressed as:

$$u_* = \sqrt{\tau/\rho} \tag{15}$$

With regard to the wave motion, the Shields parameter is defined as:

$$\theta = \frac{\tilde{\tau}}{\rho\ (s-1)\ g\ d} = \frac{1/2\ f_w\ (A\ \omega)^2}{(s-1)\ g\ d} = \frac{1}{2}\ f_w\ \psi \tag{16}$$

where $\tilde{\tau}$ is the peak bed shear stress, and f_w is friction factor. The reason why Shields parameter was not considered in this study is the shear stress in terms of the friction factor. To calculate it, many researchers have suggested and tried. There are Bagnold (1946), Carstens et al. (1969), Jonsson (1966, 1980), Kajiura (1968), Kamphuis (1975), Simons et al. (1989), Sleath (1984, 1985), Swart (1974), van Rijn (1984), etc. as a representation of the research with different flow conditions and bed conditions. However, the method to calculate the friction factor is using the empirical formula suggested in the above literature, until today. That is a reason why the mobility number was used instead of the Shields parameter in this study. Thus, it is to reduce the ambiguity, and the mobility number is enough to express the extent of sediment movement in fluids. Nevertheless, since the Shields parameter is one of the popular and important dimensionless numbers in sediment transport, it would be expressed in the square of the flow velocity according to Equation (16). Also, Jonsson (1966) presented that the friction factor is supposed to be a function of the Reynolds number, $A^2\omega/\nu$, and the relative bed roughness, r/A.

$$f_w = f_w\left(\frac{A^2\omega}{\nu}, \frac{r}{A}\right) \tag{17}$$

where r is the bed roughness (Nielsen, 1992). It is proportional to the flow velocity, $U = A\ \omega$. So, instead of expressing with the friction factor and the Shields parameter, the flow velocity and the square of it can be used as shown in Figure 43 and Figure

44. As a result, the thresholds of U and U^2 for ripple formation or release of plastics are almost $0.319\ m/s$ and $0.102\ m^2/s^2$, respectively.

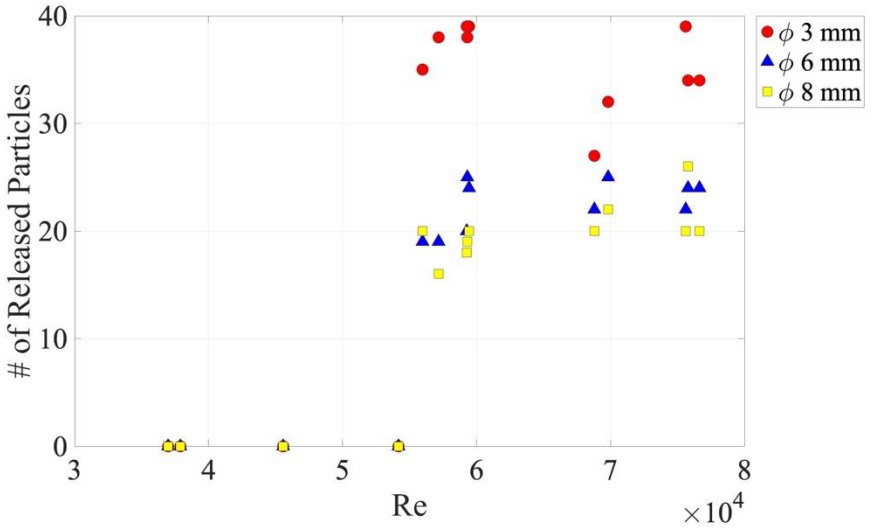

Figure 41. Number of released plastic particles with Reynolds number

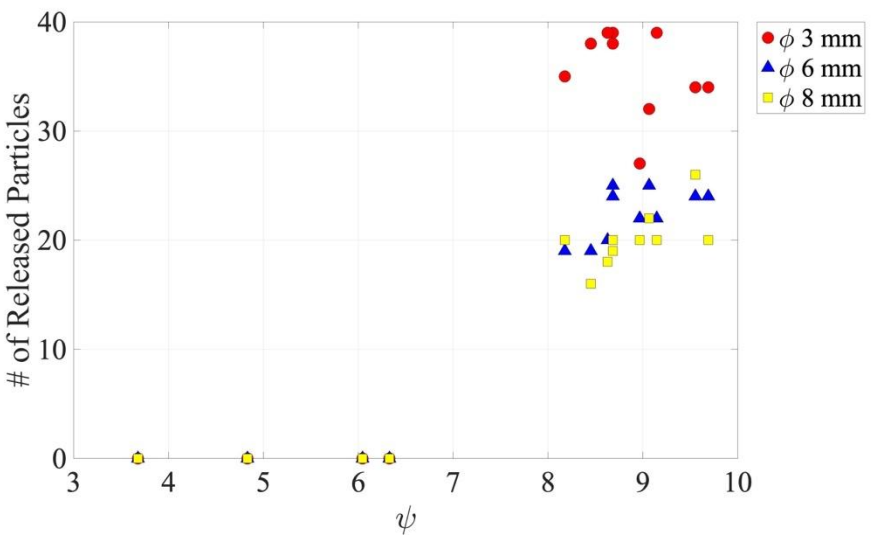

Figure 42. Number of released plastic particles with mobility number

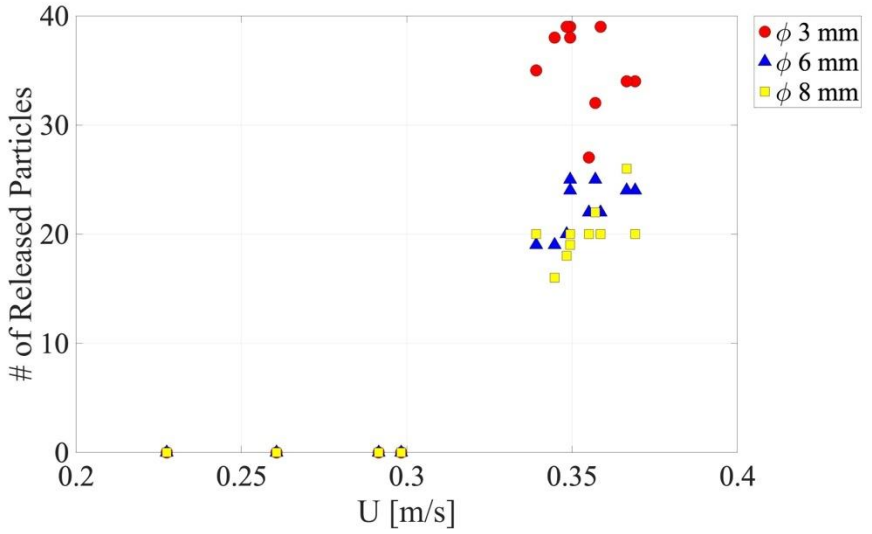

Figure 43. Number of released plastic particles with flow velocity

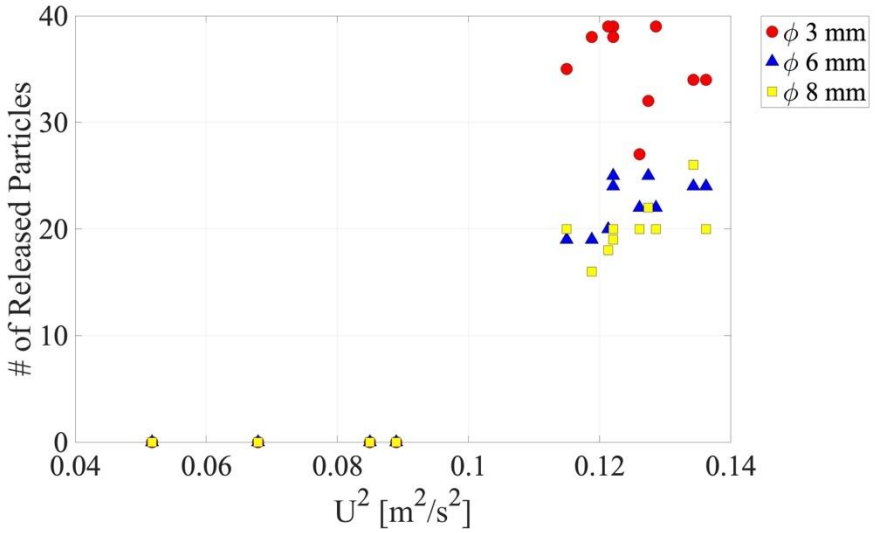

Figure 44. Number of released plastic particles with the square of flow velocity

There is another parameter that includes the flow velocity and the properties of experimental sediments. It is called the 'densimetric Froude number' or the 'particle Froude number'. It consists of the flow velocity, gravitational acceleration, and sand grain size considering specific gravity. It can be expressed as follows (Aguirre-Pe et al., 2003; Ali & Dey, 2017; García, 2008):

$$Fr = \frac{U}{\sqrt{g'\ \mathrm{d}}} = \frac{U}{\sqrt{g\ ((\rho_s - \rho)/\rho)\ d}} = \frac{U}{\sqrt{g\ (s-1)\ d}} \tag{18}$$

which is proportional to the flow velocity. Then, using the parameter, the threshold can be defined as about 2.69, according to Figure 45.

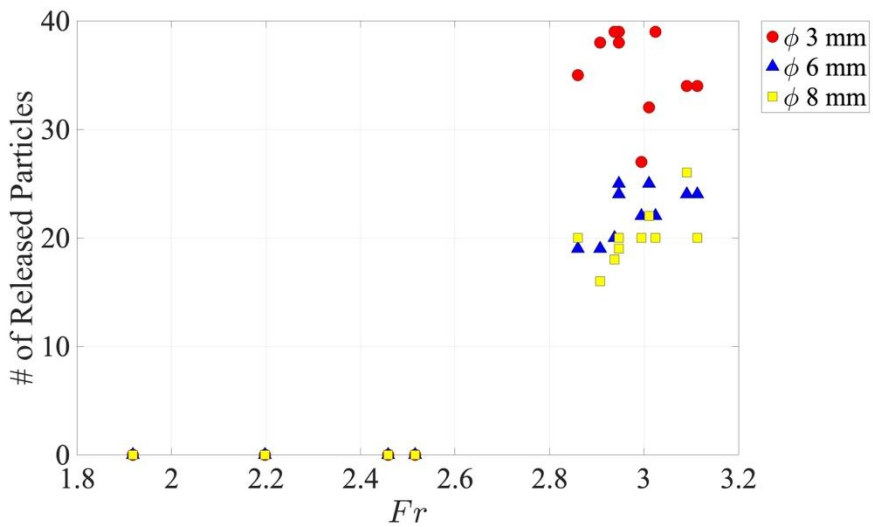

Figure 45. Number of released plastic particles with the Froude number

Moreover, the threshold of U is supported by the criterion of erosion and deposition suggested by Hjulstrom (1935). It shows the relation between the mean

velocity and the sand grain size, instead of the bottom velocity, because measuring it is harder than mean velocity. The criterion is shown in Figure 46. According to the graph, transportation of sediment occurs from $0.058\ m/s$ to $0.26\ m/s$, and the sand bed is eroded from $0.26\ m/s$ with a sediment grain size of $D_{50} = 868.6\ \mu m$. It is also based on the critical velocity introduced in Vanoni (1977). Figure 47 shows critical velocity with the grain size. From that, At the grain size, the mean critical velocity is found to be about $0.27\ m/s$, and the upper limit is almost $0.33\ m/s$.

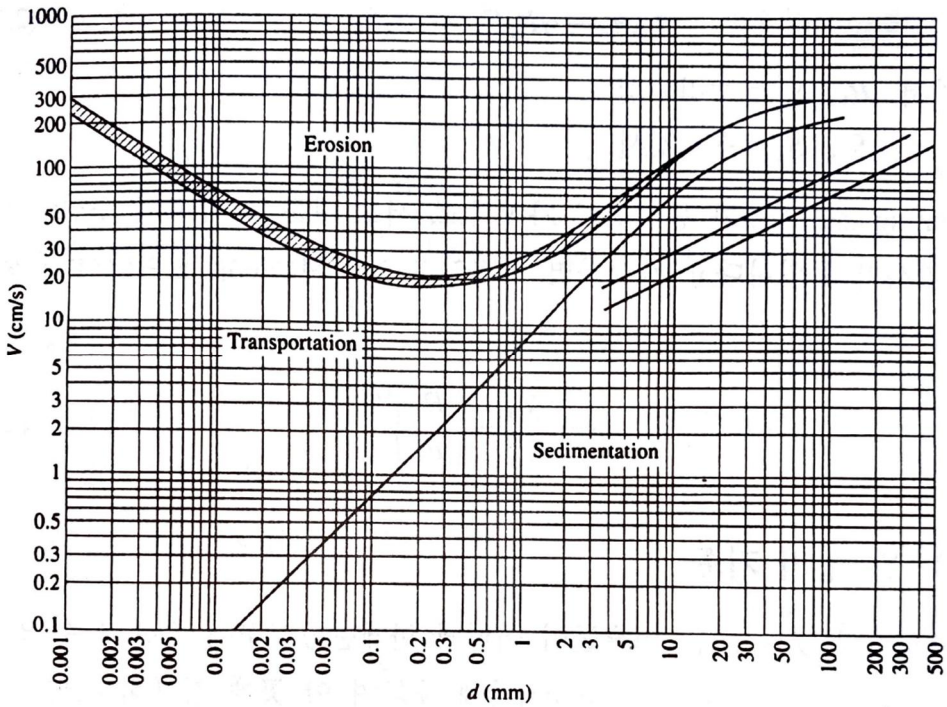

Figure 46. Criterion of erosion and deposition with mean velocity and grain size (*Figure 2.4* in Yang et al. (2007))

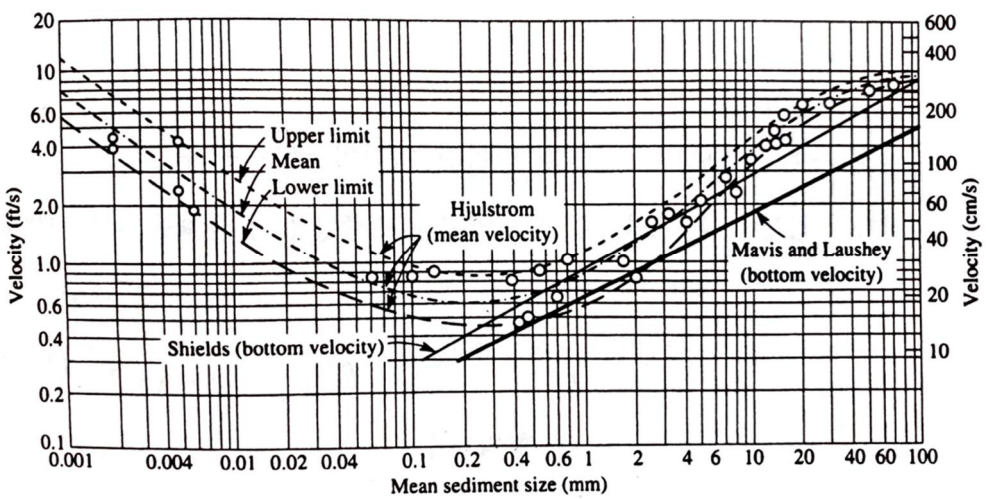

Figure 47. Critical velocity with grain size (*Figure 2.5* in Yang et al. (2007))

According to Figure 41 to Figure 44, the effect of the size of plastics on the release can be easily seen. As the plastic gets smaller, the release occurs more actively. The smallest particles with a diameter of 3 mm show the largest number of releases of them. As shown in Figure 48, the behavior of the plastics subject to their size can be found. Especially, the number of the released particles with ϕ 3 mm which fit the definition of micro-plastics is much larger than that with ϕ 6 mm and ϕ 8 mm within the category of meso-plastics. There is a clear difference between the two groups. The definition of plastic wastes in the sea was suggested by the National Oceanic and Atmospheric Administration (NOAA) as found in Figure 49. As a result, it implies that the plastics in the environment can be released from sediments to fluids by their size. Furthermore, the definition may correspond to the hydraulic perspective, although it was defined with ecological impacts of plastics such as entanglement and ingestion.

In the above five figures(Figure 41~Figure 45), the numbers of released plastics having ϕ 6 mm and ϕ 8 mm increase slightly with the growth of Re, ψ, Fr, U, and U^2. However, any pattern cannot be found in the plastics with ϕ 3 mm, because they are much influenced by the flow.

The relation between the ripple size and the release of plastics was mentioned in *Section 4.1*. shortly. The relation is illustrated in Figure 50. The ζ^- and ζ^+ were notated in Figure 26. The sum of them is the height of the ripple (η or H). They are proportional to the Reynolds number indicating the extent of the flow, and the large ζ^- means the formed ripple reached by the deeper depth. Also, the effect of the plastic size can be shown as well. Like from Figure 41 to Figure 44, the larger $\zeta^- + \zeta^+$ results in more release of the plastics as shown in (c) in Figure 50.

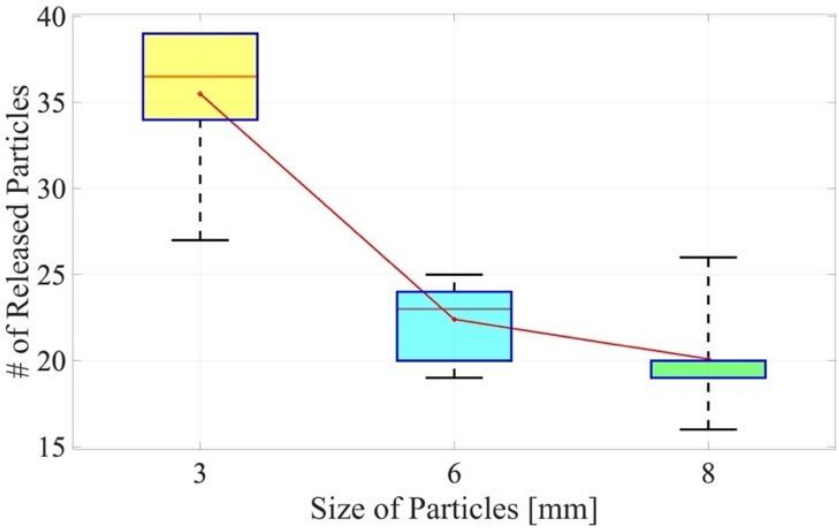

Figure 48. The number of released particles with their sizes

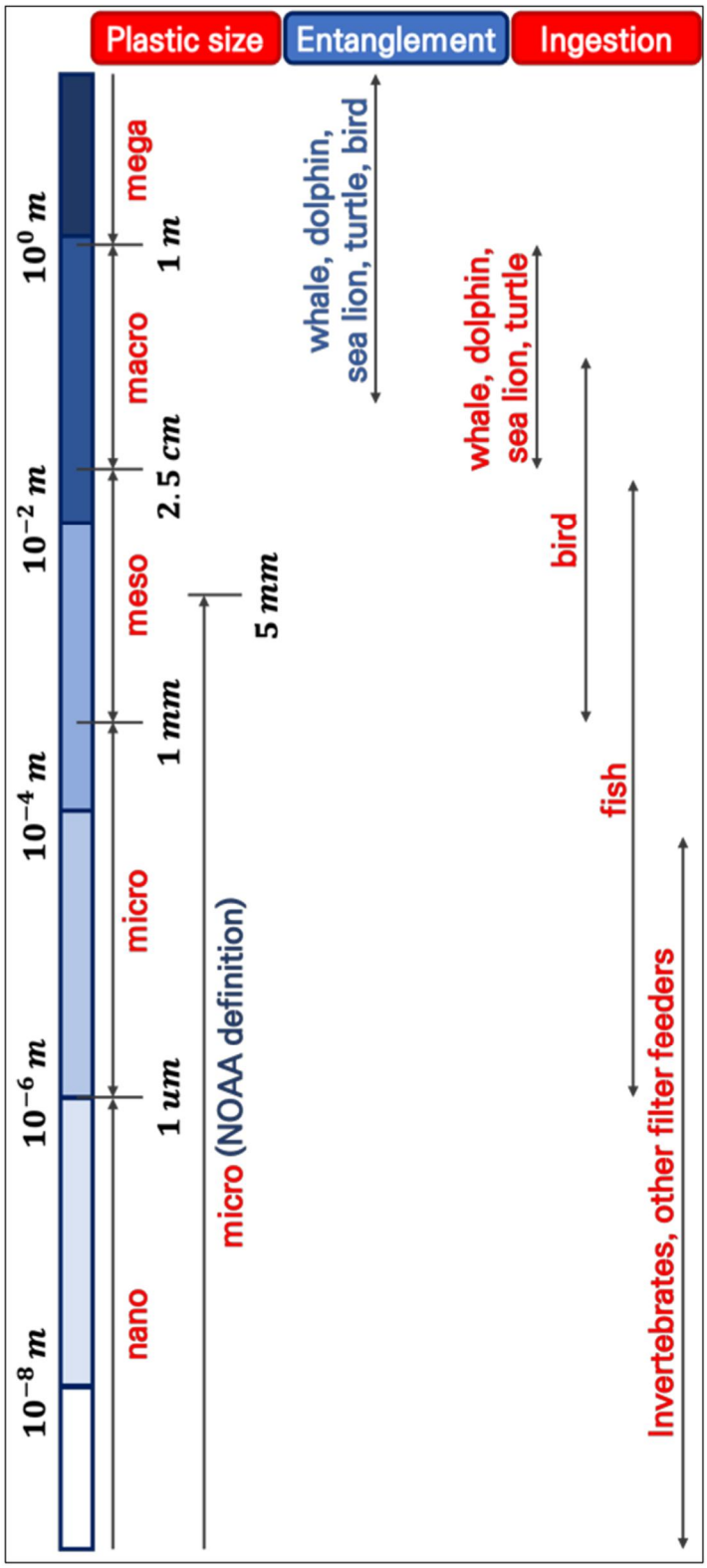

Figure 49. Definition of plastics in the ocean by size (GESAMP, 2015)

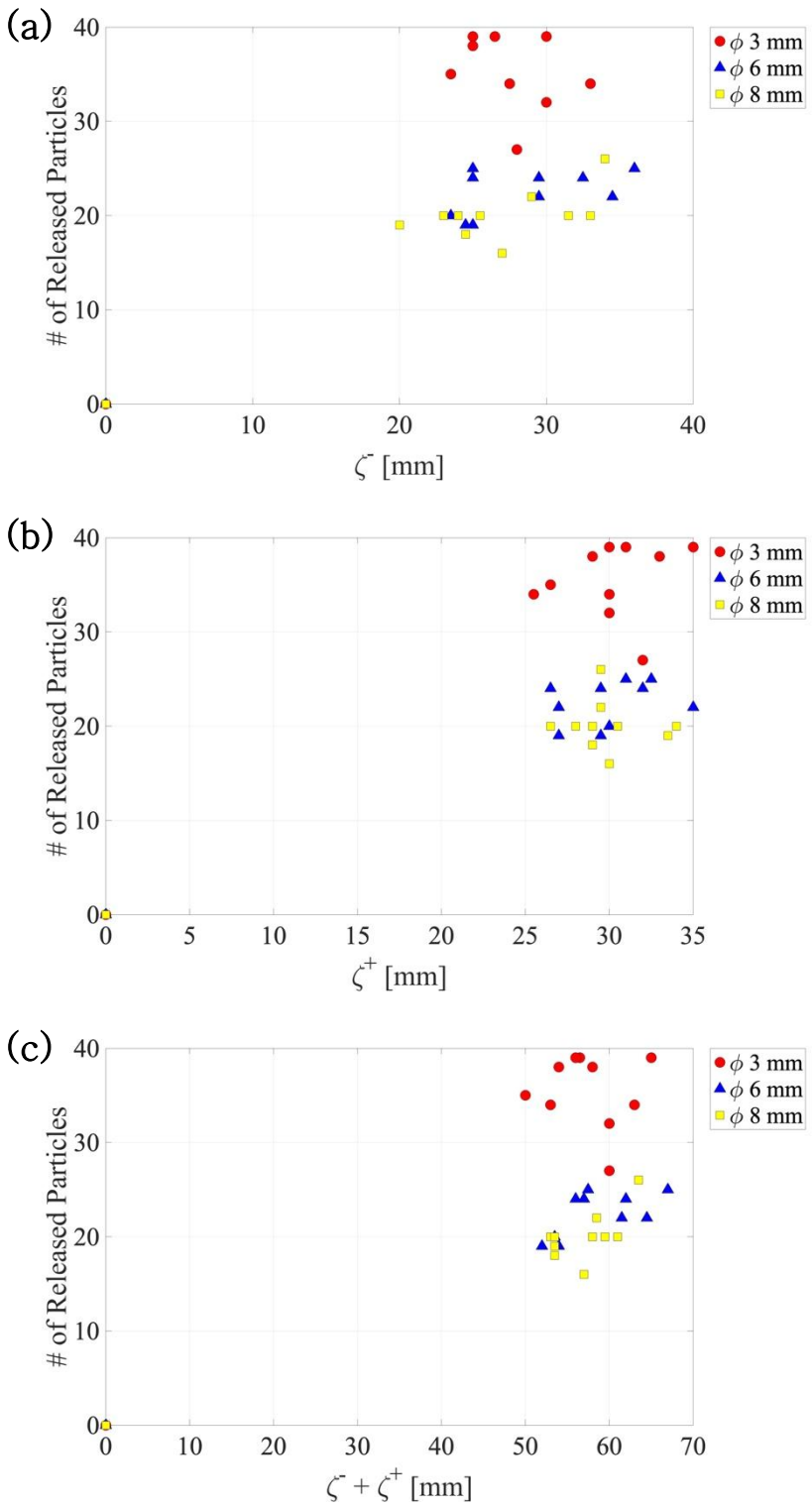

Figure 50. Relation between the ripple size and the release ((a): with ζ^-; (b): with ζ^+; (c): with $H = \zeta^- + \zeta^+$)

Chapter 5. Conclusion

Although plastic pollution has been emerging as a serious marine problem, too much plastic waste is still being dumped. Some of that flows into the ocean and coastal environments. As the waste interacts with a lot of variables therein, they experience physical and chemical reactions such as fragmentation. Also, they spend a long time in the coastal area. Therefore, this study was planned and conducted to understand the behavior of the plastic plastics in coastal sediment and to find out the variables that affect the release of the plastics from the sediment to fluid throughout experiments.

For the experiments, an oscillating water tunnel was designed and constructed to generate oscillatory flows and sediment transport at Seoul National University. The generated flows were analyzed to obtain the accurate flow velocity and period by utilizing a PIV system. Thus, the different 14 flow conditions were planned for the experiment to $Re \sim [3.70 \times 10^4,\ 7.67 \times 10^4]$. After that, the sediment basin in the oscillating water tunnel was filled with standard sand having a grain size of $D_{50} = 868.6\ \mu m$. The spherical plastic particles were used in this study, and they have different sizes of $\phi\ 3\ mm$, $\phi\ 6\ mm$, and $\phi\ 8\ mm$. Thus, 42 experimental cases were made by combining the 14 flow conditions and the 3 plastic sizes. Each case was conducted for an hour.

As a result, the ripples were not formed in 4 flow conditions that do not have enough disturbing force compared with stabilizing force. In the cases, the releases did not occur. The release of the plastics from sediments to fluids has a prior

condition. To occur that, the bedform should be changed at first, and the surface of the plastic in the sediment needs to appear on the fluid. In other words, sediment transport is the most important to the release. It might verify the research by Turner et al. (2021) which said that, if the plastics in the ocean environment are buried for some reason, they will spend several years in dunes until generating big bedform change due to some events such as tsunami. So, the higher Reynolds number flow can lead to a higher probability to release to fluids, because the ripple can reach deeper. The thresholds of Re, ψ, Fr, U, and U^2 for bedform change and release of plastics were defined to $Re_c \sim 5.5 \times 10^4$, $\psi_c \sim 7.25$, $Fr \sim 2.69$, $U_c \sim 0.319\ m/s$, and $U_c^2 \sim 0.102\ m^2/s^2$, respectively.

The comprehensive results are represented in Table 3. It shows the number of the released plastics for all cases by their occurrence probability. The ripple depths are no more than about $4\ cm$ in the condition of $Re \sim [5.50 \times 10^4,\ 7.67 \times 10^4]$. So, the probability for below $z = 0.04\ m$ is zero. Also, the larger Reynolds number of the flow results in more release, and the effect of the plastic size can be found. The small size of the plastics can be released more easily than larger plastics. The reason is the smaller particles can be much more influenced by the flow than the larger ones.

Before the experiments, the sediment basin in the oscillating water tunnel was divided into 4 sections. Each section was filled with plastic particles having different colors to investigate the transport of the plastic in the sediments. After the experiment, the plastics remaining in the sediments were sorted by the section of the basin. As a result, the plastics cannot move inside sediments from one section to another section.

This study can be developed by using a broader range of Reynolds numbers. Also, it can be conducted with sediments having different grain sizes and the other properties of plastic particles such as shapes and sizes. Then, the reliability of the study will be improved.

Table 3. The occurrence probability of the release of plastic particles from sediments to fluids

Depth in Sediment Basin	Size of Particles	Reynolds number													
		R1	R2	R3	R4	R5	R6	R7	R8	R9	R10	R11	R12	R13	R14
z = 0 m	3	0	0	0	0	1	1	1	1	1	1	1	1	1	1
	6	0	0	0	0	0.95	0.95	1	1	1	1	1	1	1	1
	8	0	0	0	0	1	0.8	0.9	0.95	1	1	1	1	1	1
z = −0.02 m	3	0	0	0	0	0.21	0.25	0.26	0.25	0.26	0.1	0.17	0.26	0.19	0.19
	6	0	0	0	0	0	0	0	0.07	0.06	0.03	0.07	0.03	0.06	0.06
	8	0	0	0	0	0	0	0	0	0	0	0.03	0	0.08	0
z = −0.045 m	3	0	0	0	0	0	0	0	0	0	0	0	0	0	0
	6	0	0	0	0	0	0	0	0	0	0	0	0	0	0
	8	0	0	0	0	0	0	0	0	0	0	0	0	0	0
z = −0.075 m	3	0	0	0	0	0	0	0	0	0	0	0	0	0	0
	6	0	0	0	0	0	0	0	0	0	0	0	0	0	0
	8	0	0	0	0	0	0	0	0	0	0	0	0	0	0

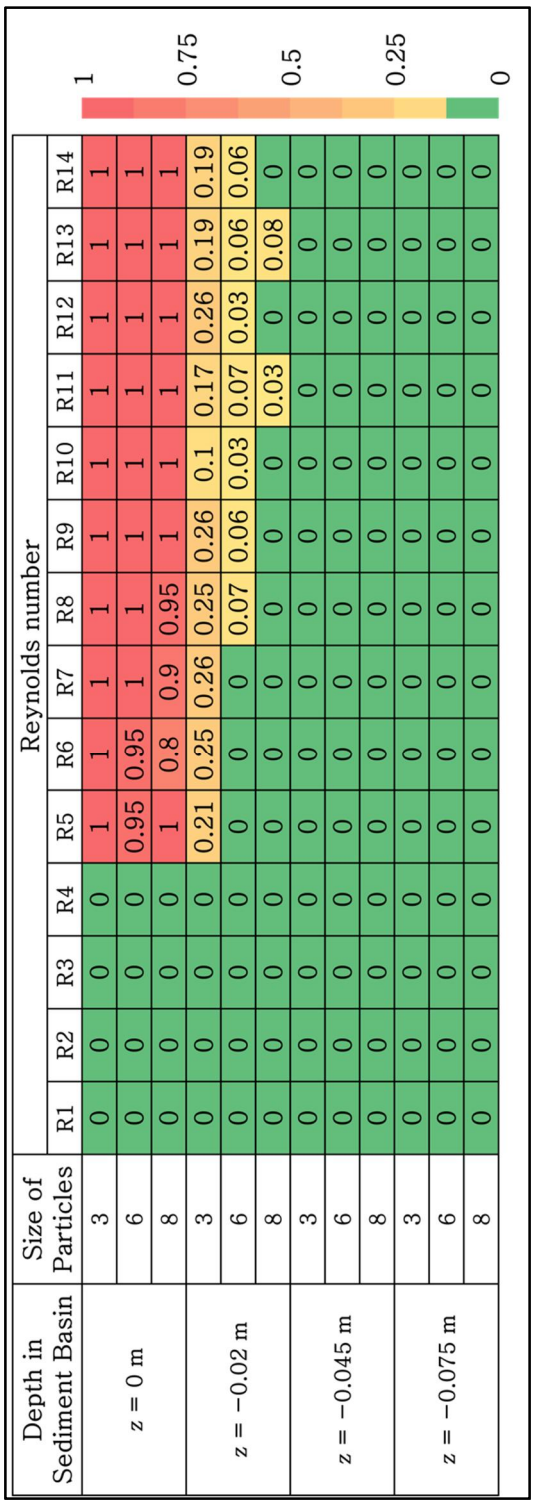

Bibliography

Aguirre-Pe, J., Olivero, M. a L., & Moncada, A. T. (2003). Particle Densimetric Froude Number for Estimating Sediment Transport. *Journal of Hydraulic Engineering*, *129*(6).

Ali, S. Z., & Dey, S. (2017). Origin of the scaling laws of sediment transport. *Proceedings of the Royal Society A: Mathematical, Physical and Engineering Sciences*, *473*(2197).

Bagnold, R. A. (1946). Motion of waves in shallow water: Interaction between waves and sand bottoms. *Proceedings of the Royal Society. Series A. Mathematical, Physical, and Engineering Sciences*, *187*(1008), 1–18.

Barnes, D. K. A. (2005). Remote islands reveal rapid rise of southern hemisphere sea debris. *TheScientificWorldJOURNAL*, *5*, 915–921.

Barnes, D. K. A., Galgani, F., Thompson, R. C., & Barlaz, M. (2009). Accumulation and fragmentation of plastic debris in global environments. *Philosophical Transactions of the Royal Society B: Biological Sciences*, *364*(1526), 1985–1998.

Bird, J. O., & Chivers, P. J. (1993). Simple harmonic motion and natural vibrations. In *Newnes Engineering and Physical Science Pocket Book* (pp. 382–386). Newnes.

Blott, S. J., & Pye, K. (2001). GRADISTAT: A grain size distribution and statistics package for the analysis of unconsolidated sediments. *Earth Surface Processes and Landforms*, *26*(11), 1237–1248.

Boucher, J., & Friot, D. (2017). *Primary microplastics in the oceans: A global evaluation of sources*. International Union for Conservation of Nature and Natural Resources (IUCN).

Brennan, E., Wilcox, C., & Hardesty, B. D. (2018). Connecting flux, deposition and resuspension in coastal debris surveys. *Science of the Total Environment*, *644*, 1019–1026.

Carpenter, E. J., Anderson, S. J., Harvey, G. R., Miklas, H. P., & Peck, B. B. (1972). Polystyrene spherules in coastal waters. *Science*, *178*(4062), 749–750.

Carpenter, E. J., & Smith, K. L. (1972). Plastics on the Sargasso sea surface. *Science*, *175*(4027), 1240–1241.

Carstens, M. R., Neilson, F. M., & Althinbilek, H. D. (1969). *Bed forms generated in the laboratory under an oscillatory flow: Analytical and experimental study*.

Chubarenko, I., Bagaev, A., Zobkov, M., & Esiukova, E. (2016). On some physical and dynamical properties of microplastic particles in marine environment. *Marine Pollution Bulletin*, *108*(1–2), 105–112.

Cózar, A., Echevarría, F., González-Gordillo, J. I., Irigoien, X., Úbeda, B., Hernández-León, S., Palma, Á. T., Navarro, S., García-de-Lomas, J., Ruiz, A., Fernández-de-Puelles, M. L., & Duarte, C. M. (2014). Plastic debris in the open ocean. *Proceedings of the*

National Academy of Sciences of the United States of America, *111*(28), 10239–10244.

Critchell, K., & Lambrechts, J. (2016). Modelling accumulation of marine plastics in the coastal zone; what are the dominant physical processes? *Estuarine, Coastal and Shelf Science*, *171*, 111–122.

Eriksen, M., Lebreton, L. C. M., Carson, H. S., Thiel, M., Moore, C. J., Borerro, J. C., Galgani, F., Ryan, P. G., & Reisser, J. (2014). Plastic pollution in the world's oceans: More than 5 trillion plastic pieces weighing over 250,000 tons afloat at sea. *PLoS ONE*, *9*(12).

Folk, R. L., & Ward, W. C. (1957). Brazos River bar [Texas]; A study in the significance of grain size parameters. *Journal of Sedimentary Research*, *27*(1), 3–26.

G20. (2017). *G20 action plan on marine litter*. http://www.g20.utoronto.ca/2017/2017-g20-marine-litter.html

García, M. H. (Ed.). (2008). *Sedimentation engineering : Processes, measurements, modeling, and practice*. American Society of Civil Engineers.

GESAMP. (2015). *Sources, fate and effects of microplastics in the marine environment: A global assessment*. www.imo.org

Geyer, R., Jambeck, J. R., & Law, K. L. (2017). Production, use, and fate of all plastics ever made. *Science Advances*, *3*(7).

Gibb, B. C. (2019). Plastics are forever. *Nature Chemistry*, *11*(5), 394–395.

Gregory, M. R. (1977). Plastic pellets on New Zealand beaches. *Marine Pollution Bulletin*, *8*(4), 82–84.

Gregory, M. R. (1978). Accumulation and distribution of virgin plastic granules on New Zealand beaches. *New Zealand Journal of Marine and Freshwater Research*, *12*(4), 399–414.

Hidalgo-Ruz, V., Gutow, L., Thompson, R. C., & Thiel, M. (2012). Microplastics in the marine environment: A review of the methods used for identification and quantification. *Environmental Science and Technology*, *46*(6), 3060–3075.

Hjulstrom, F. (1935). Studies of the morphological activity of rivers as illustrated by the Rive Fyris. *Bulletin of the Geological Institute of Uppsala*, *25*, 221–527.

Hurley, R., Woodward, J., & Rothwell, J. J. (2018). Microplastic contamination of river beds significantly reduced by catchment-wide flooding. *Nature Geoscience*, *11*(4), 251–257.

Jambeck, J. R., Geyer, R., Wilcox, C., Siegler, T. R., Perryman, M., Andrady, A., Narayan, R., & Law, K. L. (2015). Plastic waste inputs from land into the ocean. *Science*, *347*(6223), 768–771.

Jensen, B. L., Sumer, B. M., & Fredsøe, J. (1989). Turbulent oscillatory boundary layers at high Reynolds numbers. *Journal of Fluid Mechanics*, *206*, 265–297.

Jonsson, I. G. (1966). Wave boundary layers and friction factors. *Tenth International Conference on Coastal Engineering*, 127–148.

Jonsson, I. G. (1980). A new approach to oscillatory rough turbulent boundary layers. *Ocean*

Engineering, *7*(1), 109–152.

Kajiura, K. (1968). *A model of the bottom boundary layer in water waves*. University of Tokyo.

Kamphuis, J. W. (1975). Friction factor under oscillatory waves. *Journal of the Waterways, Harbors and Coastal Engineering Division*, *101*(2), 135–144.

Kaneko, S., Nakamura, T., Inada, F., Kato, M., Ishihara, K., Nishihara, T., Mureithi, N. W., & Langthjem, M. A. (2014). *Flow-induced vibrations : Classifications and lessons from practical experiences* (2nd ed.). Academic Press.

Kim, I. H., & Song, D. S. (2012). Geographical distribution of sand particle sizes on GwangWon coast. *Korean Society of Surveying, Geodesy, Photogrammetry, and Cartography*, 407–410.

Lundgren, H., & Sorensen, T. (1957). A pulsating water tunnel. *Coastal Engineering Proceedings*, *1*(6), 21.

Melling, A. (1997). Tracer particles and seeding for particle image velocimetry. *Measurement Science and Technology*, *8*(12), 1406–1416.

Melling, A., & Whitelaw, J. H. (1973). Seeding of gas flows for laser anemometry. *DISA Information*, *15*, 5–14.

Nelson, T. R., Voulgaris, G., & Traykovski, P. (2013). Predicting wave-induced ripple equilibrium geometry. *Journal of Geophysical Research: Oceans*, *118*(6), 3202–3220.

Nielsen, P. (1981). Dynamics and geometry of wave-generated ripples. *Journal of Geophysical Research*, *86*(C7), 6467–6472.

Nielsen, P. (1992). *Coastal bottom boundary layers and sediment transport* (Vol. 4). World Scientific Publishing Co. Pte. Ltd.

PlasticsEurope. (2021). *Plastics - the Facts 2021 - An analysis of European plastics production, demand and waste data*. https://plasticseurope.org/knowledge-hub/plastics-the-facts-2021/

Reynolds, O. (1883). III. An experimental investigation of the circumstances which determine whether the motion of water shall be direct or sinuous, and of the law of resistance in parallel channels. *Proceedings of the Royal Society of London*, *35*(224–226), 84–99.

Rhew, H., & Kang, J. (2020). Morphological and textural characteristics of the beach-dune system in South Korea, with the possibility of a dune type scheme based on grain-size trend. *JOURNAL OF THE GEOMORPHOLOGICAL ASSOCIATION OF KOREA*, *27*(3), 53–73.

Ribberink, J. S., & Al-Salem, A. A. (1994). Sediment transport in oscillatory boundary layers in cases of rippled beds and sheet flow. *Journal of Geophysical Research*, *99*(C6), 12707–12727.

Scandura, P. (2007). Steady streaming in a turbulent oscillating boundary layer. *Journal of Fluid Mechanics*, *571*, 265–280.

Schmidt, C., Krauth, T., & Wagner, S. (2017). Export of plastic debris by rivers into the sea. *Environmental Science and Technology*, *51*(21), 12246–12253.

Shields, A. (1936a). *Anwendung der Aehnlichkeitsmechanik und der Turbulenzforschung auf die Geschiebebewegung* [PhD Thesis]. Preußische Versuchsanstalt für Wasserbau.

Shields, A. (1936b). *Application of similarity principles and turbulence research to bed-load movement*.

Shim, W. J., Hong, S. H., & Eo, S. (2018). Marine microplastics: Abundance, distribution, and composition. In *Microplastic Contamination in Aquatic Environments: An Emerging Matter of Environmental Urgency* (pp. 1–26). Elsevier.

Shim, W. J., & Thomposon, R. C. (2015). Microplastics in the ocean. *Archives of Environmental Contamination and Toxicology*, *69*(3).

Simons, R. R., Grass, A. J., & Kyriacou, A. (1989). The influence of currents on wave attenuation. *Coastal Engineering 1988*, 363–376.

Sleath, J. F. A. (1984). *Sea bed mechanics*. Wiley Interscience.

Sleath, J. F. A. (1985). Energy dissipation in oscillatory flow over rippled beds. *Coastal Engineering*, *9*(2), 159–170.

Soulsby, R. L., & Whitehouse, R. J. S. (2005). *Prediction of ripple properties in shelf seas - Mark 2 predictor for time evolution*.

Sumer, B. M., & Fuhrman, D. R. (2020). *Turbulence in coastal and civil engineering* (Vol. 51). World Scientific Publishing Co. Pte. Ltd.

Swart, D. H. (1974). *Offshore sediment transport and equilibrium beach profiles* [Ph.D. Thesis]. Delft University of Technology.

Thielicke, W., & Stamhuis, E. J. (2014). PIVlab – Towards user-friendly, affordable and accurate digital particle image velocimetry in MATLAB. *Journal of Open Research Software*, *2*(1).

Thompson, R. C., Olson, Y., Mitchell, R. P., Davis, A., Rowland, S. J., John, A. W. G., McGonigle, D., & Russell, A. E. (2004). Lost at Sea: Where Is All the Plastic? *Science*, *304*(5672), 838.

Thompson, R. C., Swan, S. H., Moore, C. J., & vom Saal, F. S. (2009). Our plastic age. *Philosophical Transactions of the Royal Society B: Biological Sciences*, *364*(1526), 1973–1976.

Turner, A., Amos, S. L., & Williams, T. (2021). Coastal dunes as a sink and secondary source of marine plastics: A study at Perran Beach, southwest England. *Marine Pollution Bulletin*, *173*(113133).

Turra, A., Manzano, A. B., Dias, R. J. S., Mahiques, M. M., Barbosa, L., Balthazar-Silva, D., & Moreira, F. T. (2014). Three-dimensional distribution of plastic pellets in sandy beaches: Shifting paradigms. *Scientific Reports*, *4*(4435).

Udden, J. A. (1914). Mechanical compostion of clastic sediments. *Bulletin of the Geological Society of America*, *25*(1), 655–744.

UNEP. (2017). *Exploring the potential for adopting alternative materials to reduce marine plastic litter*.

van der Werf, J. J., Doucette, J. S., O'Donoghue, T., & Ribberink, J. S. (2007). Detailed measurements of velocities and suspended sand concentrations over full-scale ripples in regular oscillatory flow. *Journal of Geophysical Research: Earth Surface*, *112*(F2).

van Rijn, L. C. (1984). Sediment transport, Part I: Bed load transport. *Journal of Hydraulic Engineering*, *110*(10), 1431–1456.

Vanoni, V. A. (1977). *Sedimentation engineering*.

Wentworth, C. K. (1922). A scale of grade and class terms for clastic sediments. *Journal of Geology*, *30*(5), 377–392.

Willis, K., Denise Hardesty, B., Kriwoken, L., & Wilcox, C. (2017). Differentiating littering, urban runoff and marine transport as sources of marine debris in coastal and estuarine environments. *Scientific Reports*, *7*(44479).

Yang, T. C., 우효섭, 정관수, 이삼희, 류권규, 최성욱, & 손광익. (2007). *유사 이송: 이론과 실무*. 청문각.

Yuan, J., & Madsen, O. S. (2014). Experimental study of turbulent oscillatory boundary layers in an oscillating water tunnel. *Coastal Engineering*, *89*, 63–84.

Yuan, J., & Wang, D. (2018). Experimental investigation of total bottom shear stress for oscillatory flows over sand ripples. *Journal of Geophysical Research: Oceans*, *123*(9), 6481–6502.

남정호. (2004). *해양쓰레기의 국가간 이동에 대한 대응방향 연구*.

진정일. (2013, April 9). 석기시대, 청동기시대, 철기시대를 건너, 지금 우리는 플라스틱 시대에 살고 있다. GS칼텍스 미디어허브. https://gscaltexmediahub.com/energy/plastics-all-around/

천권필. (2021, June 22). 낙동강→북한→독도...버려진 페트병 충격적 "1000km 여정." *The JoongAng*. https://www.joongang.co.kr/article/24087734#home

탁성제. (2020). *플라스틱 규제 동향과 대응방안*.

해양수산부, & 해양환경공단. (2020). *2020 국가 해안쓰레기 일제·모니터링 조사 용역 최종보고서*. https://www.koem.or.kr/site/koem/ex/board/View.do?cbIdx=370&bcIdx=30182

APPENDIX A:
Bedform change over time

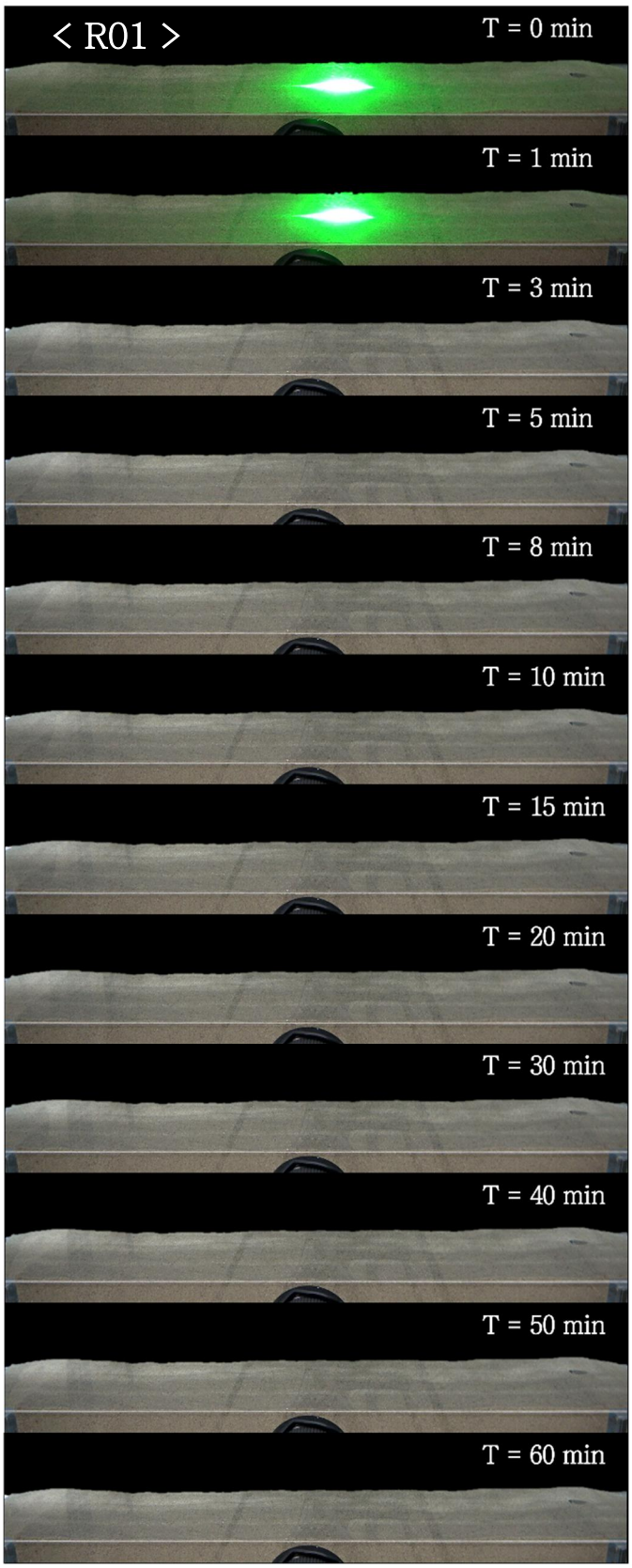
< R01 >
T = 0 min
T = 1 min
T = 3 min
T = 5 min
T = 8 min
T = 10 min
T = 15 min
T = 20 min
T = 30 min
T = 40 min
T = 50 min
T = 60 min

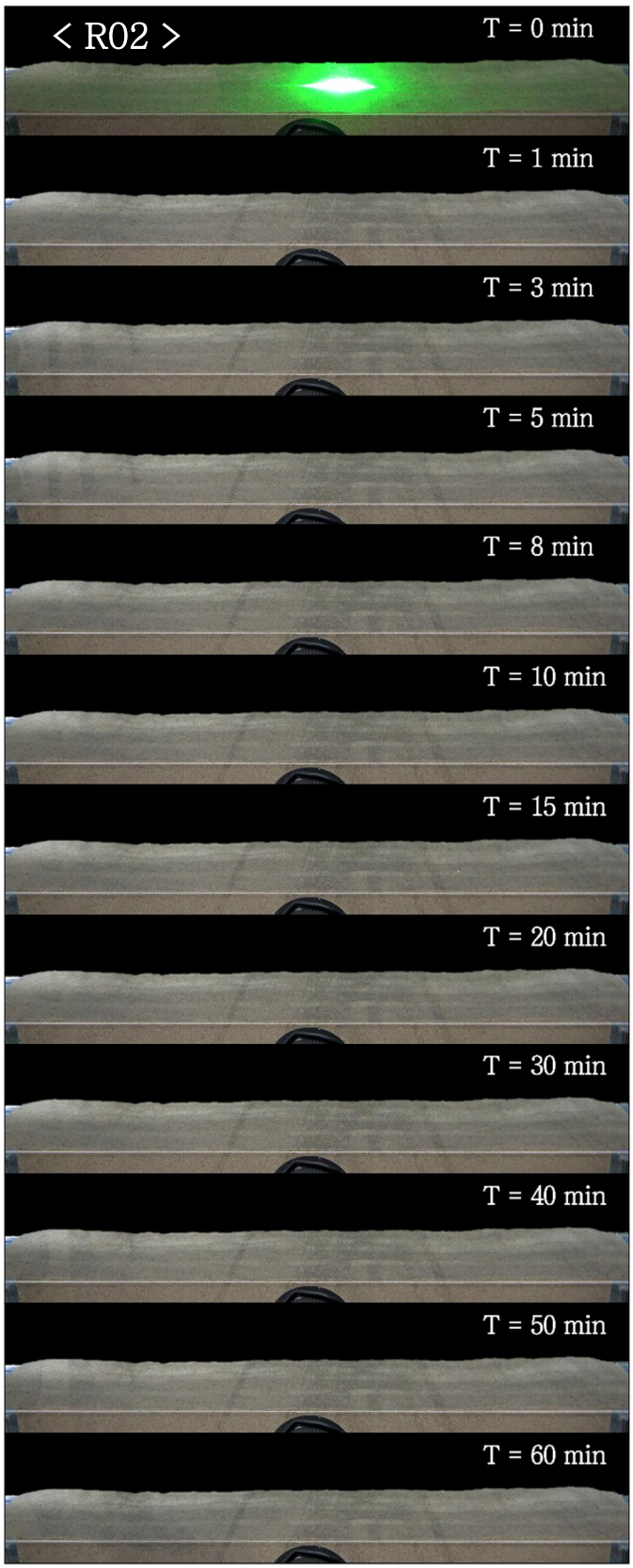
< R02 >
T = 0 min
T = 1 min
T = 3 min
T = 5 min
T = 8 min
T = 10 min
T = 15 min
T = 20 min
T = 30 min
T = 40 min
T = 50 min
T = 60 min

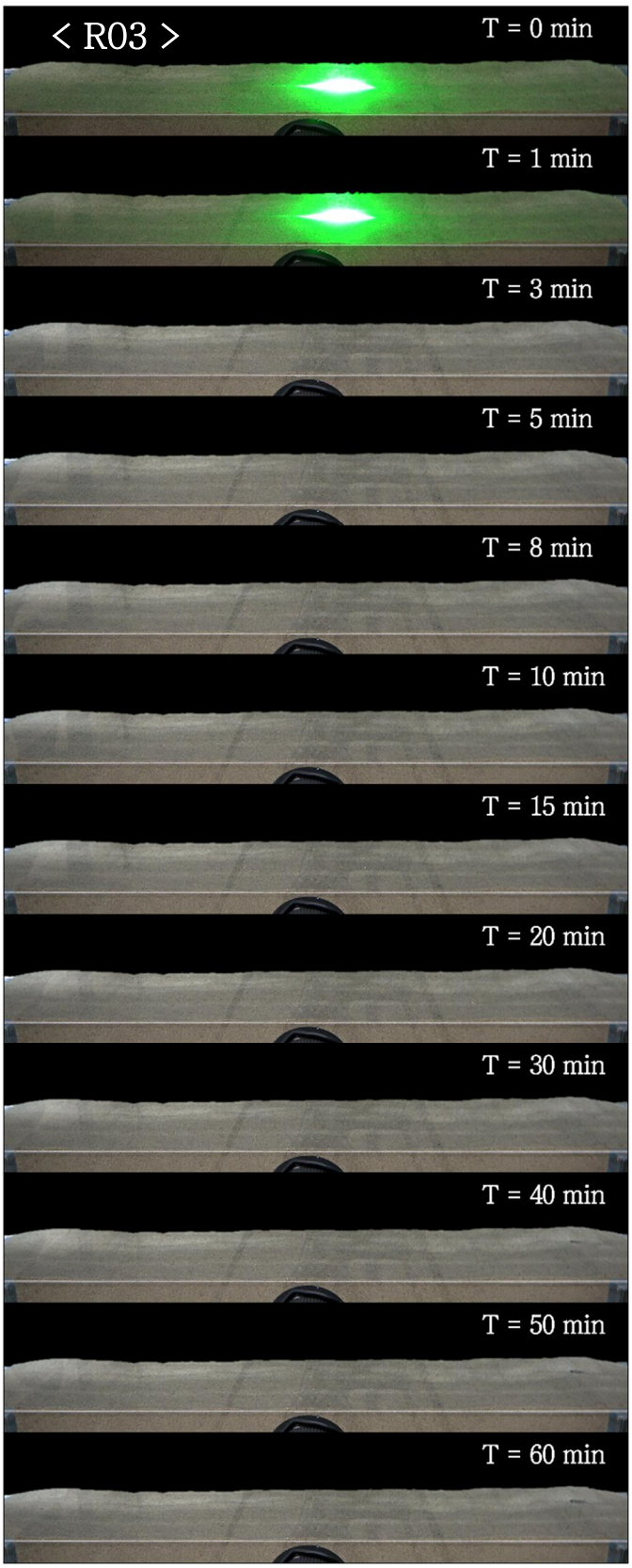
< R03 >
T = 0 min
T = 1 min
T = 3 min
T = 5 min
T = 8 min
T = 10 min
T = 15 min
T = 20 min
T = 30 min
T = 40 min
T = 50 min
T = 60 min

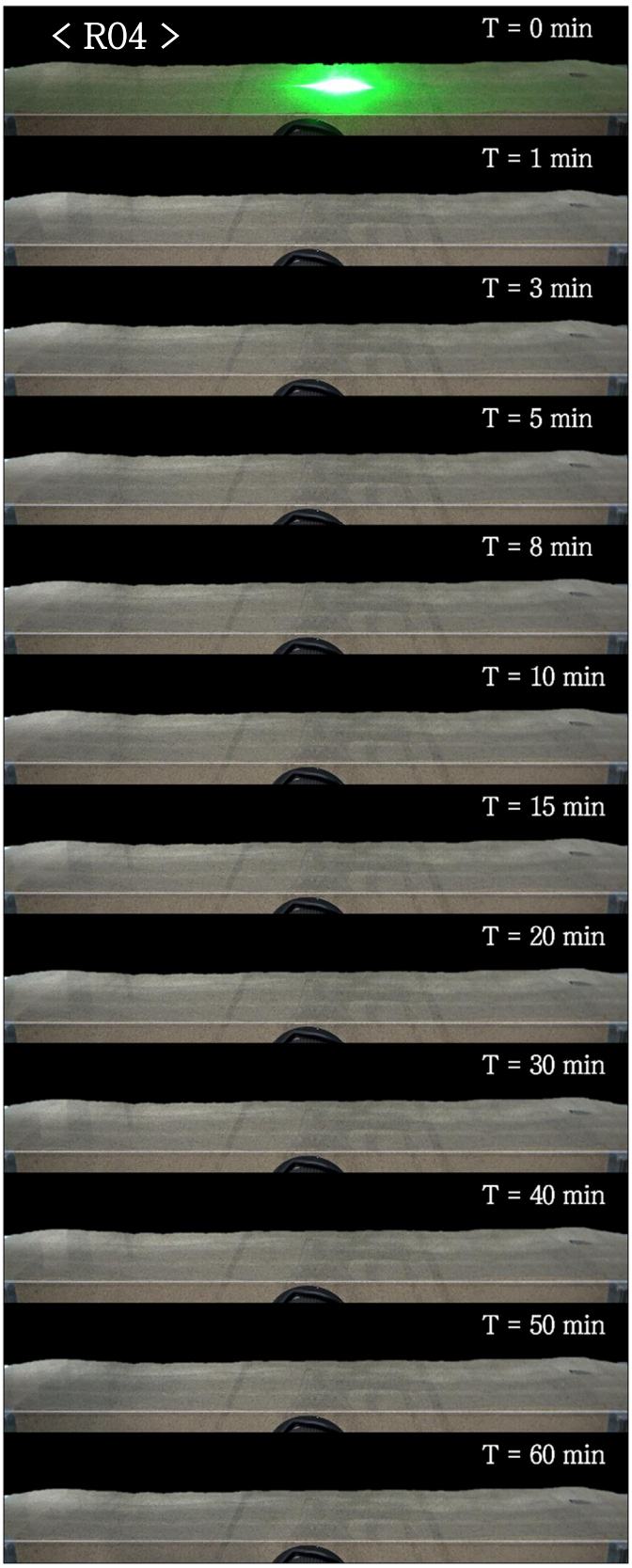
< R04 >
T = 0 min
T = 1 min
T = 3 min
T = 5 min
T = 8 min
T = 10 min
T = 15 min
T = 20 min
T = 30 min
T = 40 min
T = 50 min
T = 60 min

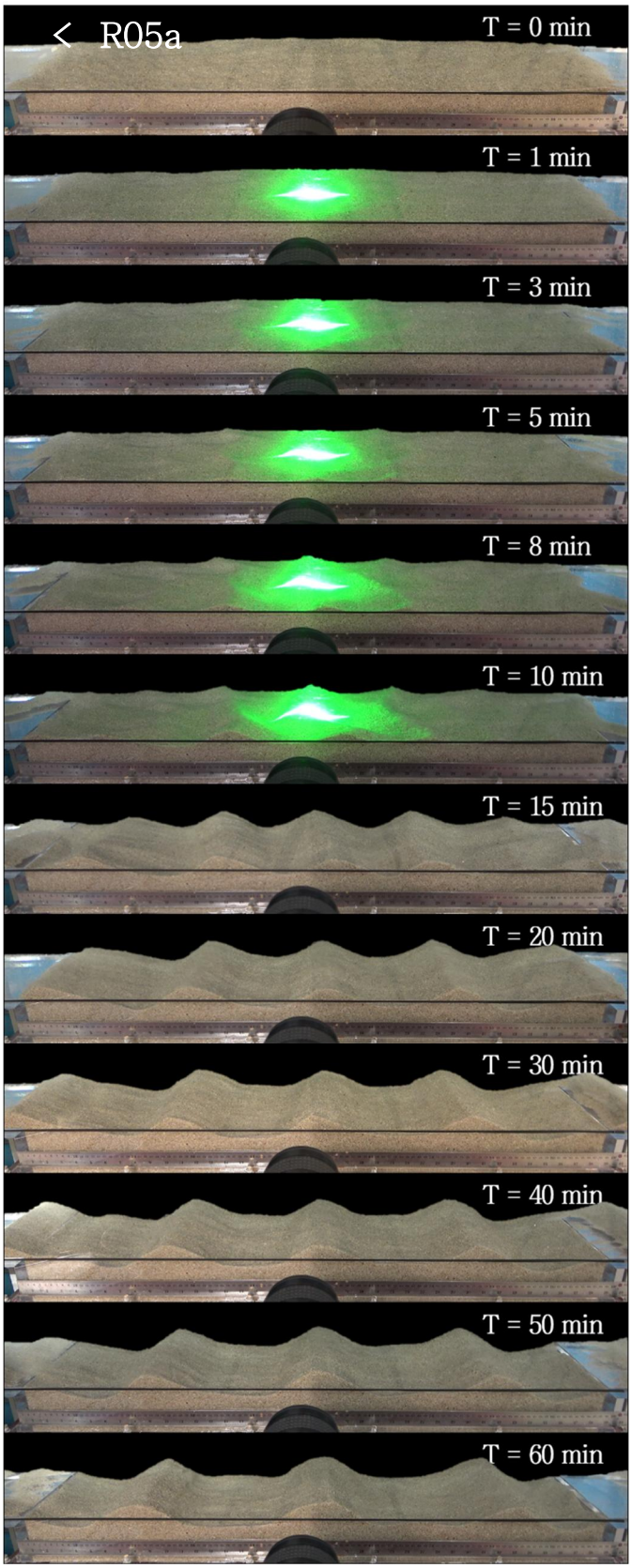
< R05a
T = 0 min
T = 1 min
T = 3 min
T = 5 min
T = 8 min
T = 10 min
T = 15 min
T = 20 min
T = 30 min
T = 40 min
T = 50 min
T = 60 min

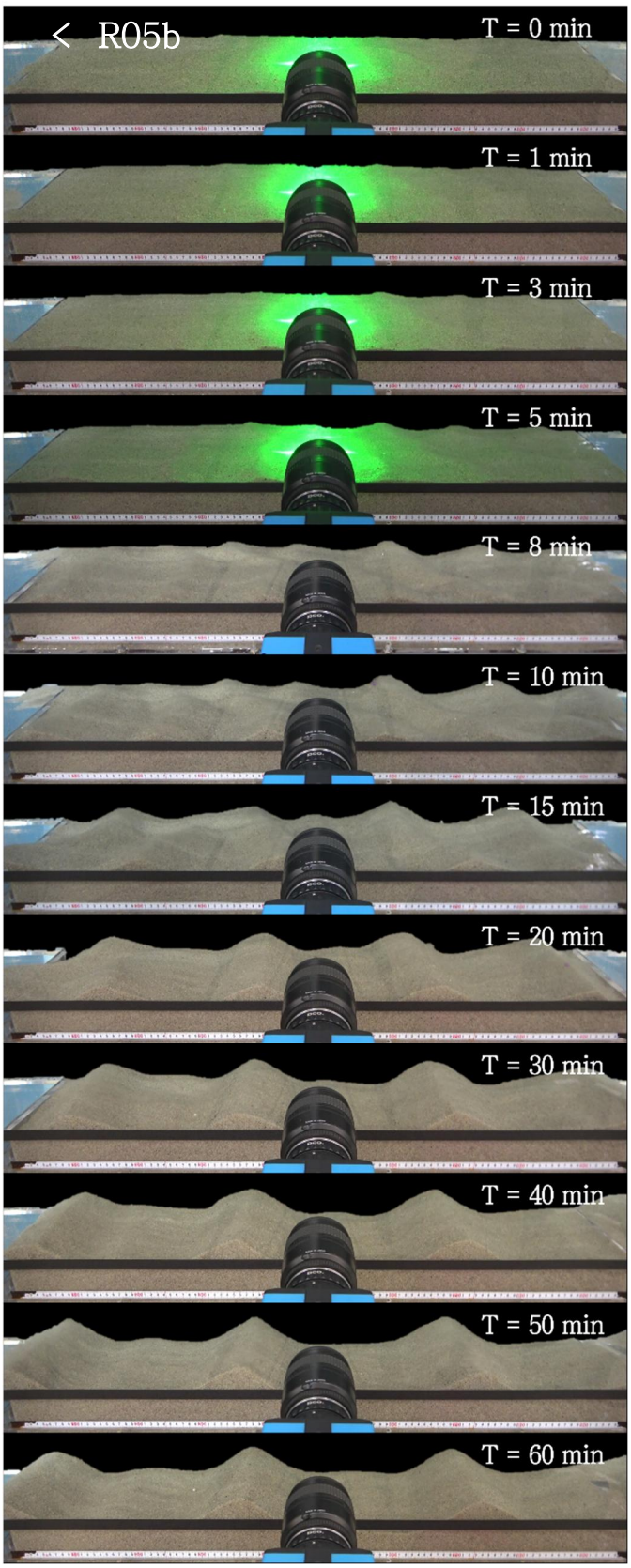
R05b
T = 0 min
T = 1 min
T = 3 min
T = 5 min
T = 8 min
T = 10 min
T = 15 min
T = 20 min
T = 30 min
T = 40 min
T = 50 min
T = 60 min

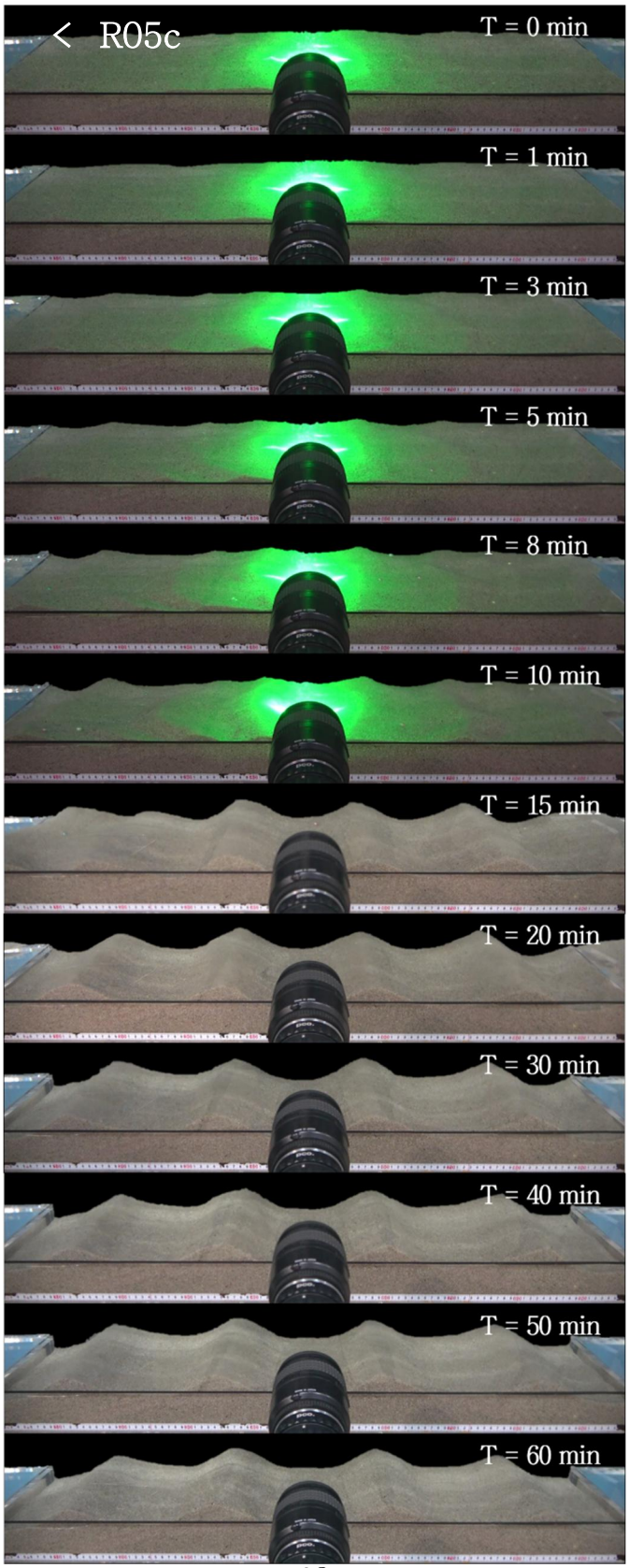
R05c
T = 0 min
T = 1 min
T = 3 min
T = 5 min
T = 8 min
T = 10 min
T = 15 min
T = 20 min
T = 30 min
T = 40 min
T = 50 min
T = 60 min

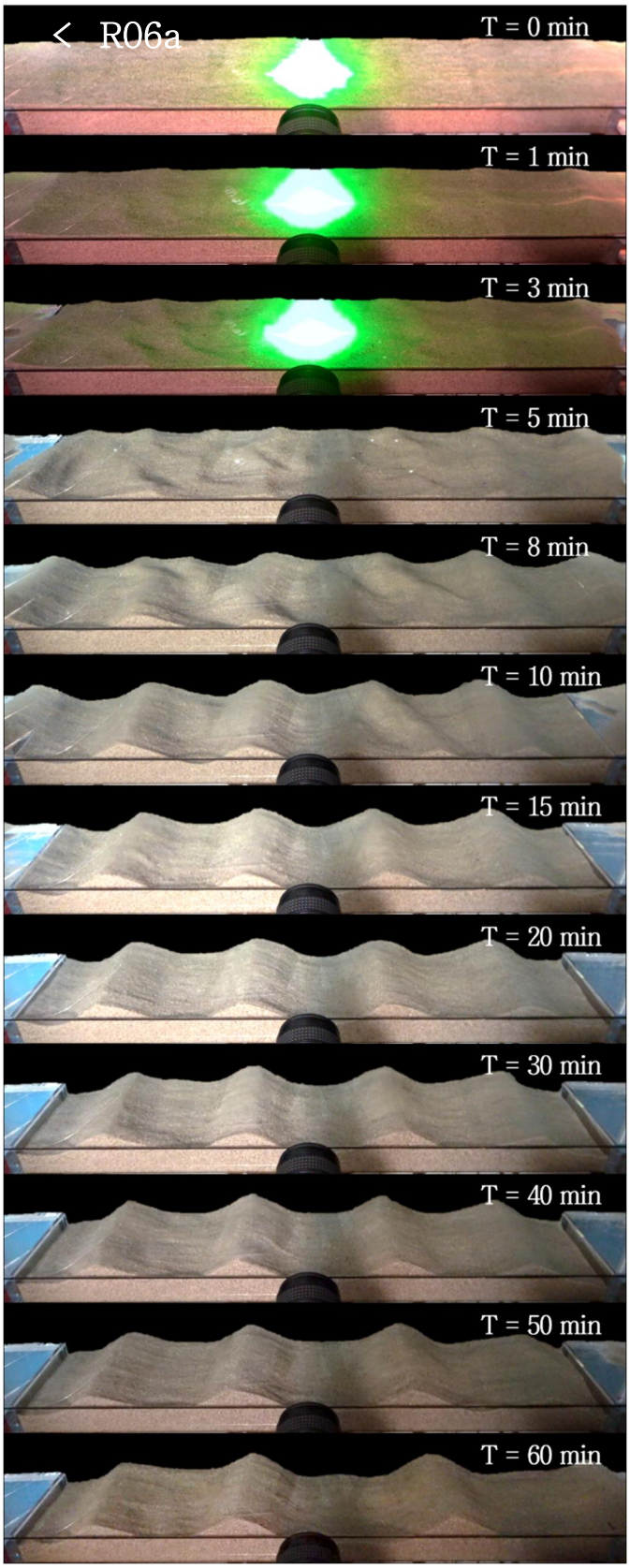
< R06a
T = 0 min
T = 1 min
T = 3 min
T = 5 min
T = 8 min
T = 10 min
T = 15 min
T = 20 min
T = 30 min
T = 40 min
T = 50 min
T = 60 min

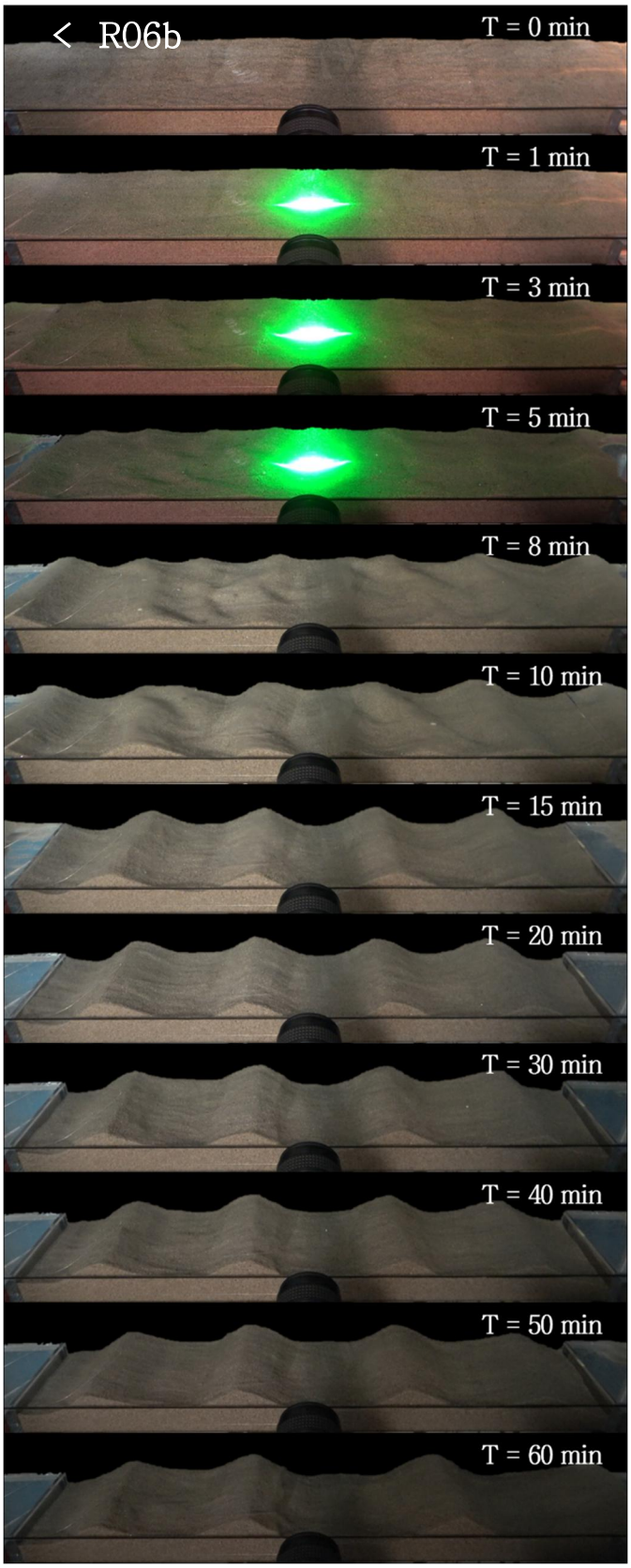
< R06b
T = 0 min
T = 1 min
T = 3 min
T = 5 min
T = 8 min
T = 10 min
T = 15 min
T = 20 min
T = 30 min
T = 40 min
T = 50 min
T = 60 min

< R06c
T = 0 min
T = 1 min
T = 3 min
T = 5 min
T = 8 min
T = 10 min
T = 15 min
T = 20 min
T = 30 min
T = 40 min
T = 50 min
T = 60 min

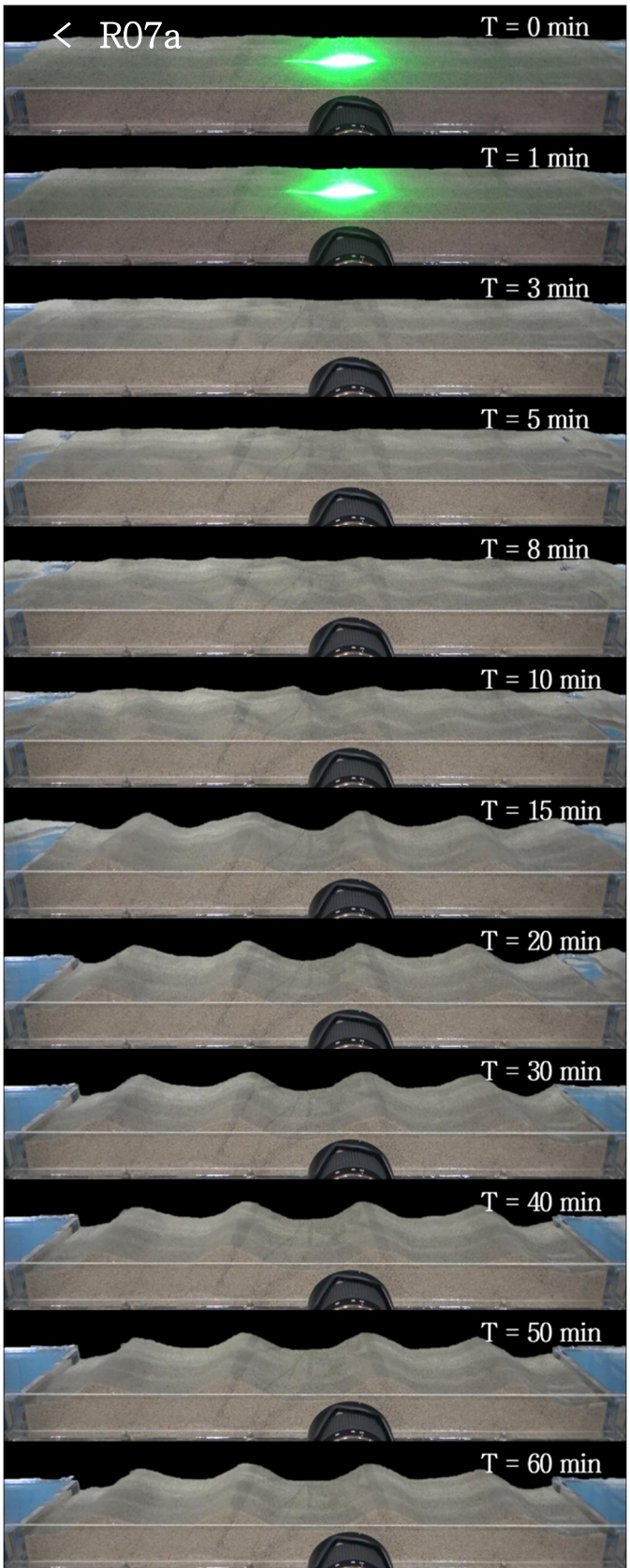
R07a
T = 0 min
T = 1 min
T = 3 min
T = 5 min
T = 8 min
T = 10 min
T = 15 min
T = 20 min
T = 30 min
T = 40 min
T = 50 min
T = 60 min

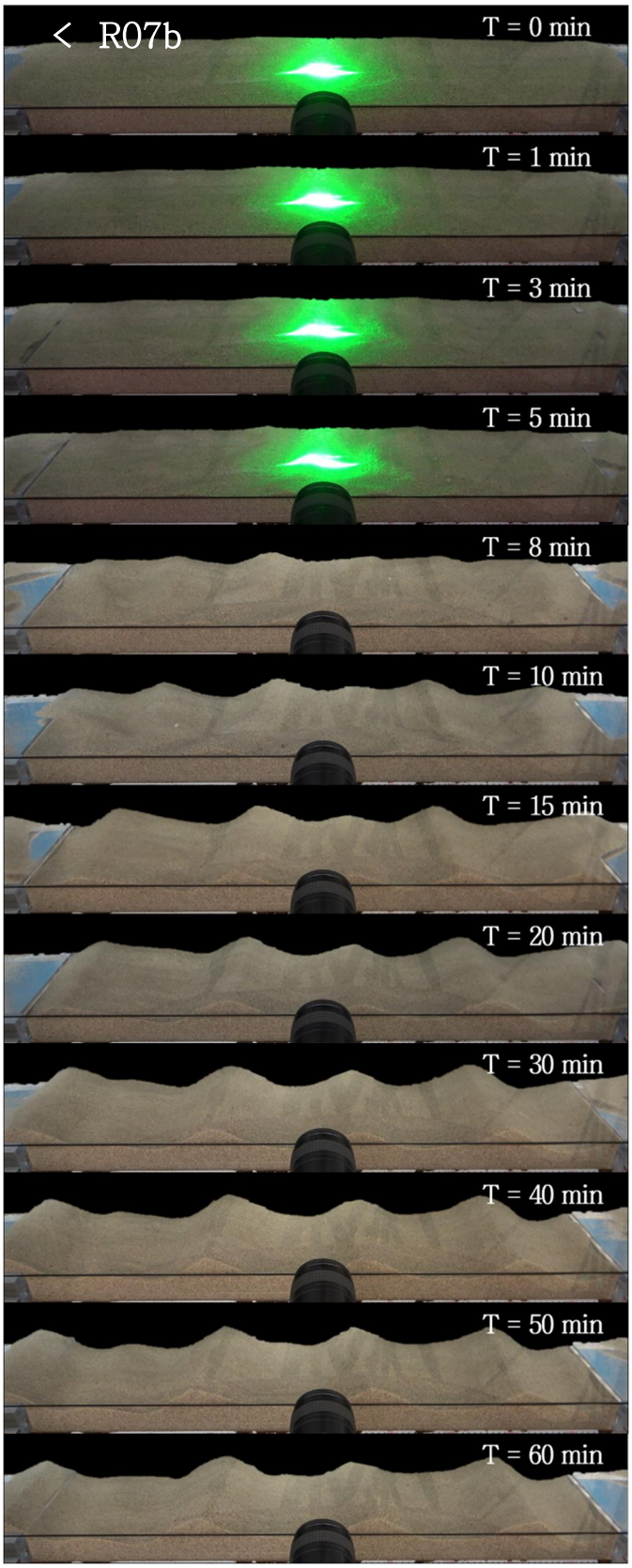
< R07b
T = 0 min
T = 1 min
T = 3 min
T = 5 min
T = 8 min
T = 10 min
T = 15 min
T = 20 min
T = 30 min
T = 40 min
T = 50 min
T = 60 min

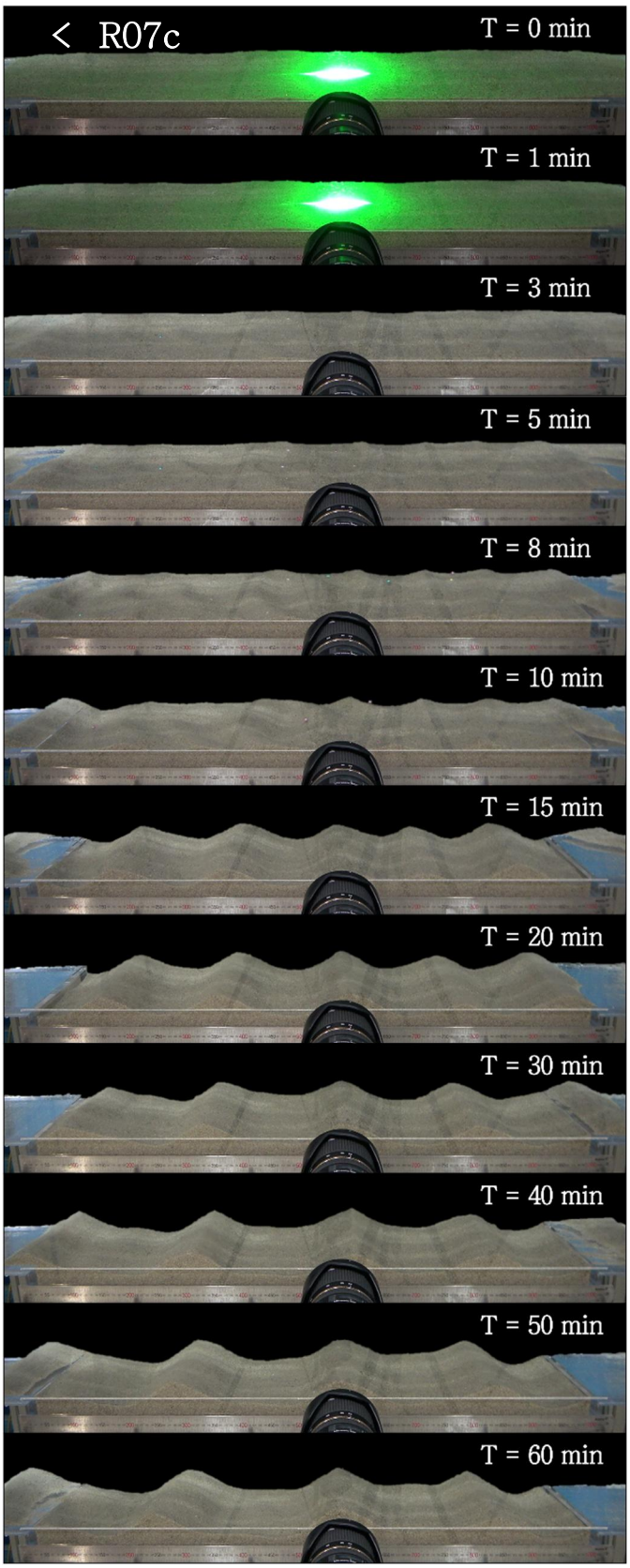
< R07c
T = 0 min
T = 1 min
T = 3 min
T = 5 min
T = 8 min
T = 10 min
T = 15 min
T = 20 min
T = 30 min
T = 40 min
T = 50 min
T = 60 min

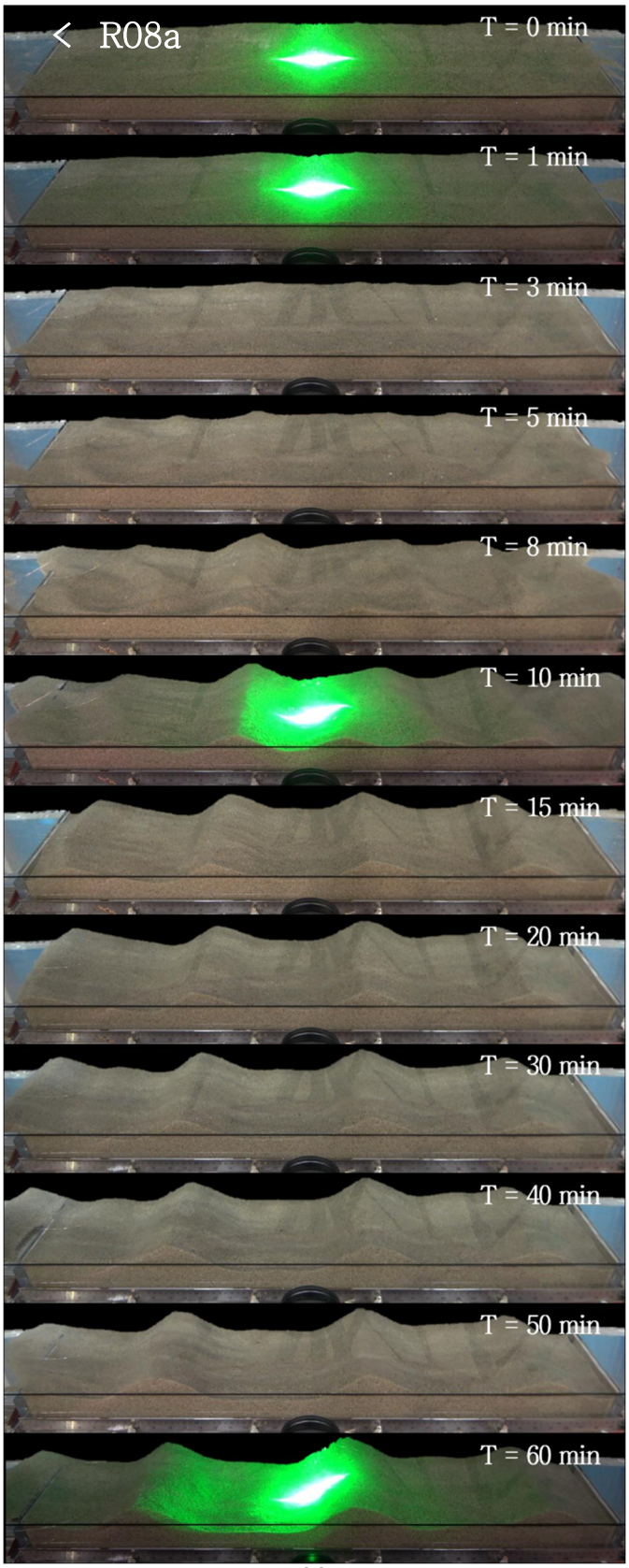
R08a
T = 0 min
T = 1 min
T = 3 min
T = 5 min
T = 8 min
T = 10 min
T = 15 min
T = 20 min
T = 30 min
T = 40 min
T = 50 min
T = 60 min

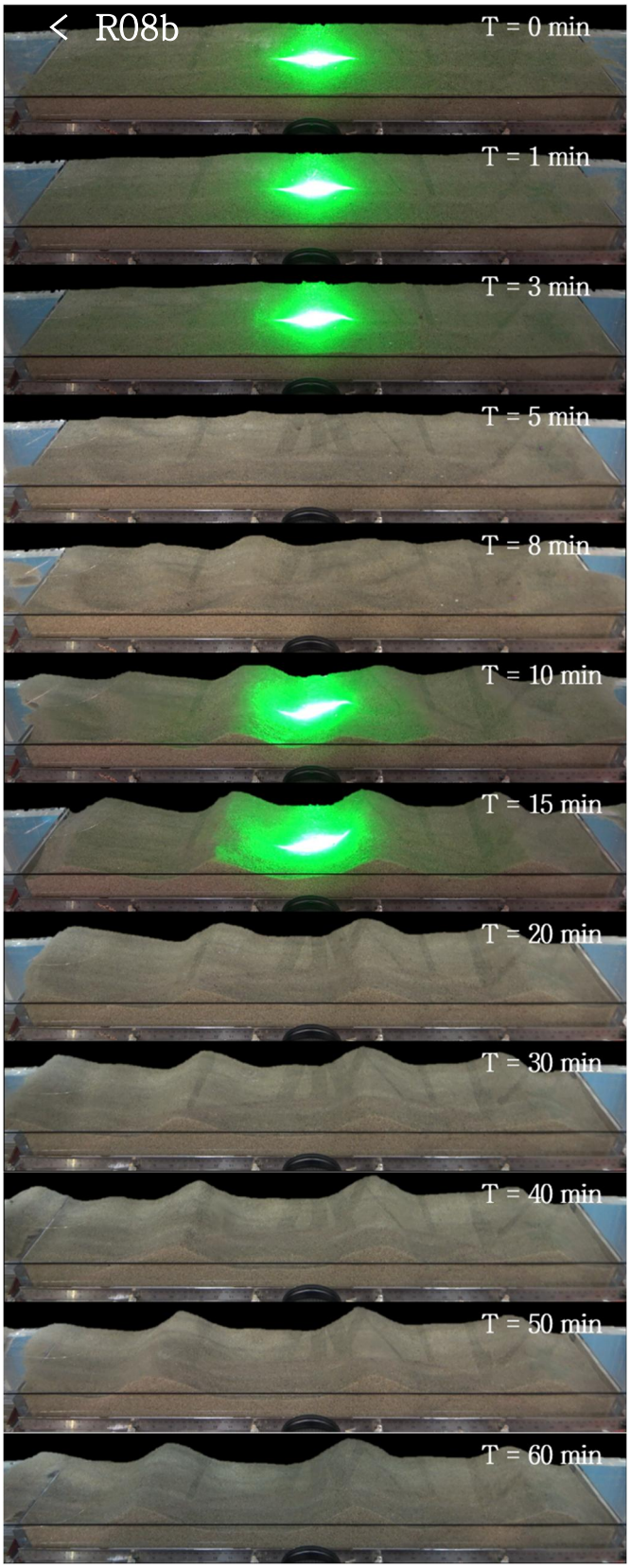
R08b
T = 0 min
T = 1 min
T = 3 min
T = 5 min
T = 8 min
T = 10 min
T = 15 min
T = 20 min
T = 30 min
T = 40 min
T = 50 min
T = 60 min

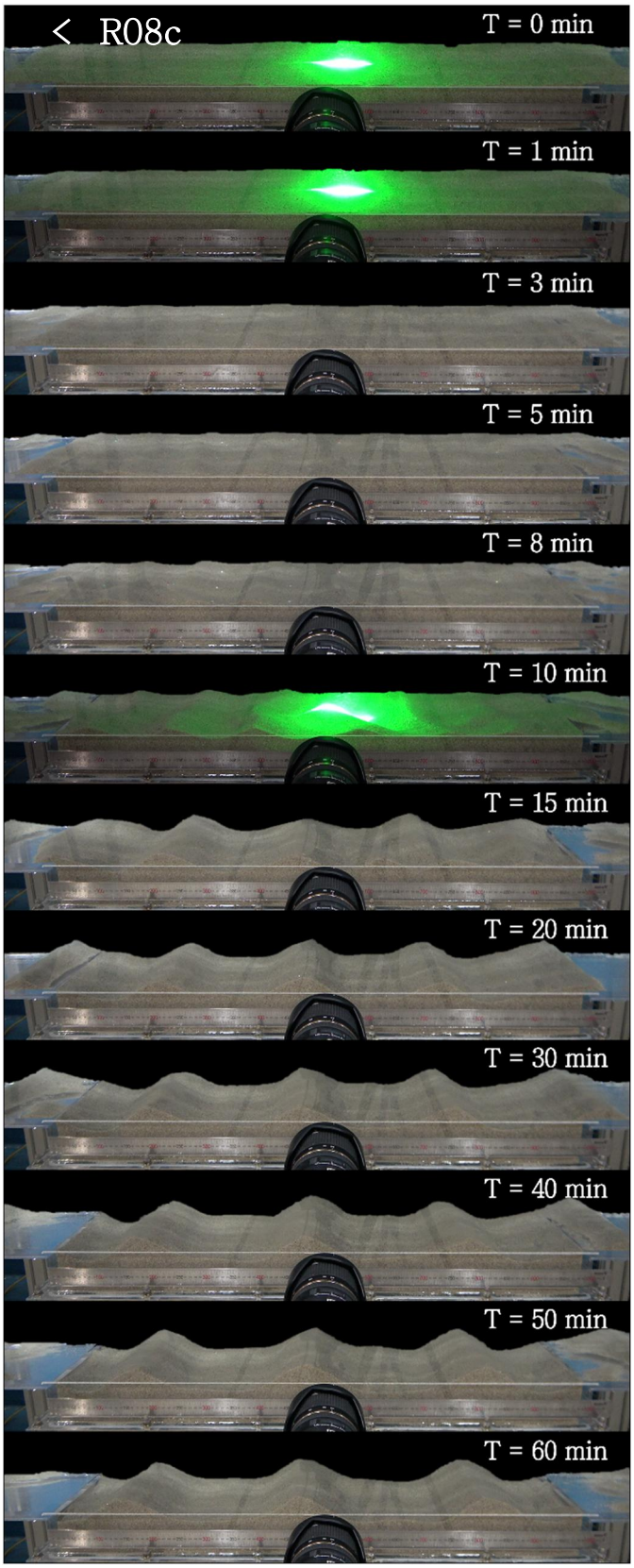
< R08c
T = 0 min
T = 1 min
T = 3 min
T = 5 min
T = 8 min
T = 10 min
T = 15 min
T = 20 min
T = 30 min
T = 40 min
T = 50 min
T = 60 min

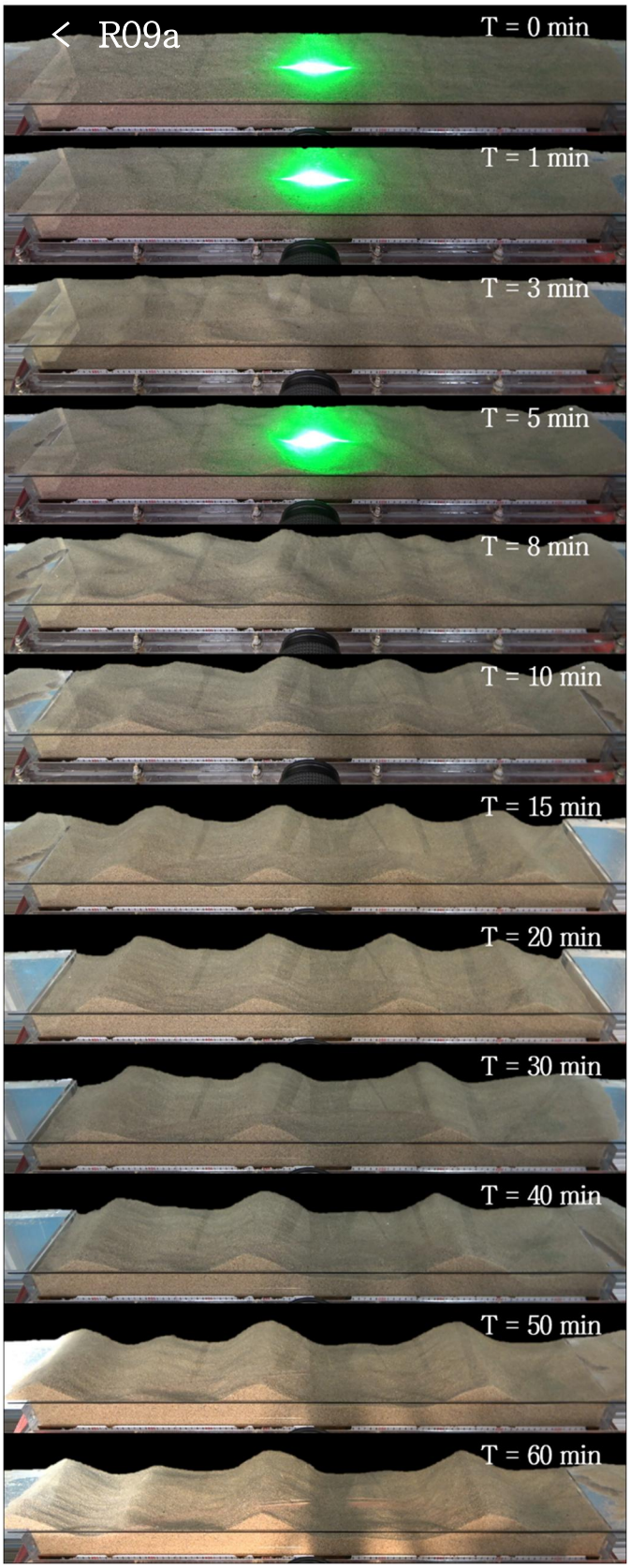
R09a
T = 0 min
T = 1 min
T = 3 min
T = 5 min
T = 8 min
T = 10 min
T = 15 min
T = 20 min
T = 30 min
T = 40 min
T = 50 min
T = 60 min

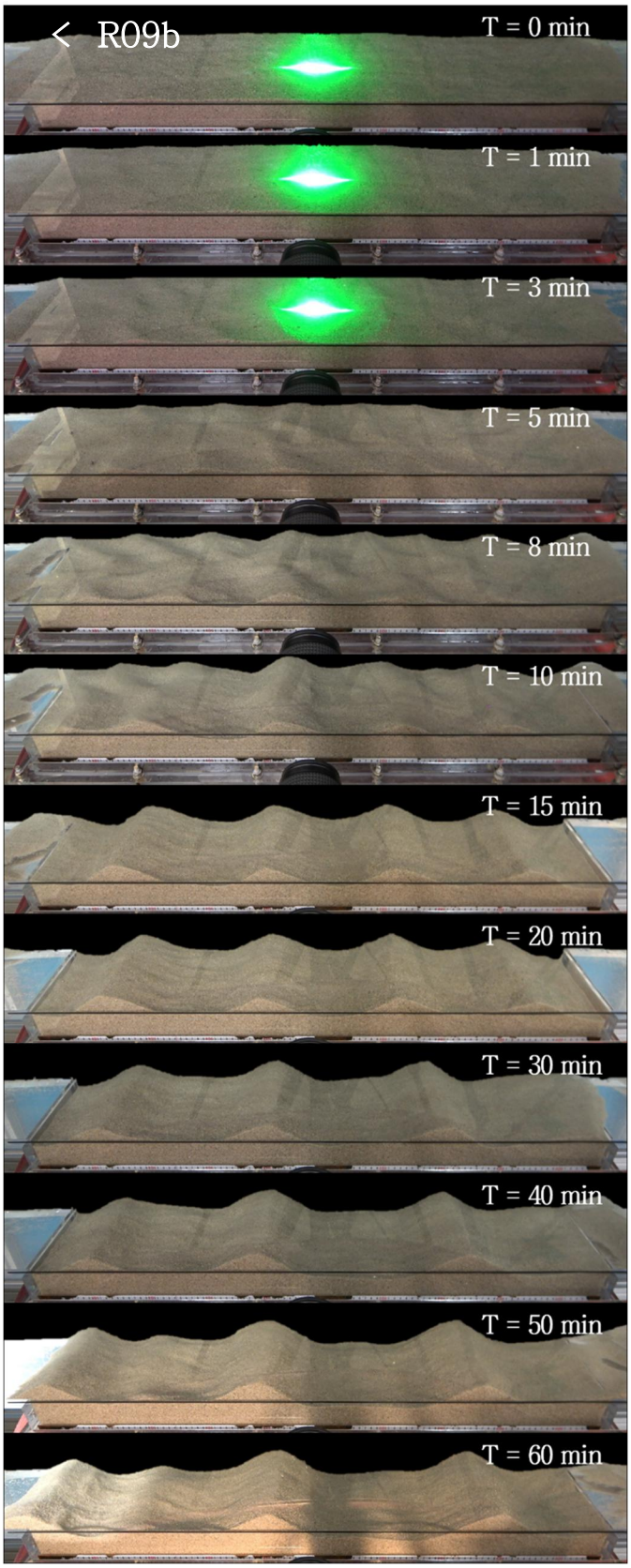
R09b
T = 0 min
T = 1 min
T = 3 min
T = 5 min
T = 8 min
T = 10 min
T = 15 min
T = 20 min
T = 30 min
T = 40 min
T = 50 min
T = 60 min

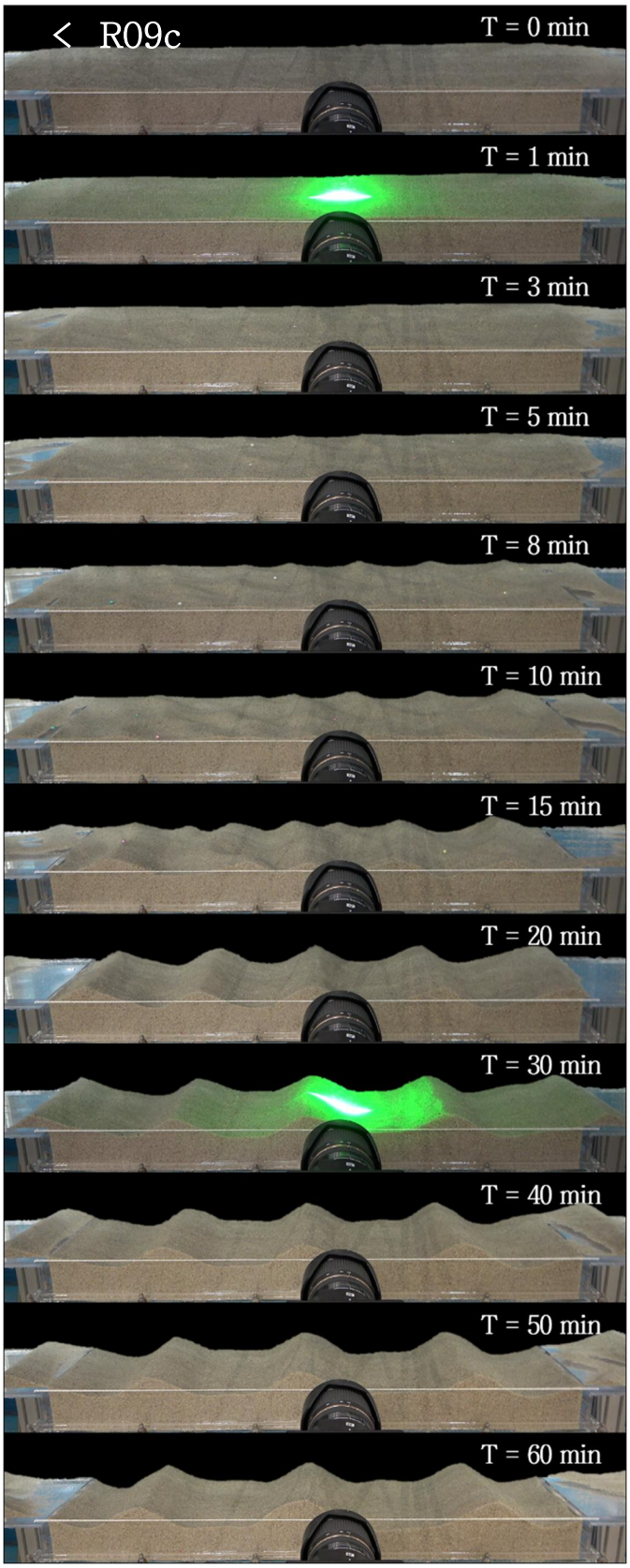
< R09c
T = 0 min
T = 1 min
T = 3 min
T = 5 min
T = 8 min
T = 10 min
T = 15 min
T = 20 min
T = 30 min
T = 40 min
T = 50 min
T = 60 min

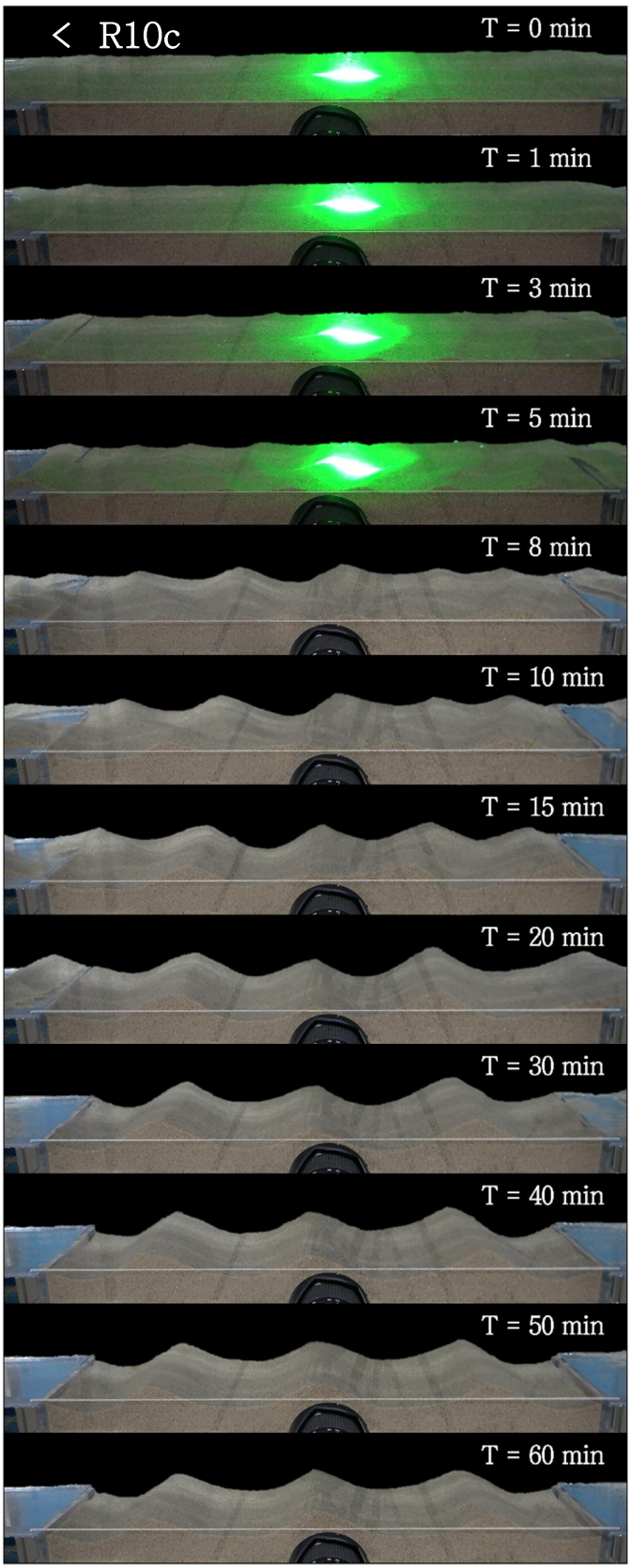
< R10c
T = 0 min
T = 1 min
T = 3 min
T = 5 min
T = 8 min
T = 10 min
T = 15 min
T = 20 min
T = 30 min
T = 40 min
T = 50 min
T = 60 min

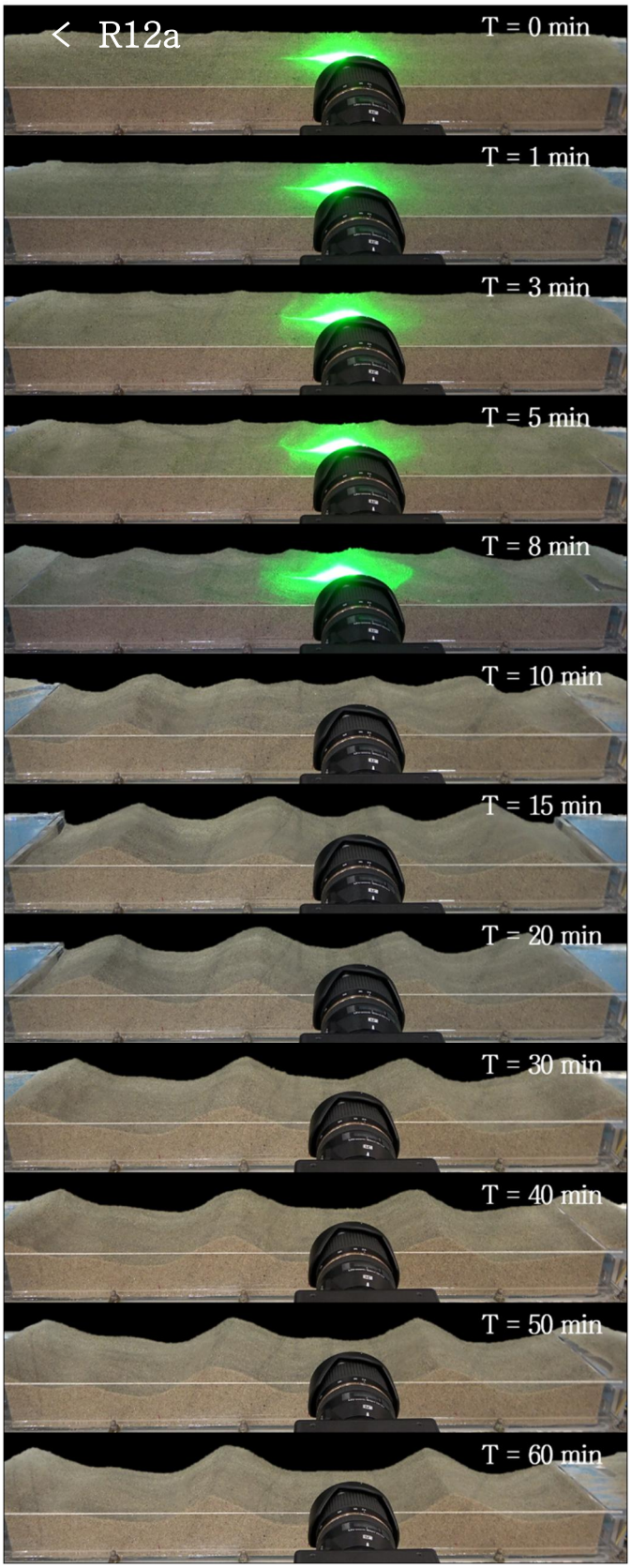
R12a
T = 0 min
T = 1 min
T = 3 min
T = 5 min
T = 8 min
T = 10 min
T = 15 min
T = 20 min
T = 30 min
T = 40 min
T = 50 min
T = 60 min

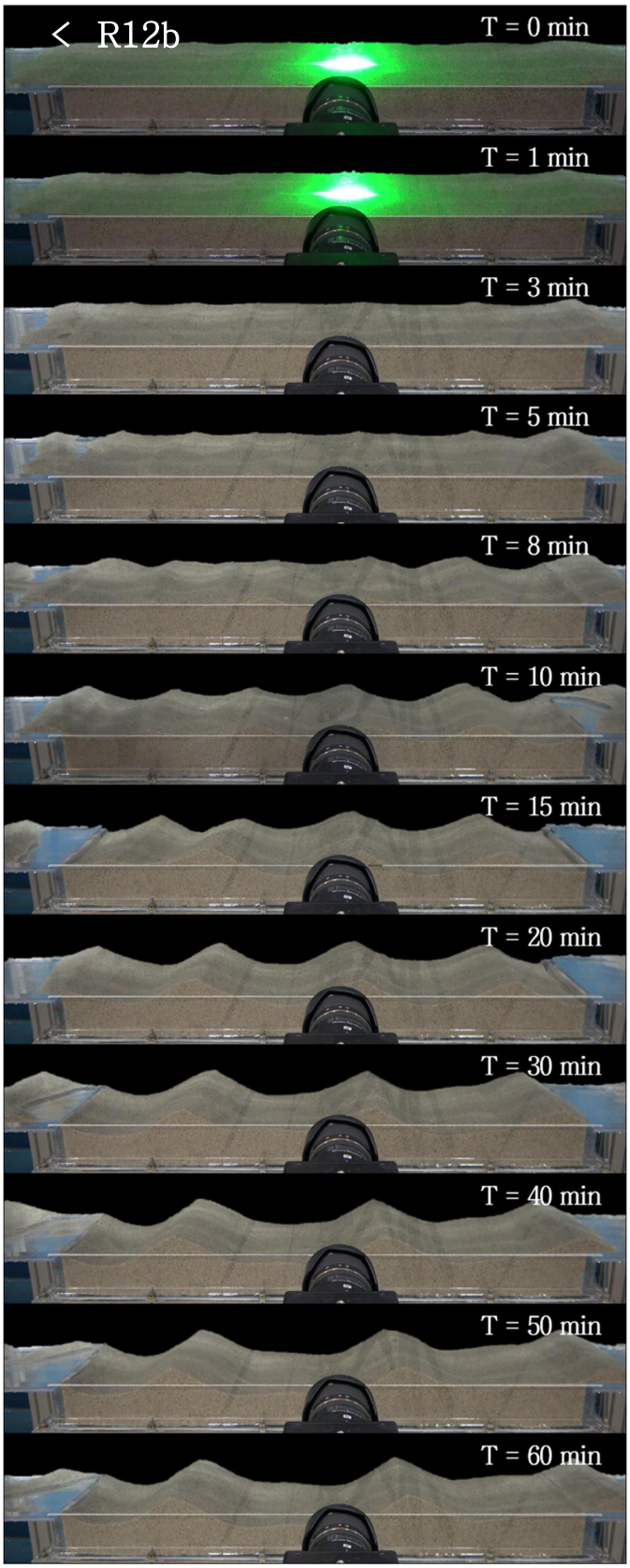
< R12b
T = 0 min
T = 1 min
T = 3 min
T = 5 min
T = 8 min
T = 10 min
T = 15 min
T = 20 min
T = 30 min
T = 40 min
T = 50 min
T = 60 min

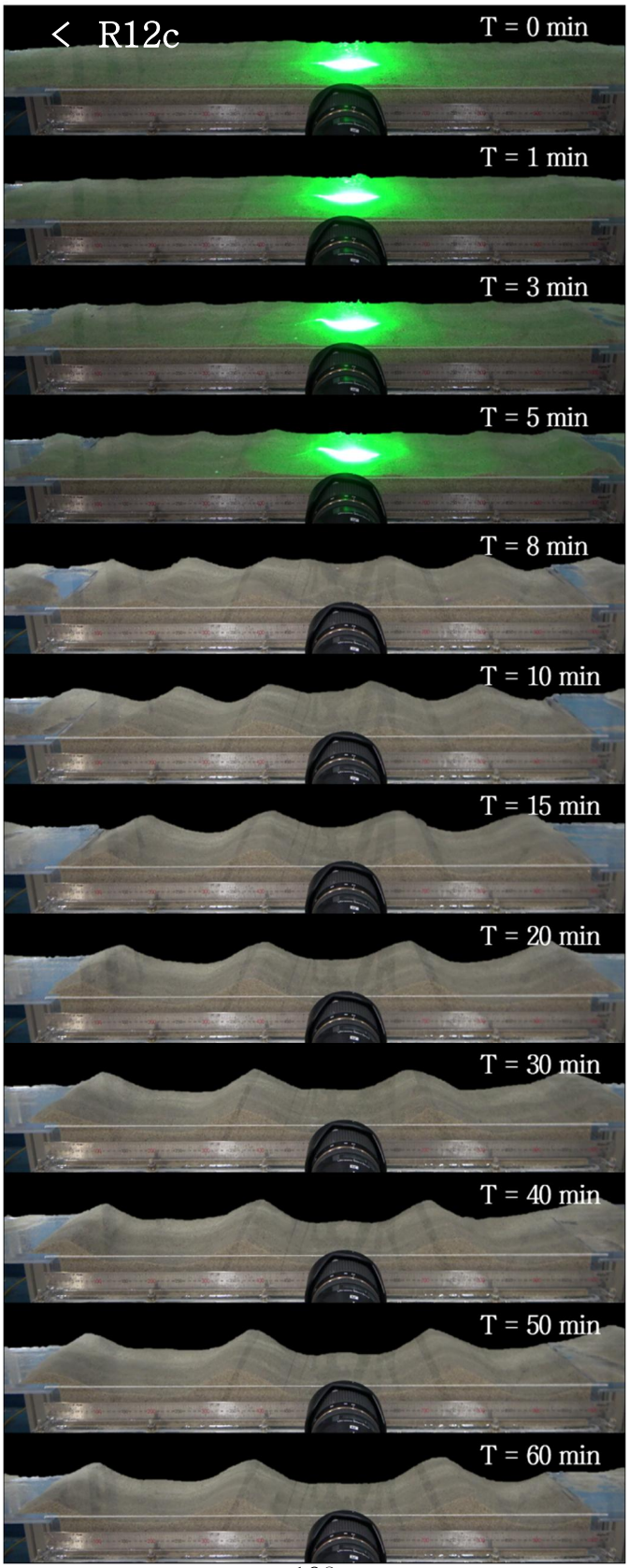
< R12c
T = 0 min
T = 1 min
T = 3 min
T = 5 min
T = 8 min
T = 10 min
T = 15 min
T = 20 min
T = 30 min
T = 40 min
T = 50 min
T = 60 min

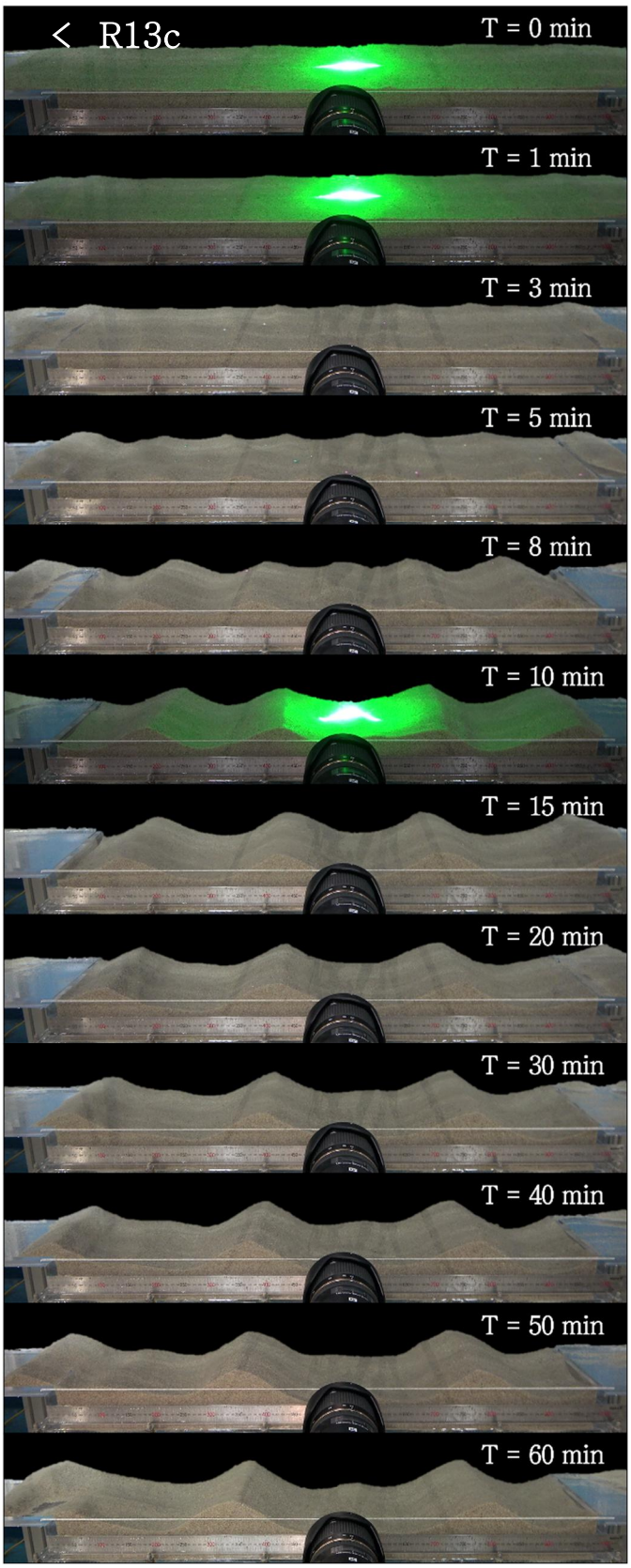
< R13c
T = 0 min
T = 1 min
T = 3 min
T = 5 min
T = 8 min
T = 10 min
T = 15 min
T = 20 min
T = 30 min
T = 40 min
T = 50 min
T = 60 min

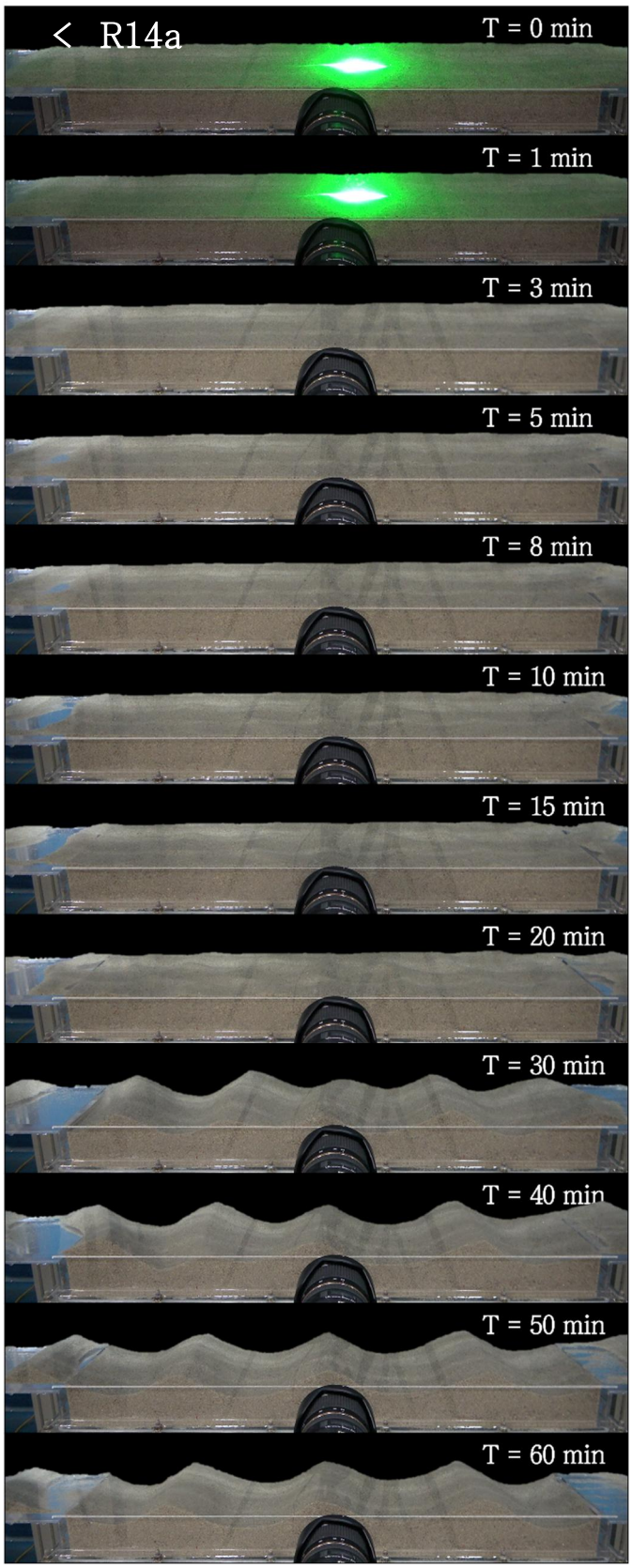
< R14a
T = 0 min
T = 1 min
T = 3 min
T = 5 min
T = 8 min
T = 10 min
T = 15 min
T = 20 min
T = 30 min
T = 40 min
T = 50 min
T = 60 min

APPENDIX B:
Digitized two-dimensional bedform over time

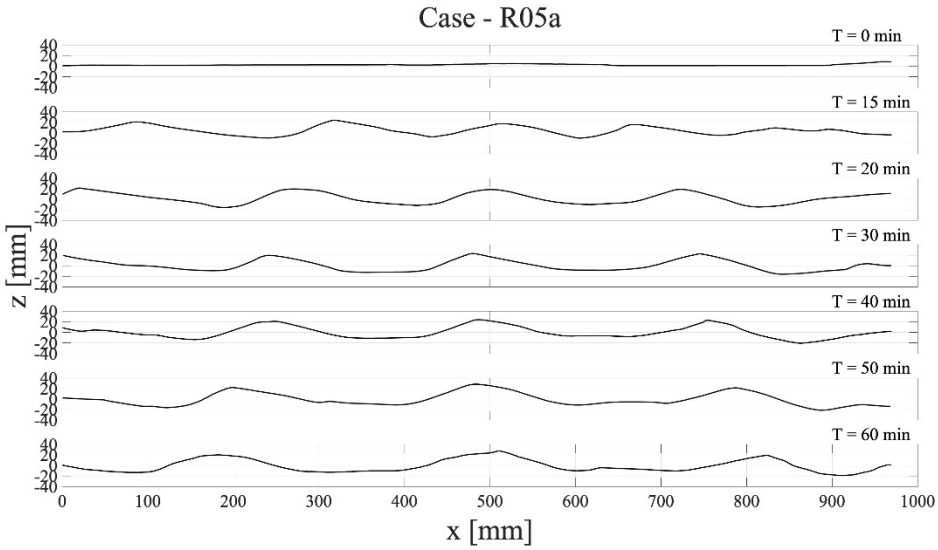
Case - R05a
T = 0 min
T = 15 min
T = 20 min
T = 30 min
T = 40 min
T = 50 min
T = 60 min
z [mm]
x [mm]

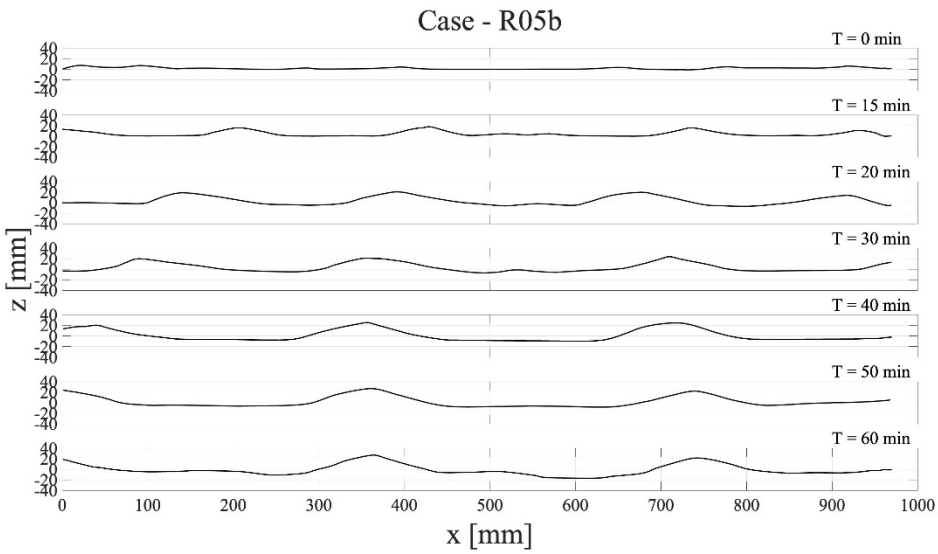
Case - R05b
T = 0 min
T = 15 min
T = 20 min
T = 30 min
T = 40 min
T = 50 min
T = 60 min
z [mm]
x [mm]

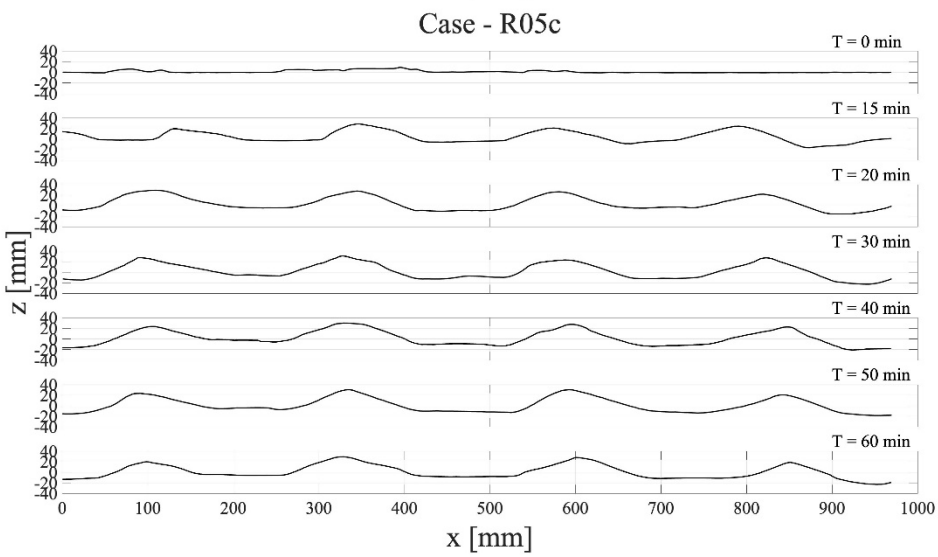
Case - R05c
T = 0 min
T = 15 min
T = 20 min
T = 30 min
T = 40 min
T = 50 min
T = 60 min
z [mm]
x [mm]

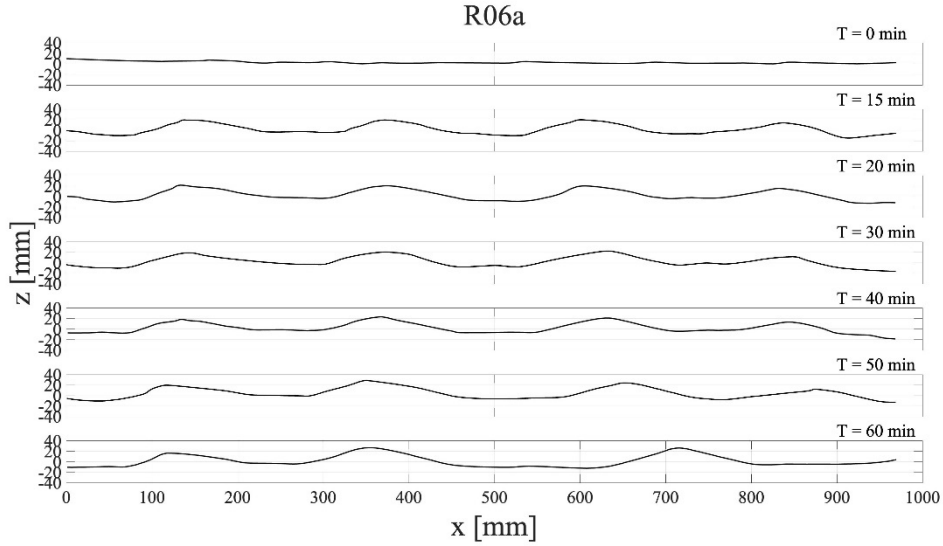
R06a
T = 0 min
T = 15 min
T = 20 min
T = 30 min
T = 40 min
T = 50 min
T = 60 min
z [mm]
x [mm]

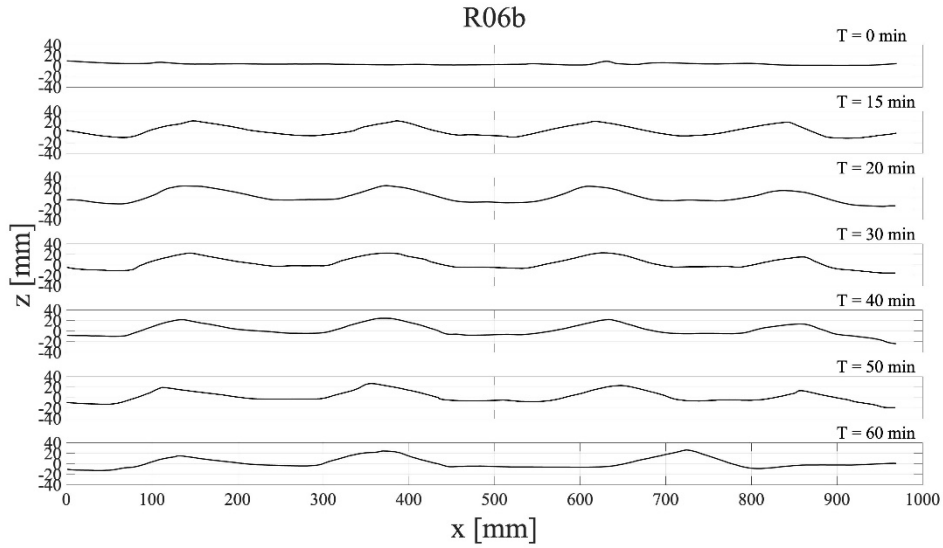
R06b
T = 0 min
T = 15 min
T = 20 min
T = 30 min
T = 40 min
T = 50 min
T = 60 min
z [mm]
x [mm]

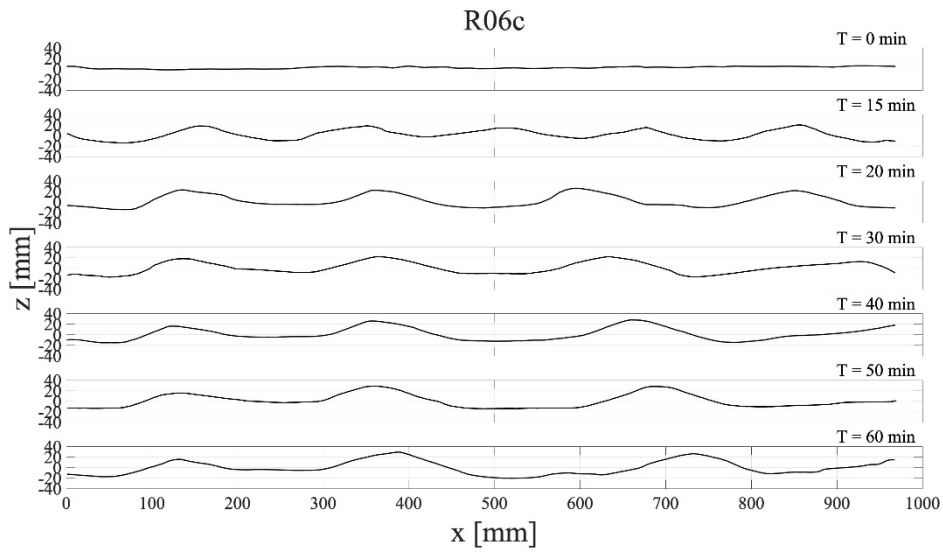
R06c
T = 0 min
T = 15 min
T = 20 min
T = 30 min
T = 40 min
T = 50 min
T = 60 min
z [mm]
x [mm]

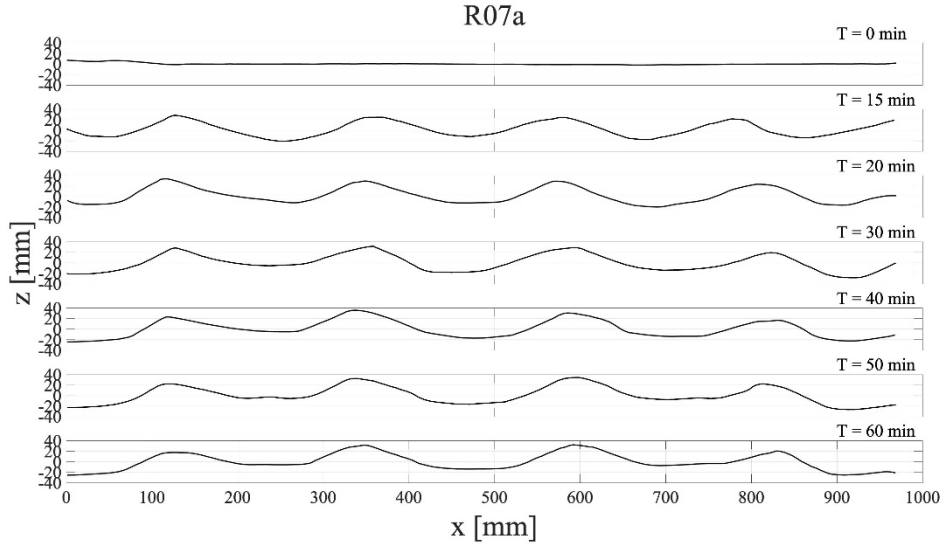
R07a
T = 0 min
T = 15 min
T = 20 min
T = 30 min
T = 40 min
T = 50 min
T = 60 min
z [mm]
x [mm]

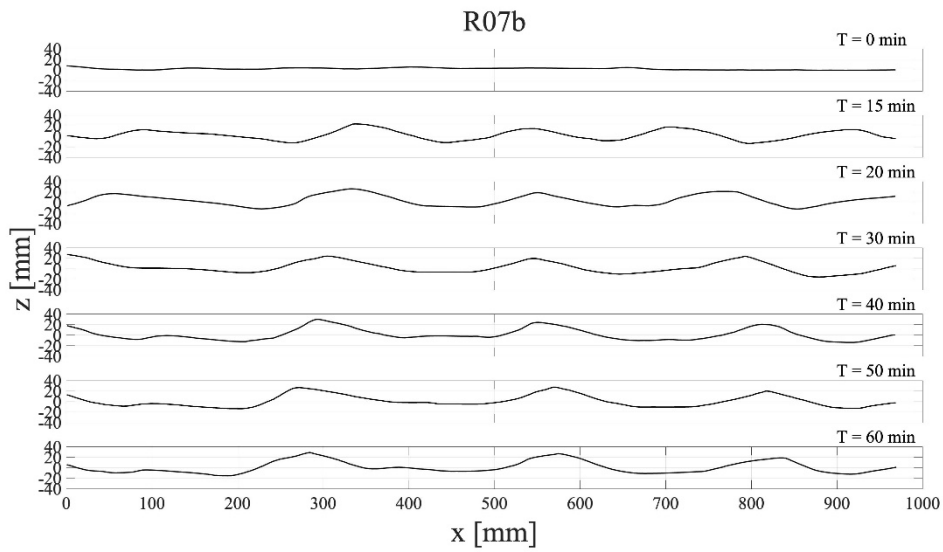
R07b
T = 0 min
T = 15 min
T = 20 min
T = 30 min
T = 40 min
T = 50 min
T = 60 min
z [mm]
x [mm]

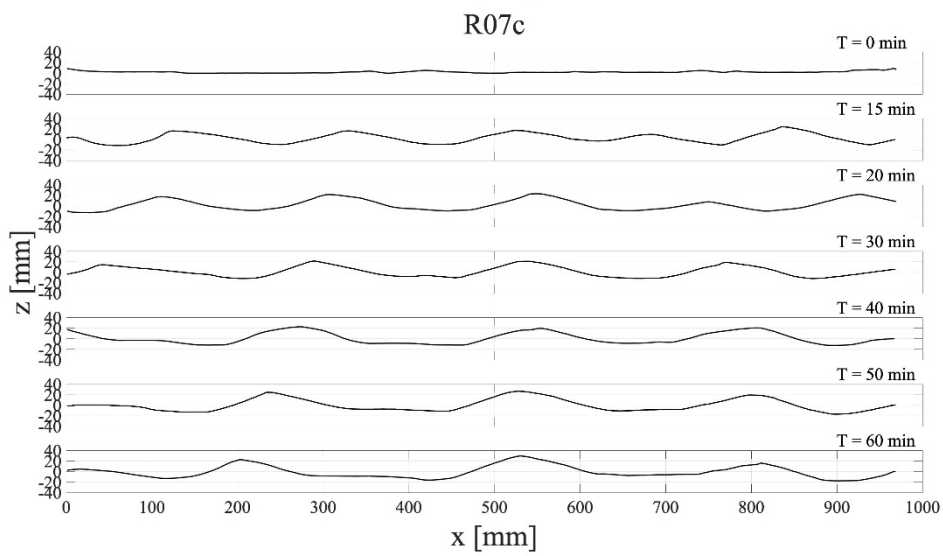
R07c
T = 0 min
T = 15 min
T = 20 min
T = 30 min
T = 40 min
T = 50 min
T = 60 min
z [mm]
x [mm]

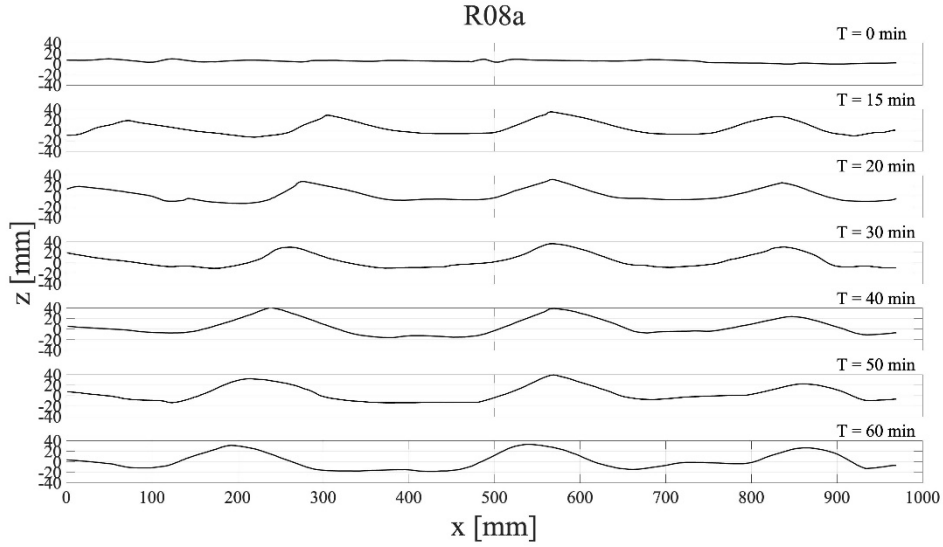
R08a
T = 0 min
T = 15 min
T = 20 min
T = 30 min
T = 40 min
T = 50 min
T = 60 min
z [mm]
x [mm]

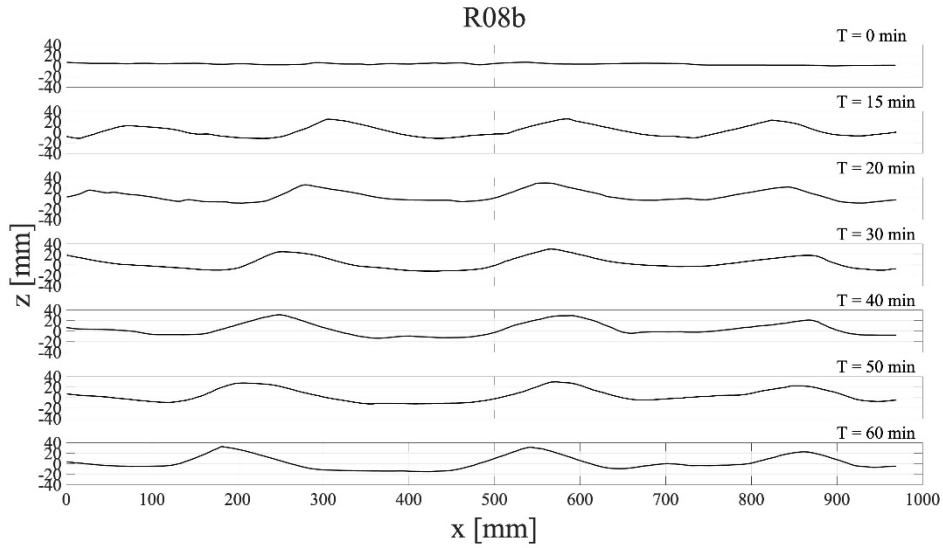
R08b
T = 0 min
T = 15 min
T = 20 min
T = 30 min
T = 40 min
T = 50 min
T = 60 min
z [mm]
x [mm]

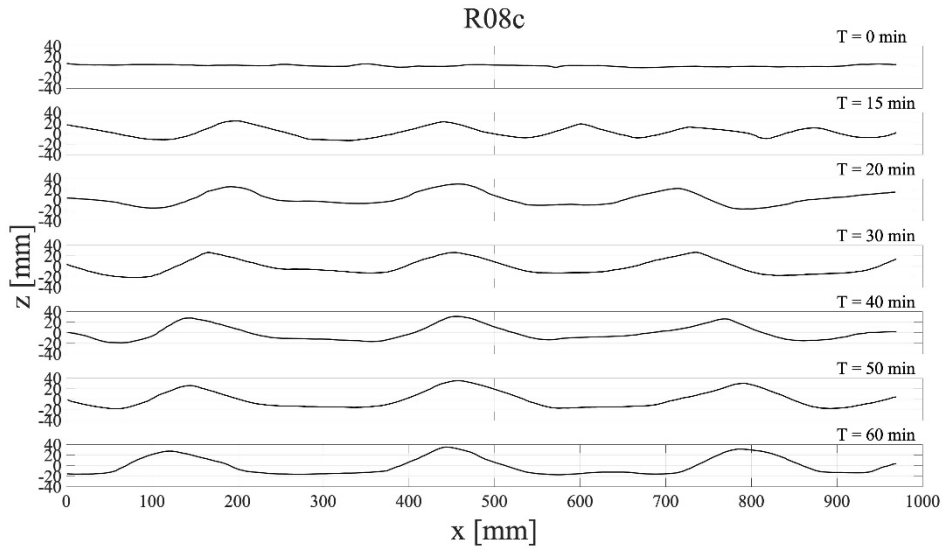
R08c
T = 0 min
T = 15 min
T = 20 min
T = 30 min
T = 40 min
T = 50 min
T = 60 min
z [mm]
x [mm]

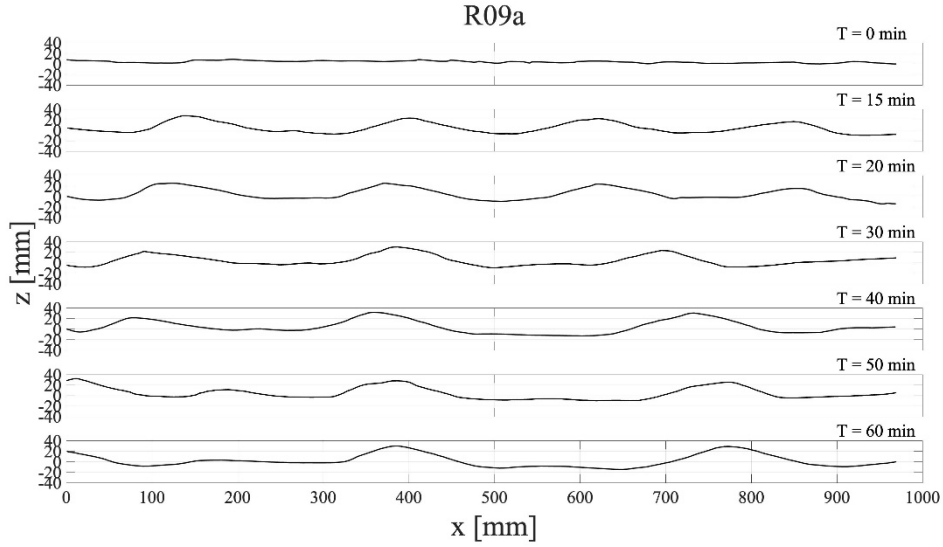
R09a
T = 0 min
T = 15 min
T = 20 min
T = 30 min
T = 40 min
T = 50 min
T = 60 min
z [mm]
x [mm]

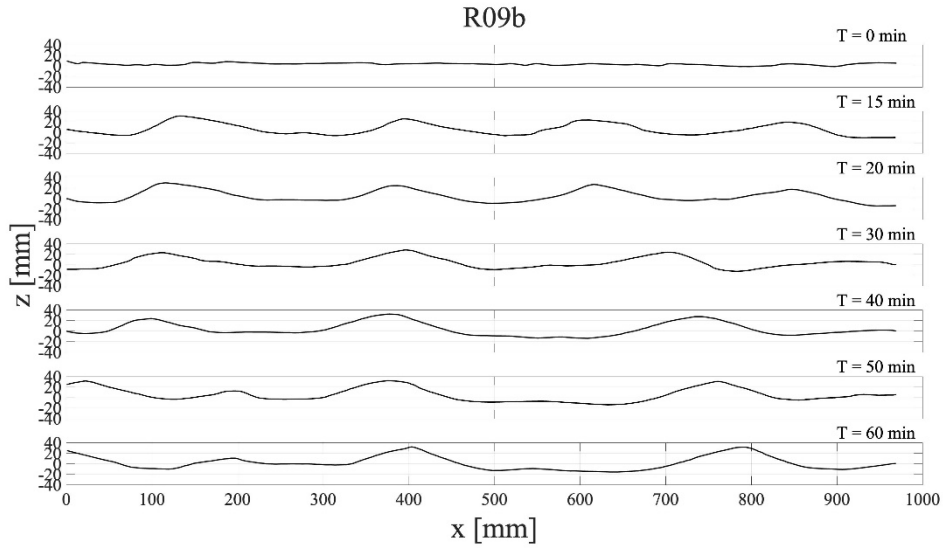
R09b
T = 0 min
T = 15 min
T = 20 min
T = 30 min
T = 40 min
T = 50 min
T = 60 min
z [mm]
x [mm]

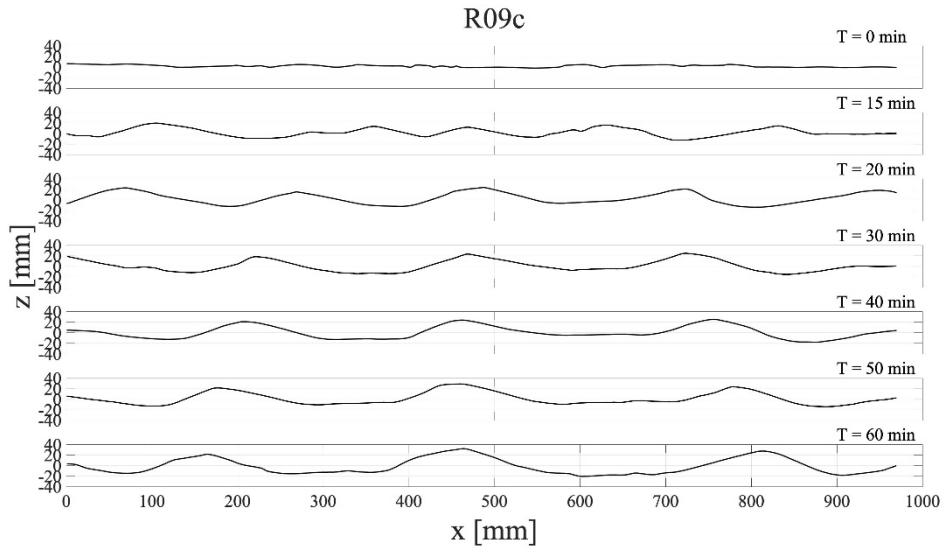
R09c
T = 0 min
T = 15 min
T = 20 min
T = 30 min
T = 40 min
T = 50 min
T = 60 min
z [mm]
x [mm]

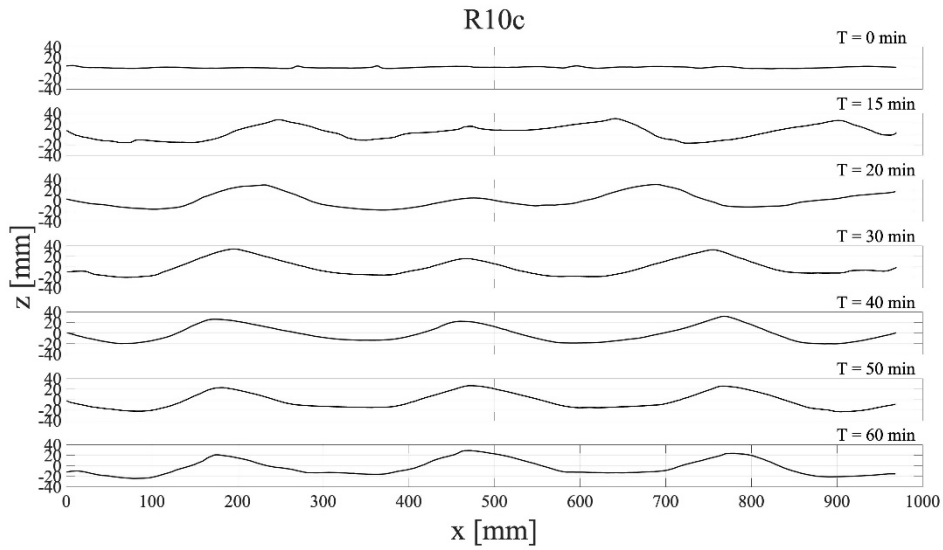
R10c
T = 0 min
T = 15 min
T = 20 min
T = 30 min
T = 40 min
T = 50 min
T = 60 min
z [mm]
x [mm]

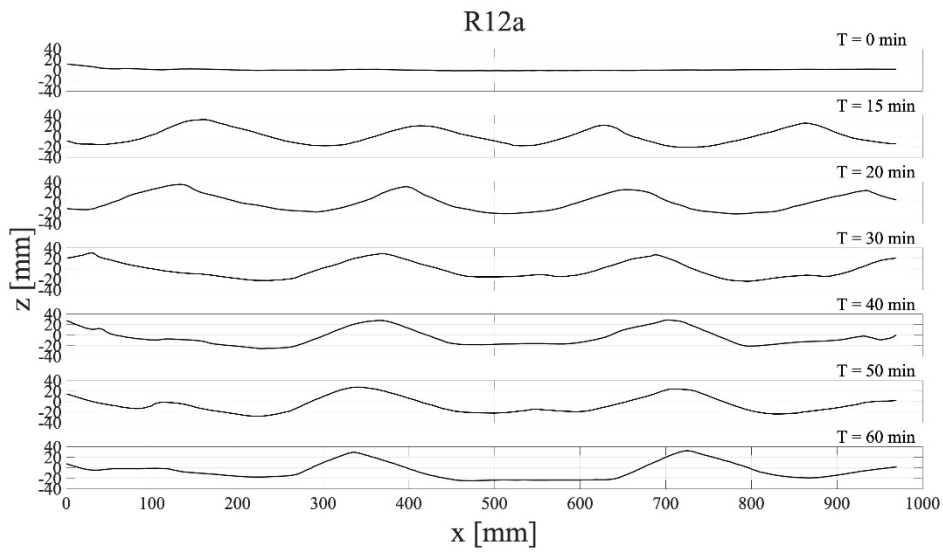
R12a
T = 0 min
T = 15 min
T = 20 min
T = 30 min
T = 40 min
T = 50 min
T = 60 min
z [mm]
x [mm]

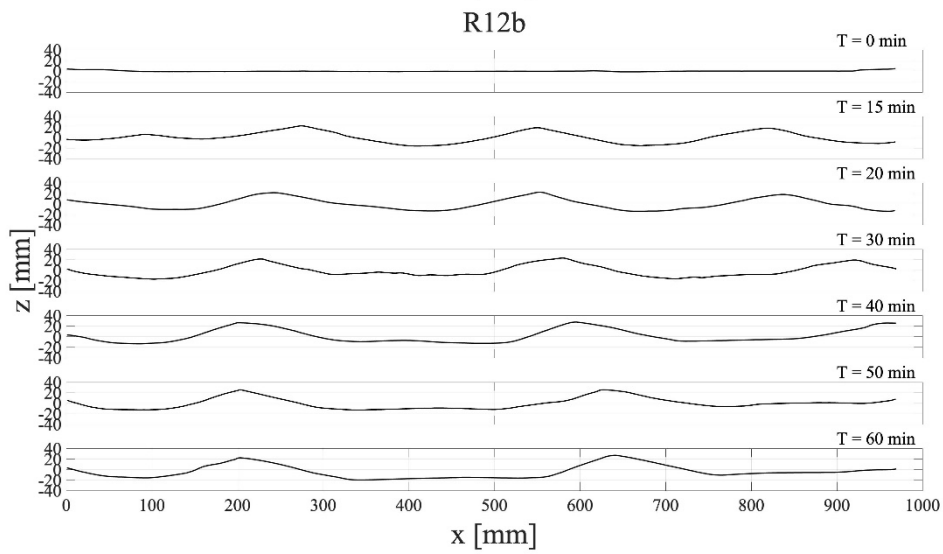
R12b
T = 0 min
T = 15 min
T = 20 min
T = 30 min
T = 40 min
T = 50 min
T = 60 min
z [mm]
x [mm]

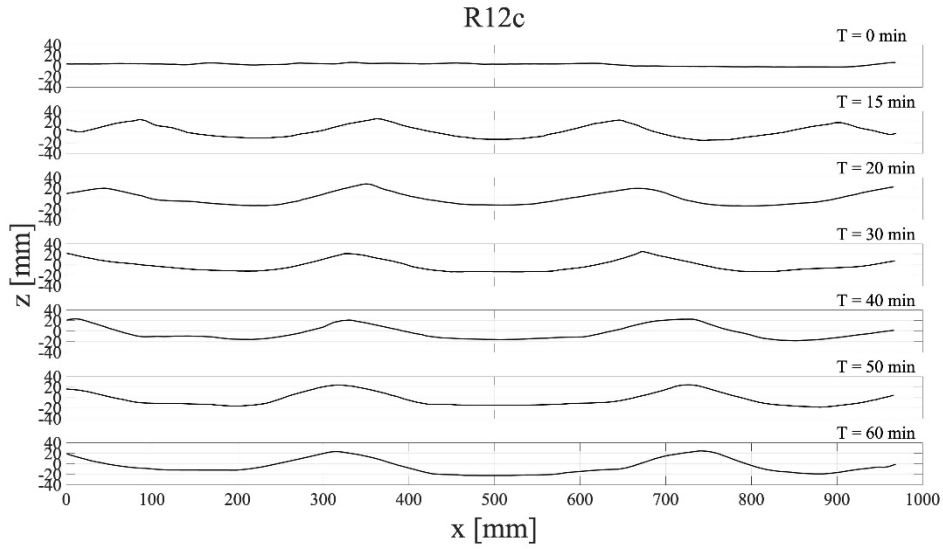
R12c
T = 0 min
T = 15 min
T = 20 min
T = 30 min
T = 40 min
T = 50 min
T = 60 min
z [mm]
x [mm]

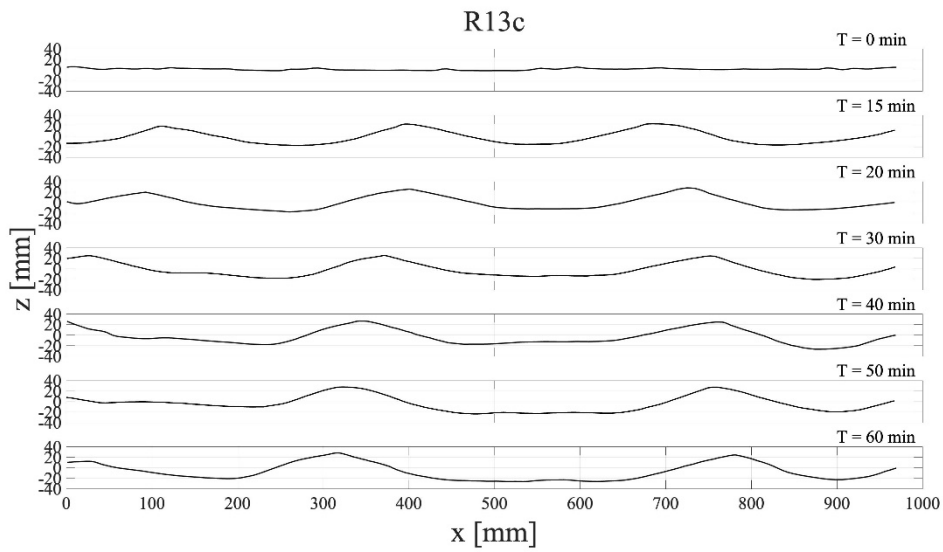
R13c
T = 0 min
T = 15 min
T = 20 min
T = 30 min
T = 40 min
T = 50 min
T = 60 min
z [mm]
x [mm]

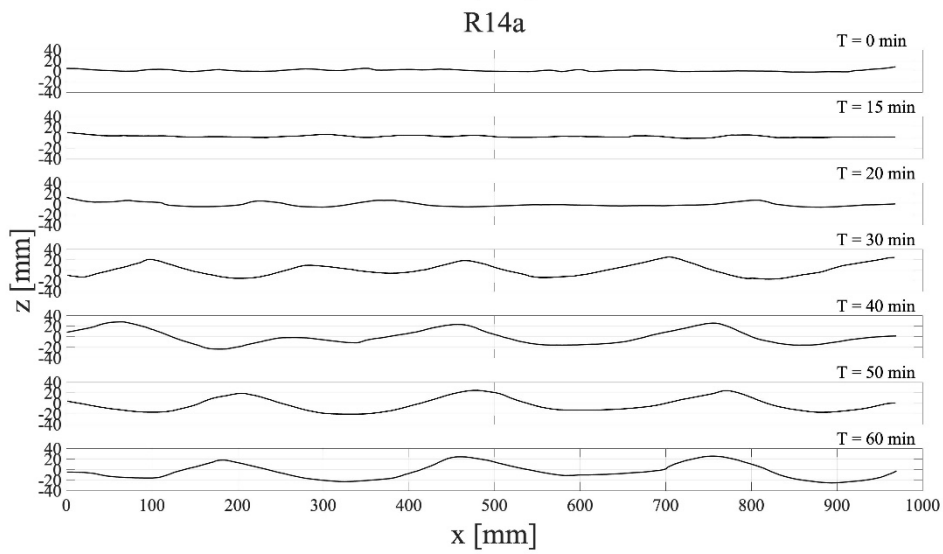
R14a
T = 0 min
T = 15 min
T = 20 min
T = 30 min
T = 40 min
T = 50 min
T = 60 min
z [mm]
x [mm]

APPENDIX C:
Length between ripples on reference depths over time

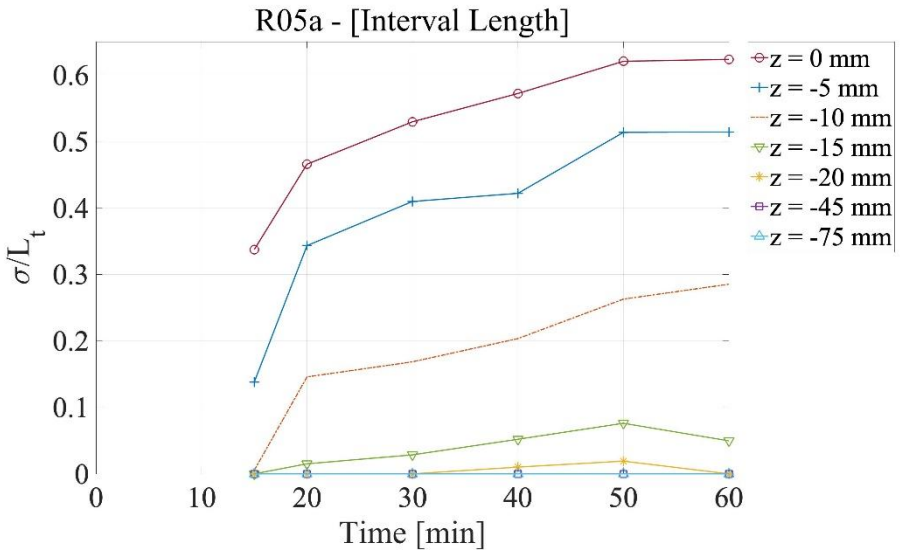
R05a - [Interval Length]
σ/L_t
Time [min]
z = 0 mm
z = -5 mm
z = -10 mm
z = -15 mm
z = -20 mm
z = -45 mm
z = -75 mm

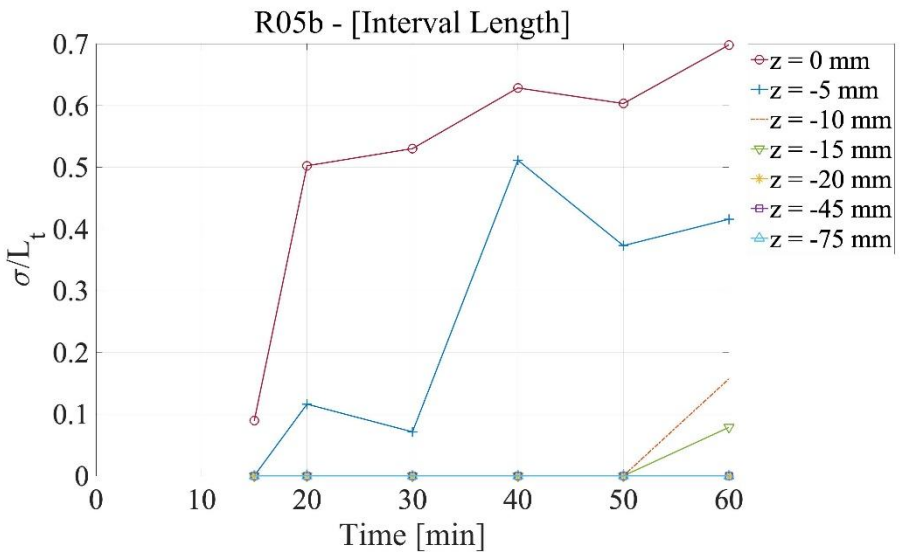
R05b - [Interval Length]
σ/L_t
Time [min]
z = 0 mm
z = -5 mm
z = -10 mm
z = -15 mm
z = -20 mm
z = -45 mm
z = -75 mm

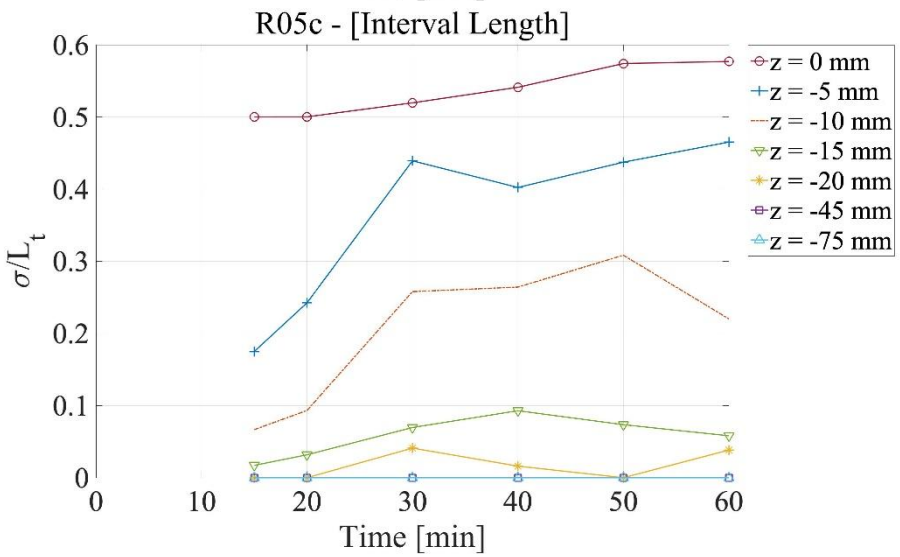
R05c - [Interval Length]
σ/L_t
Time [min]
z = 0 mm
z = -5 mm
z = -10 mm
z = -15 mm
z = -20 mm
z = -45 mm
z = -75 mm

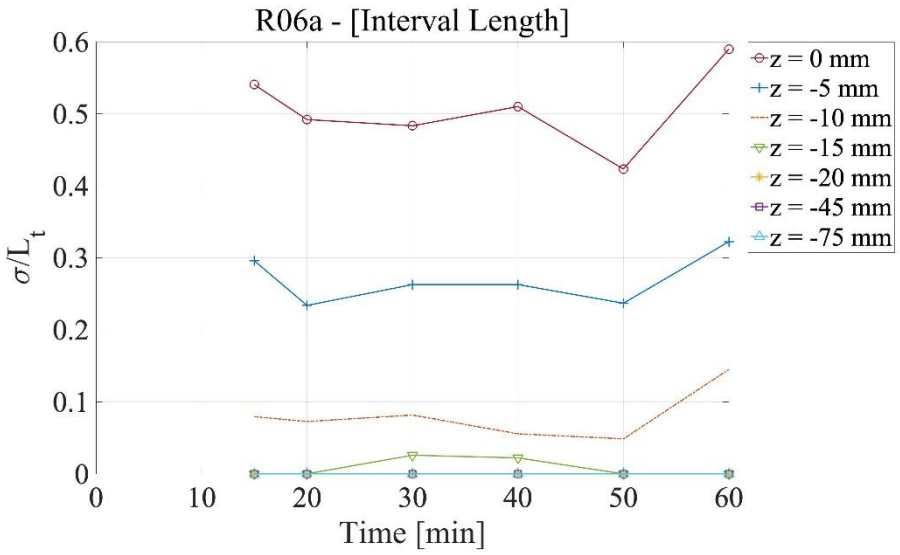
R06a - [Interval Length]
σ/L_t
Time [min]
z = 0 mm
z = -5 mm
z = -10 mm
z = -15 mm
z = -20 mm
z = -45 mm
z = -75 mm

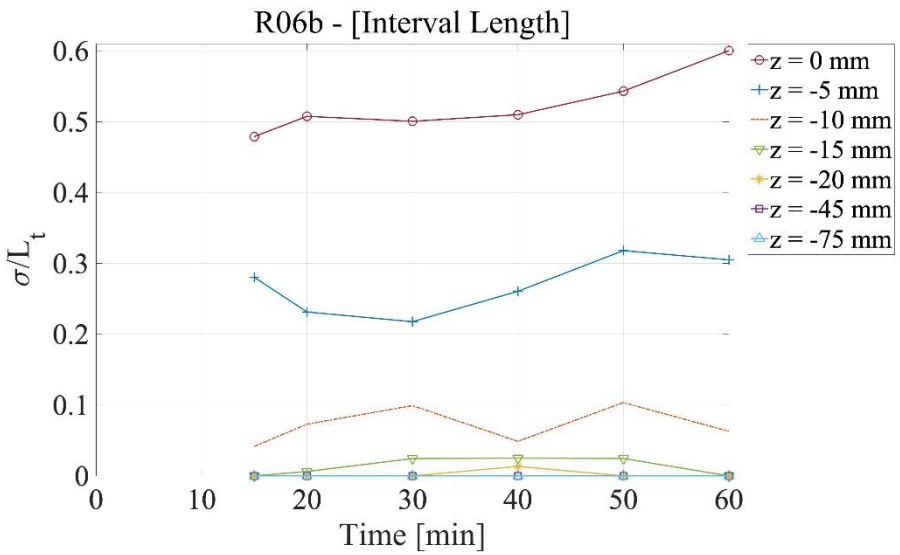
R06b - [Interval Length]
σ/L_t
Time [min]
z = 0 mm
z = -5 mm
z = -10 mm
z = -15 mm
z = -20 mm
z = -45 mm
z = -75 mm

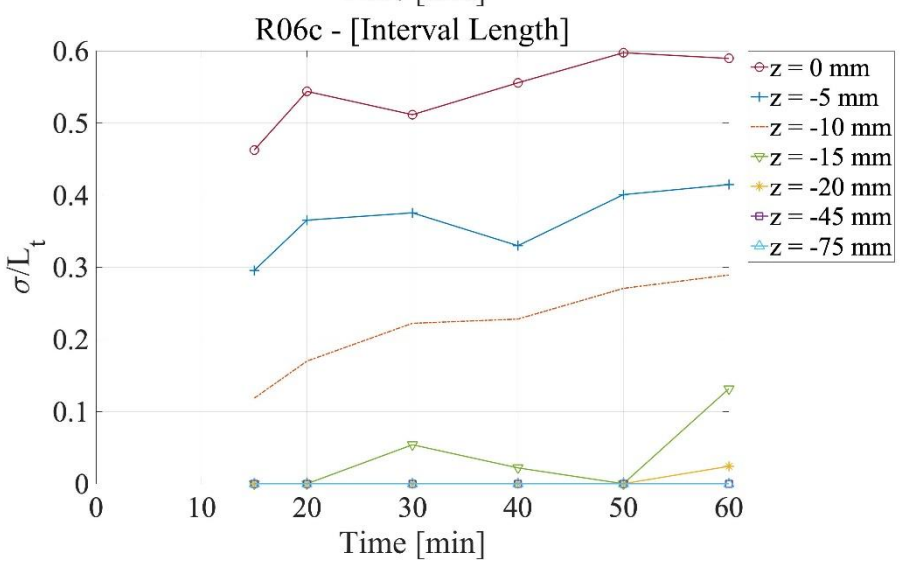
R06c - [Interval Length]
σ/L_t
Time [min]
z = 0 mm
z = -5 mm
z = -10 mm
z = -15 mm
z = -20 mm
z = -45 mm
z = -75 mm

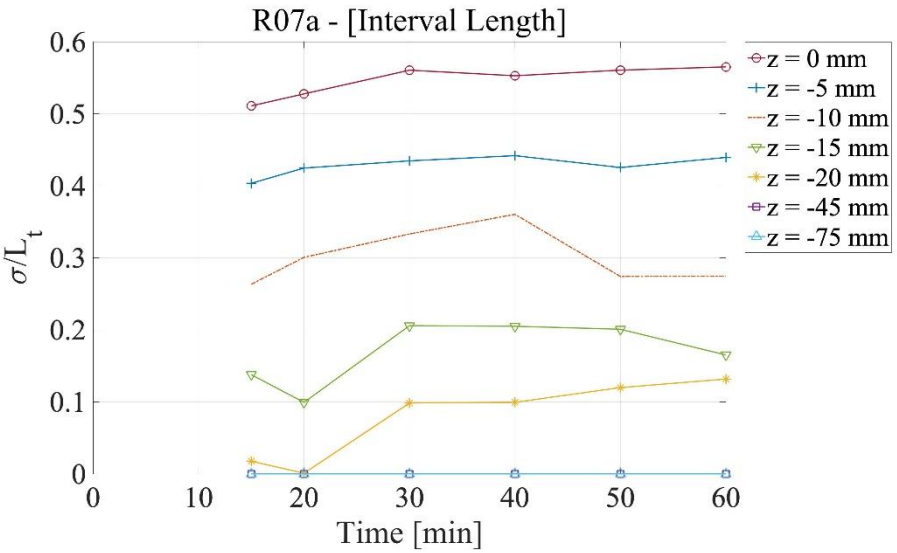
R07a - [Interval Length]
σ/L_t
Time [min]
z = 0 mm
z = -5 mm
z = -10 mm
z = -15 mm
z = -20 mm
z = -45 mm
z = -75 mm

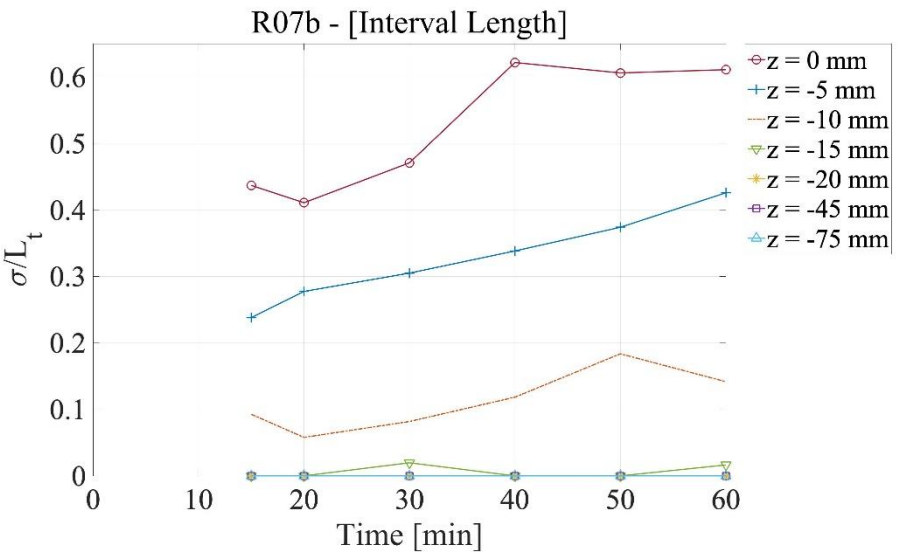
R07b - [Interval Length]
σ/L_t
Time [min]
z = 0 mm
z = -5 mm
z = -10 mm
z = -15 mm
z = -20 mm
z = -45 mm
z = -75 mm

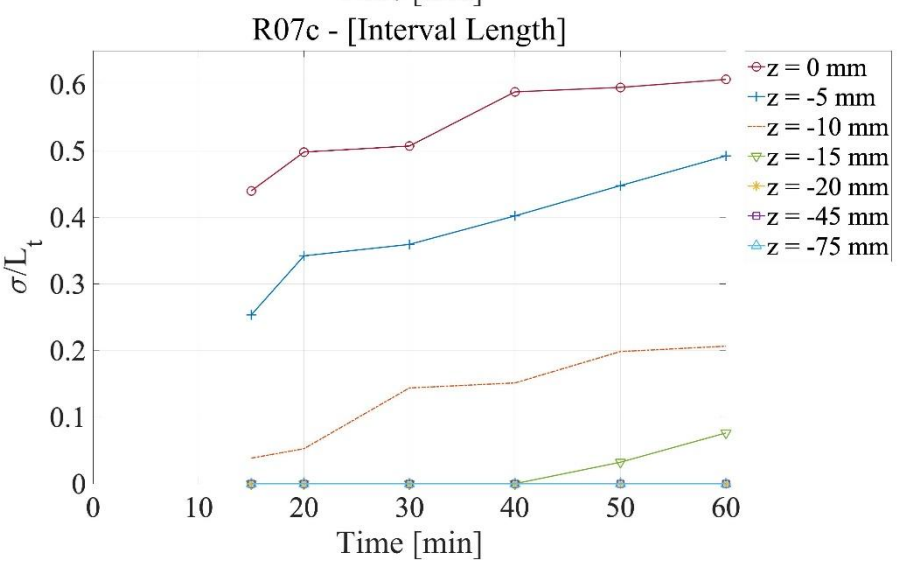
R07c - [Interval Length]
σ/L_t
Time [min]
z = 0 mm
z = -5 mm
z = -10 mm
z = -15 mm
z = -20 mm
z = -45 mm
z = -75 mm

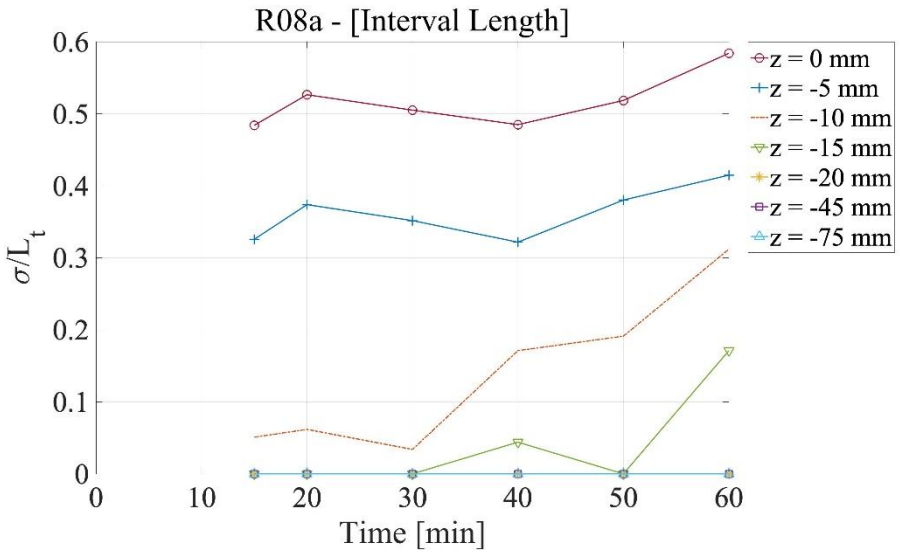
R08a - [Interval Length]
σ/L_t
Time [min]
z = 0 mm
z = -5 mm
z = -10 mm
z = -15 mm
z = -20 mm
z = -45 mm
z = -75 mm

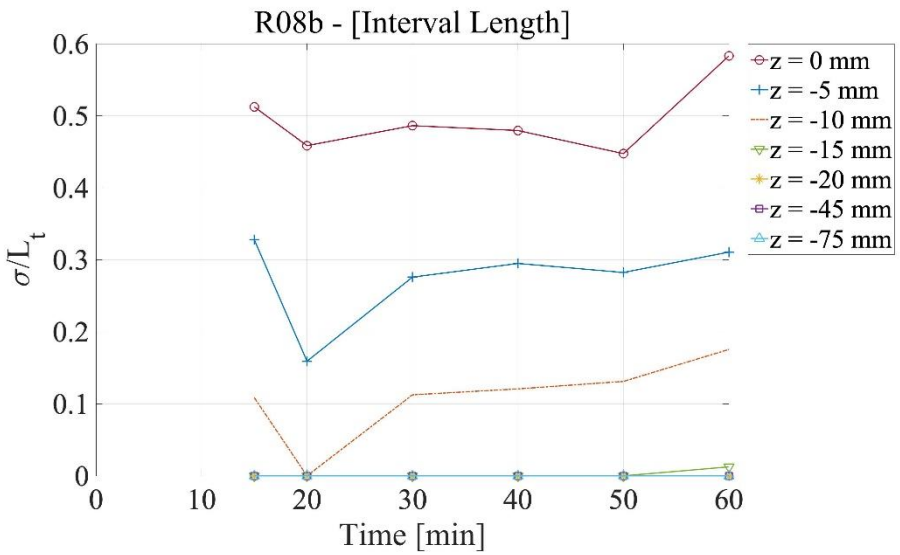
R08b - [Interval Length]
σ/L_t
Time [min]
z = 0 mm
z = -5 mm
z = -10 mm
z = -15 mm
z = -20 mm
z = -45 mm
z = -75 mm

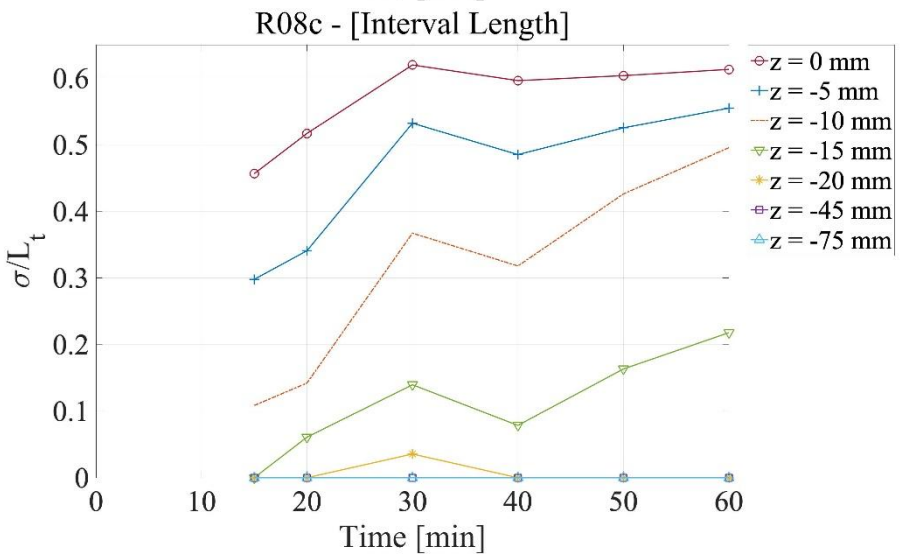
R08c - [Interval Length]
σ/L_t
Time [min]
z = 0 mm
z = -5 mm
z = -10 mm
z = -15 mm
z = -20 mm
z = -45 mm
z = -75 mm

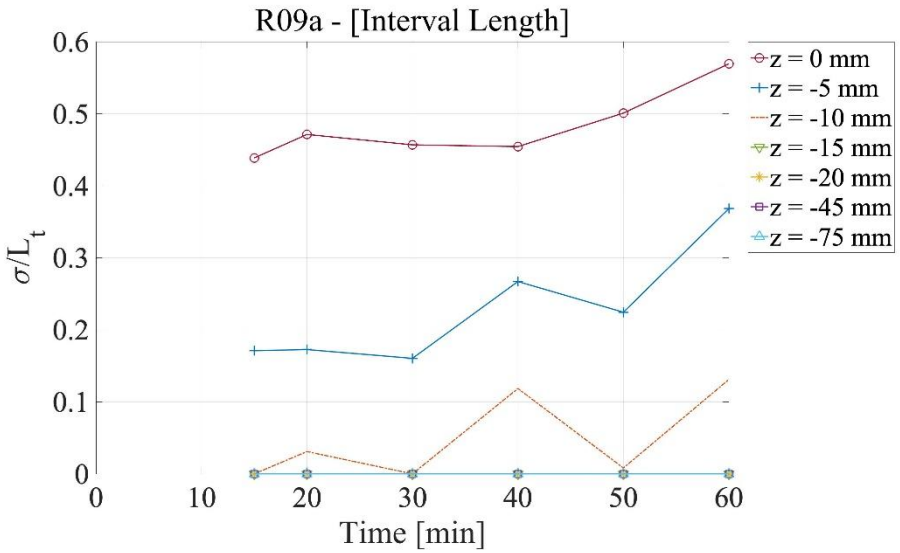
R09a - [Interval Length]
σ/L_t
Time [min]
z = 0 mm
z = -5 mm
z = -10 mm
z = -15 mm
z = -20 mm
z = -45 mm
z = -75 mm

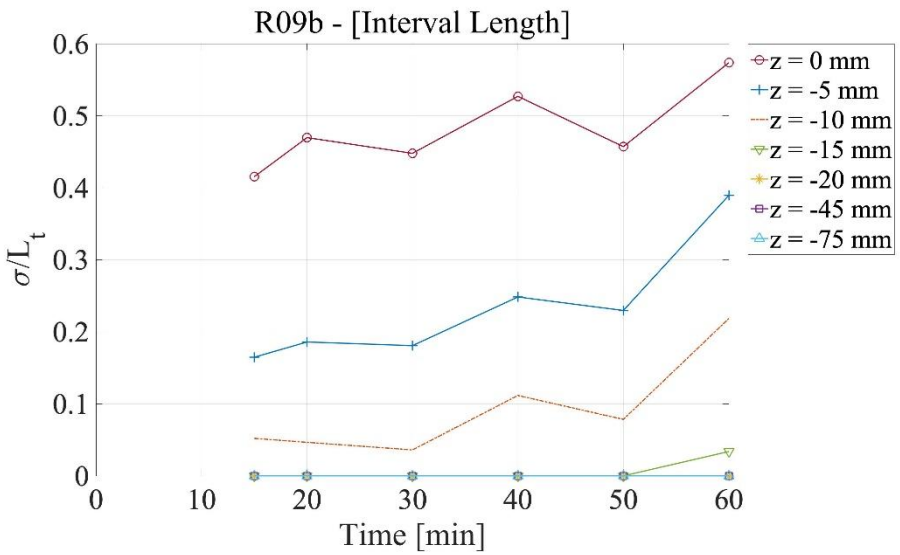
R09b - [Interval Length]
σ/L_t
Time [min]
z = 0 mm
z = -5 mm
z = -10 mm
z = -15 mm
z = -20 mm
z = -45 mm
z = -75 mm

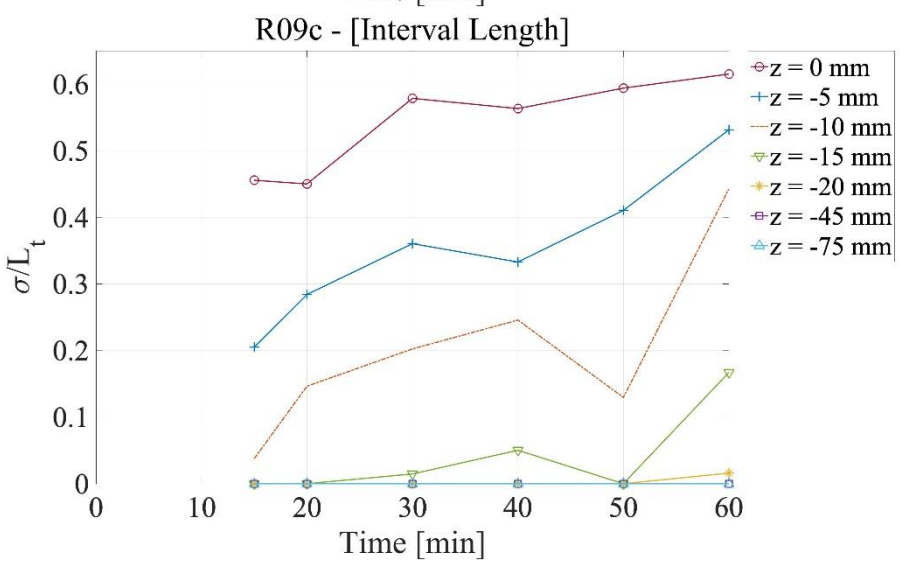
R09c - [Interval Length]
σ/L_t
Time [min]
z = 0 mm
z = -5 mm
z = -10 mm
z = -15 mm
z = -20 mm
z = -45 mm
z = -75 mm

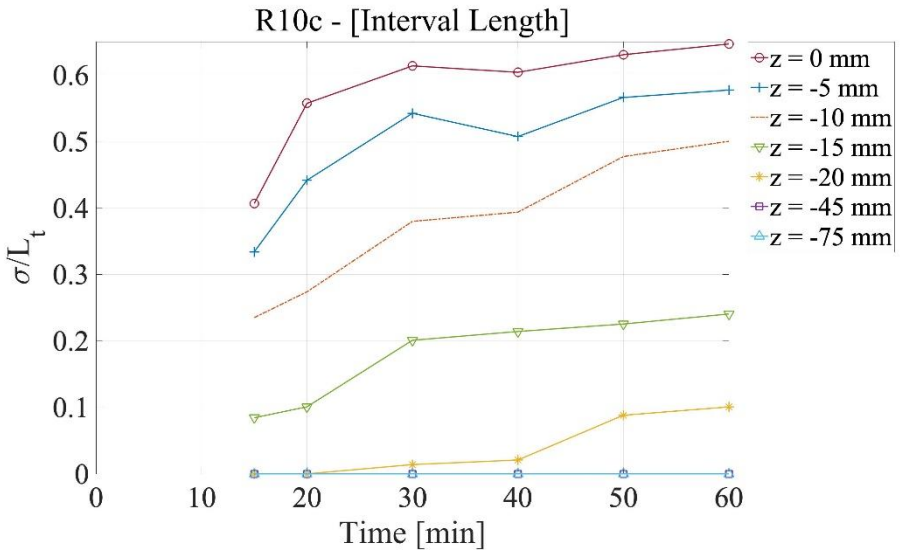
R10c - [Interval Length]
σ/L_t
Time [min]
z = 0 mm
z = -5 mm
z = -10 mm
z = -15 mm
z = -20 mm
z = -45 mm
z = -75 mm

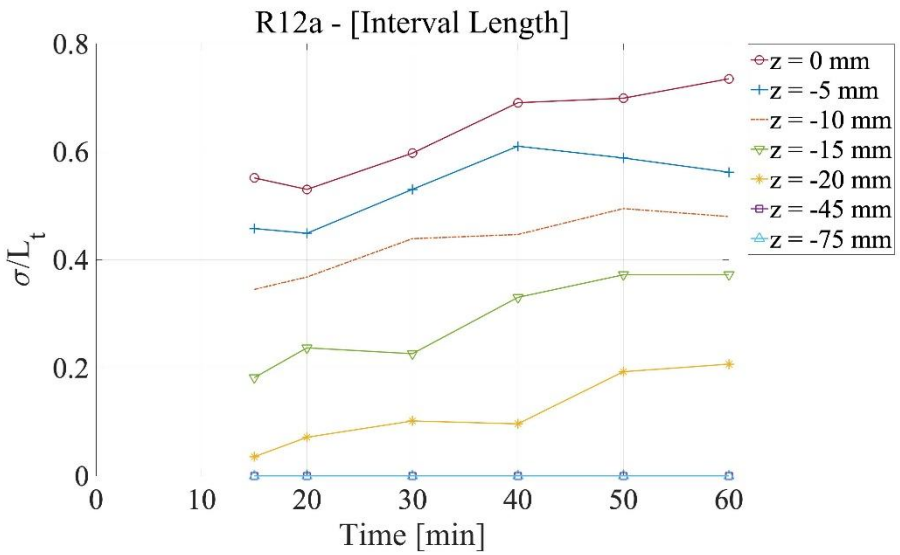
R12a - [Interval Length]
σ/L_t
Time [min]
z = 0 mm
z = -5 mm
z = -10 mm
z = -15 mm
z = -20 mm
z = -45 mm
z = -75 mm

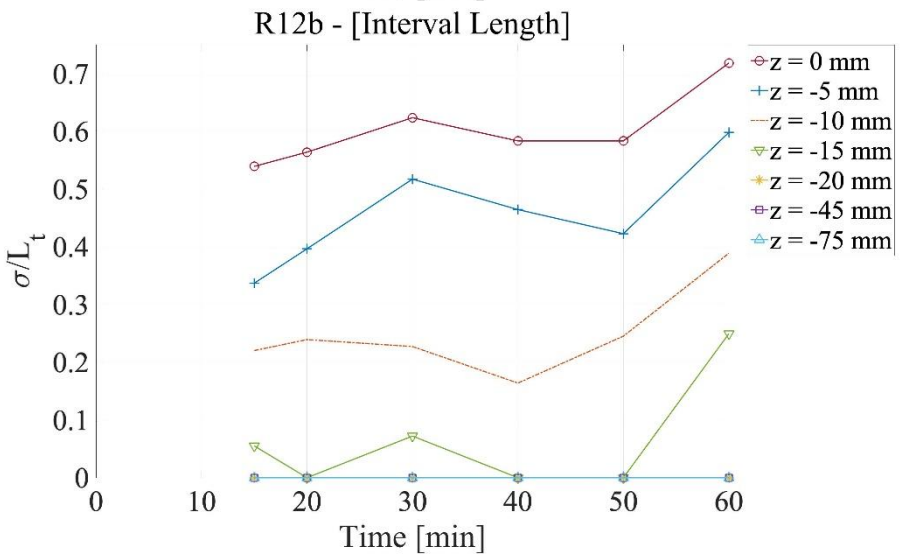
R12b - [Interval Length]
σ/L_t
Time [min]
z = 0 mm
z = -5 mm
z = -10 mm
z = -15 mm
z = -20 mm
z = -45 mm
z = -75 mm

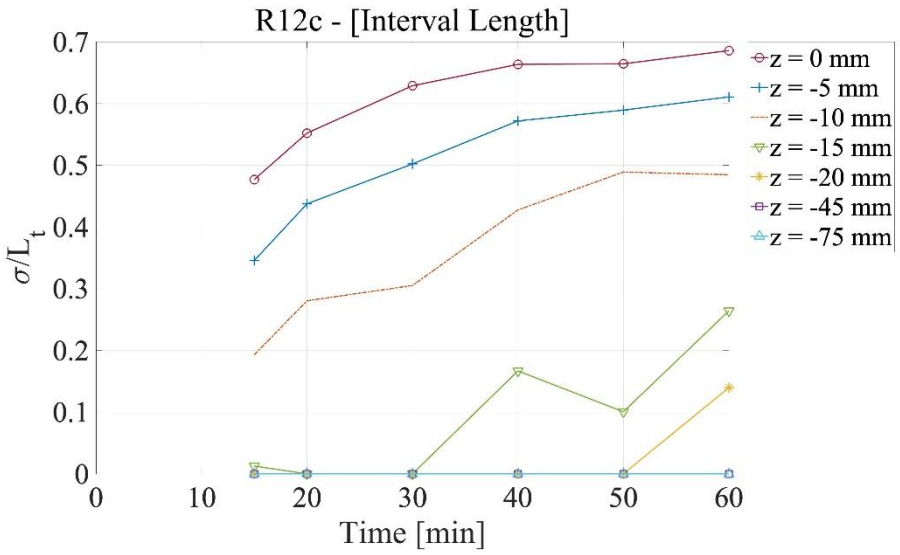
R12c - [Interval Length]
σ/L_t
Time [min]
z = 0 mm
z = -5 mm
z = -10 mm
z = -15 mm
z = -20 mm
z = -45 mm
z = -75 mm

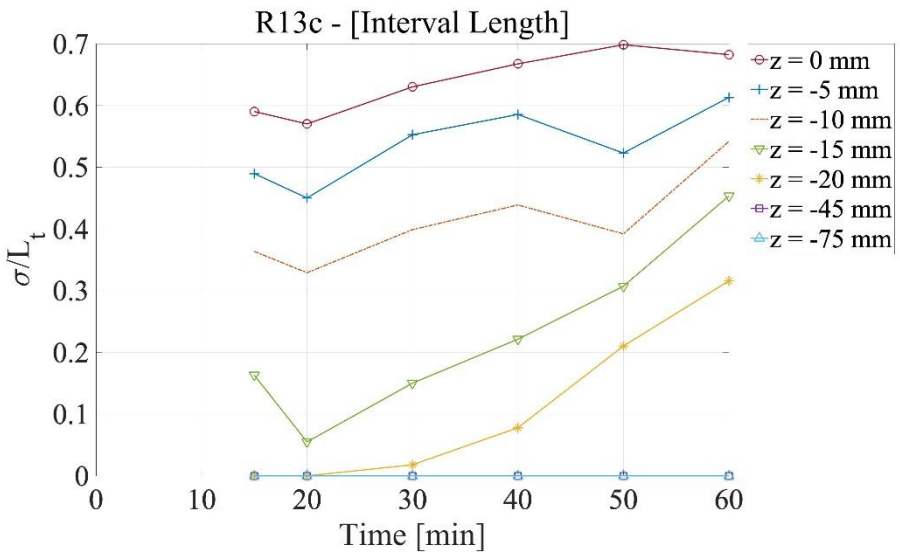
R13c - [Interval Length]
σ/L_t
Time [min]
z = 0 mm
z = -5 mm
z = -10 mm
z = -15 mm
z = -20 mm
z = -45 mm
z = -75 mm

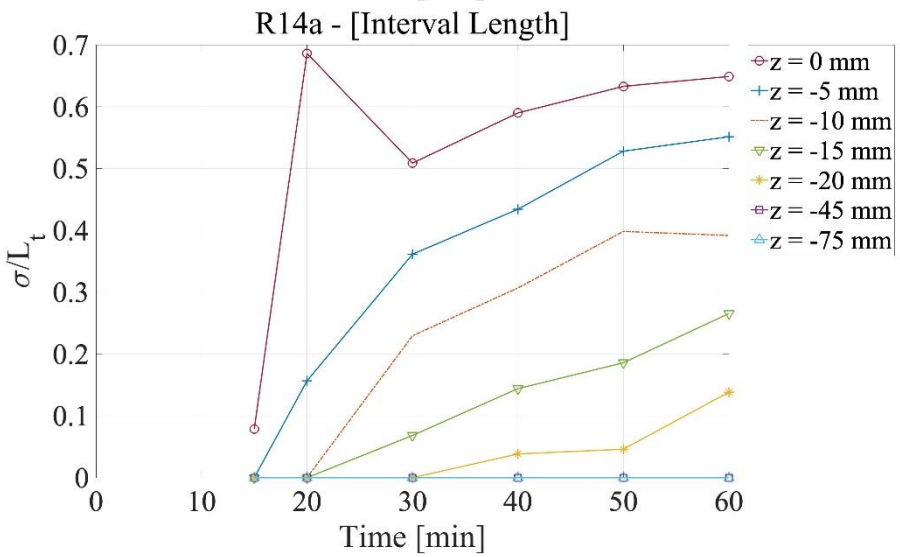
R14a - [Interval Length]
σ/L_t
Time [min]
z = 0 mm
z = -5 mm
z = -10 mm
z = -15 mm
z = -20 mm
z = -45 mm
z = -75 mm

APPENDIX D:
Two-dimensional area of ripple under reference depths over time

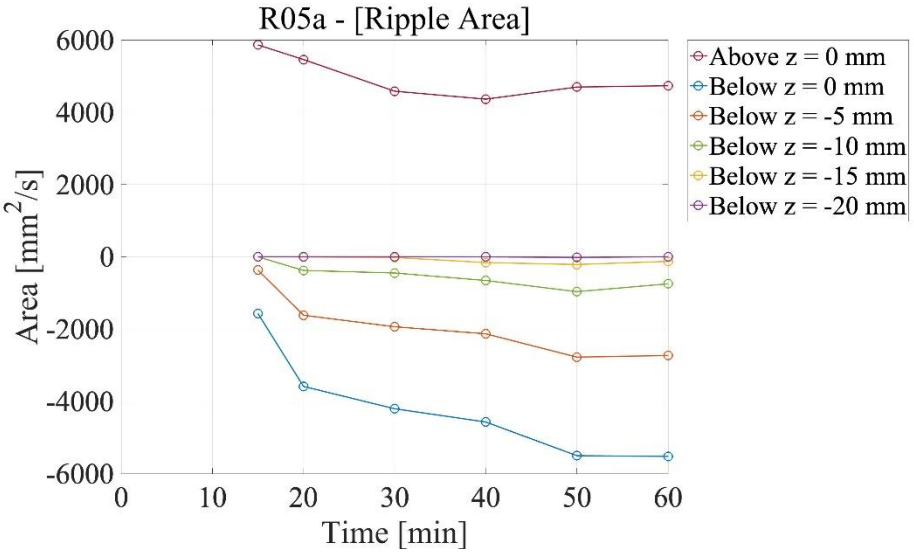
R05a - [Ripple Area]
Area [mm²/s]
Time [min]
Above z = 0 mm
Below z = 0 mm
Below z = -5 mm
Below z = -10 mm
Below z = -15 mm
Below z = -20 mm

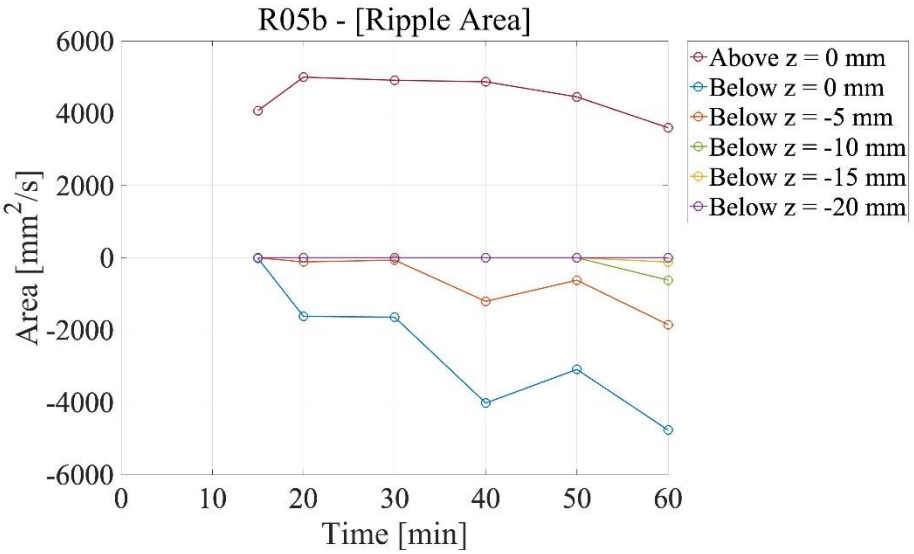
R05b - [Ripple Area]
Area [mm²/s]
Time [min]
Above z = 0 mm
Below z = 0 mm
Below z = -5 mm
Below z = -10 mm
Below z = -15 mm
Below z = -20 mm

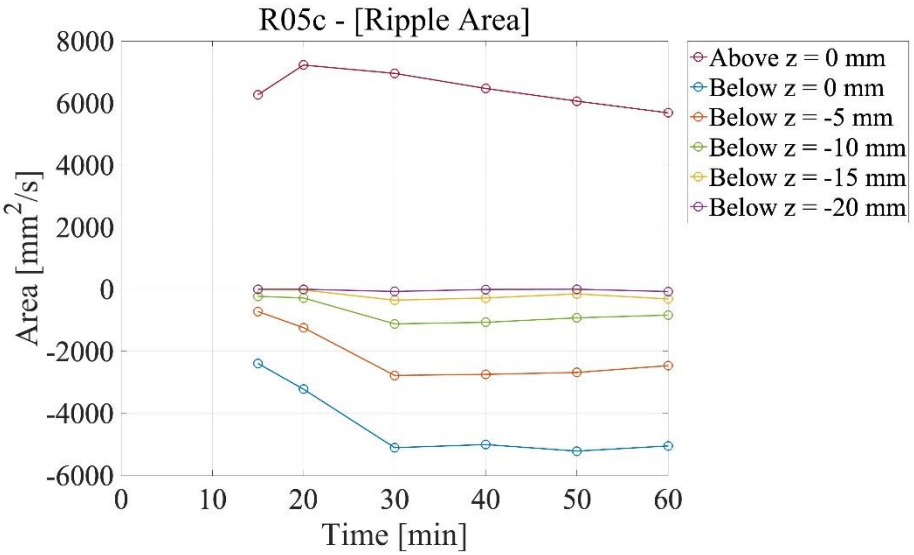
R05c - [Ripple Area]
Area [mm²/s]
Time [min]
Above z = 0 mm
Below z = 0 mm
Below z = -5 mm
Below z = -10 mm
Below z = -15 mm
Below z = -20 mm

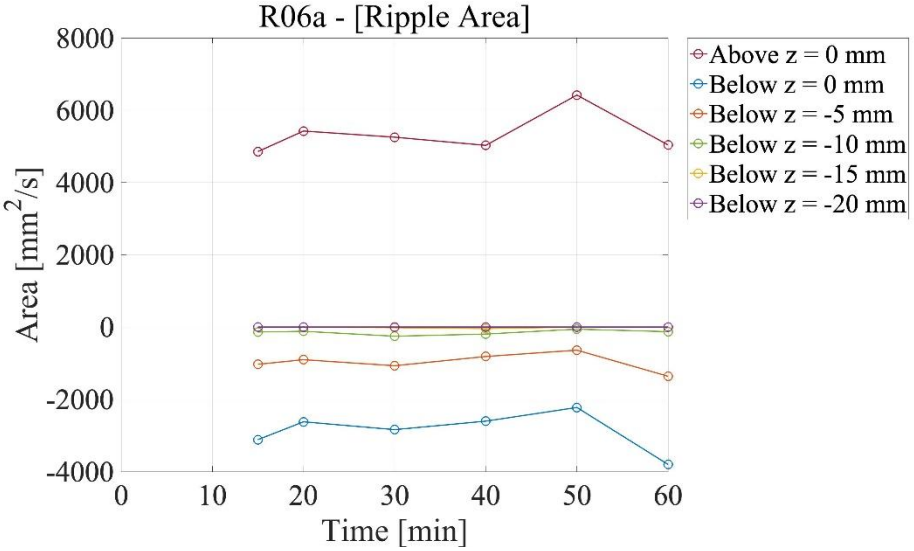
R06a - [Ripple Area]
Area [mm²/s]
Time [min]
Above z = 0 mm
Below z = 0 mm
Below z = -5 mm
Below z = -10 mm
Below z = -15 mm
Below z = -20 mm

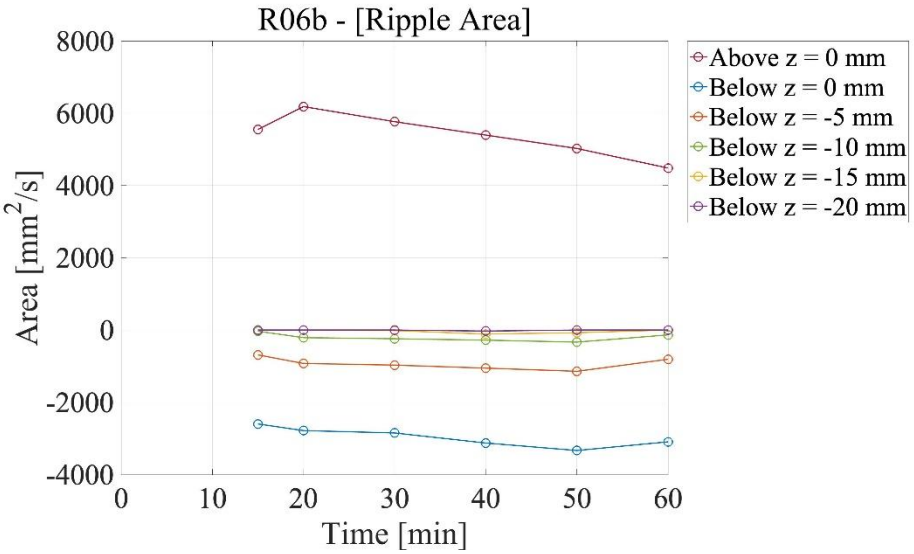
R06b - [Ripple Area]
Area [mm²/s]
Time [min]
Above z = 0 mm
Below z = 0 mm
Below z = -5 mm
Below z = -10 mm
Below z = -15 mm
Below z = -20 mm

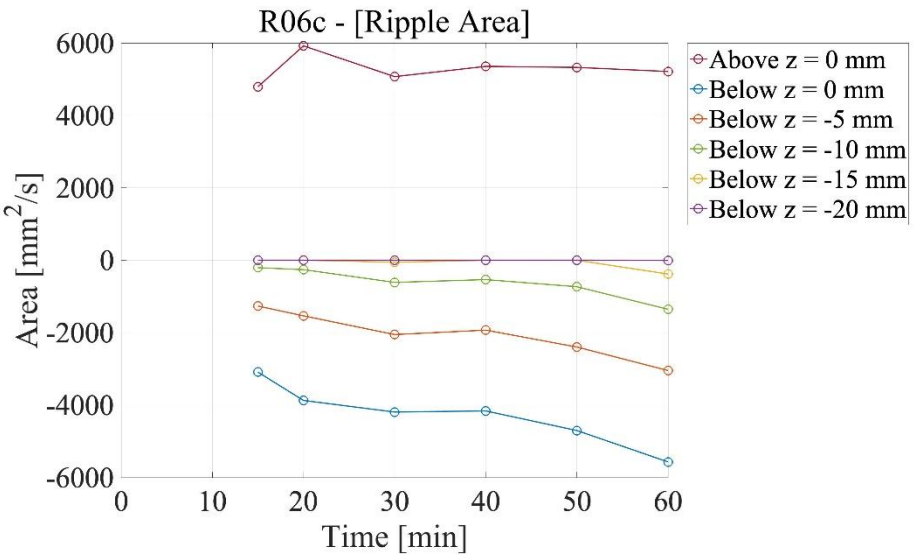
R06c - [Ripple Area]
Area [mm²/s]
Time [min]
Above z = 0 mm
Below z = 0 mm
Below z = -5 mm
Below z = -10 mm
Below z = -15 mm
Below z = -20 mm

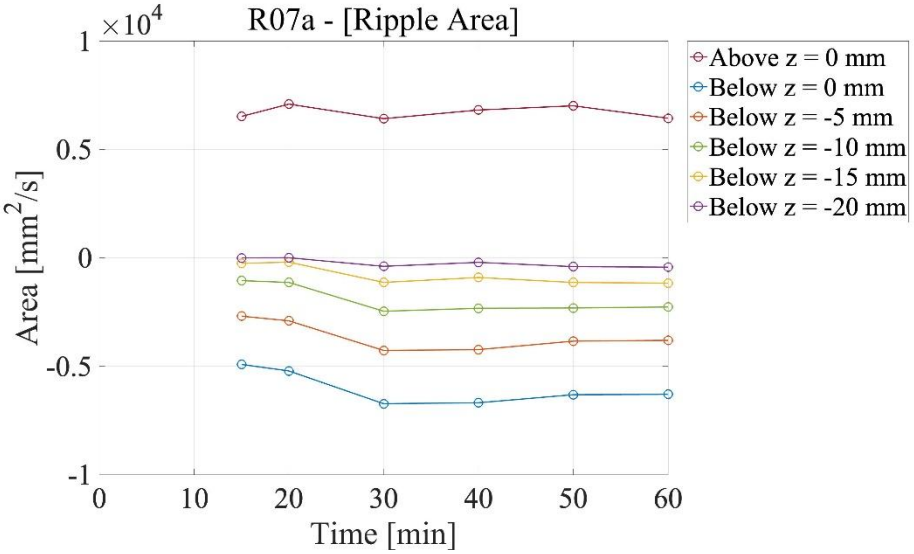
R07a - [Ripple Area]
×10^4
1
0.5
0
-0.5
-1
Area [mm^2/s]
0
10
20
30
40
50
60
Time [min]
Above z = 0 mm
Below z = 0 mm
Below z = -5 mm
Below z = -10 mm
Below z = -15 mm
Below z = -20 mm

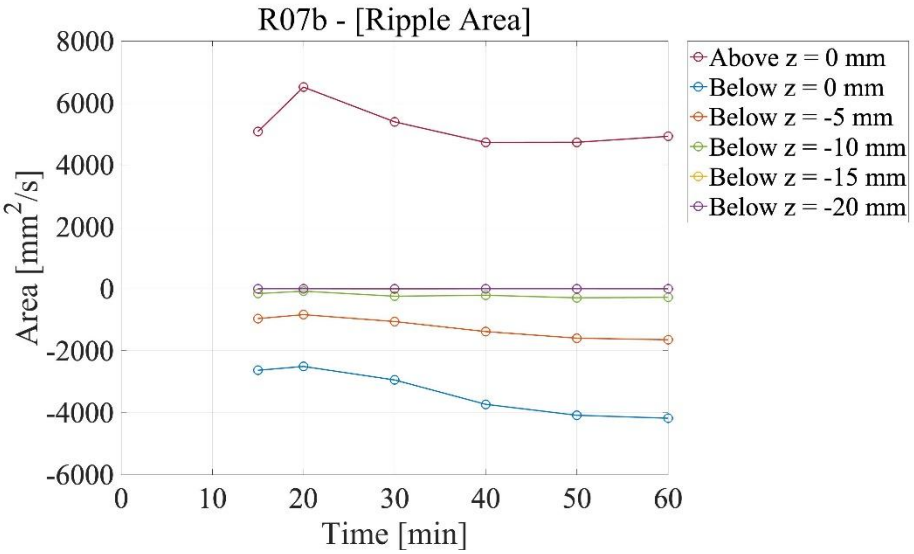
R07b - [Ripple Area]
8000
6000
4000
2000
0
-2000
-4000
-6000
Area [mm^2/s]
0
10
20
30
40
50
60
Time [min]
Above z = 0 mm
Below z = 0 mm
Below z = -5 mm
Below z = -10 mm
Below z = -15 mm
Below z = -20 mm

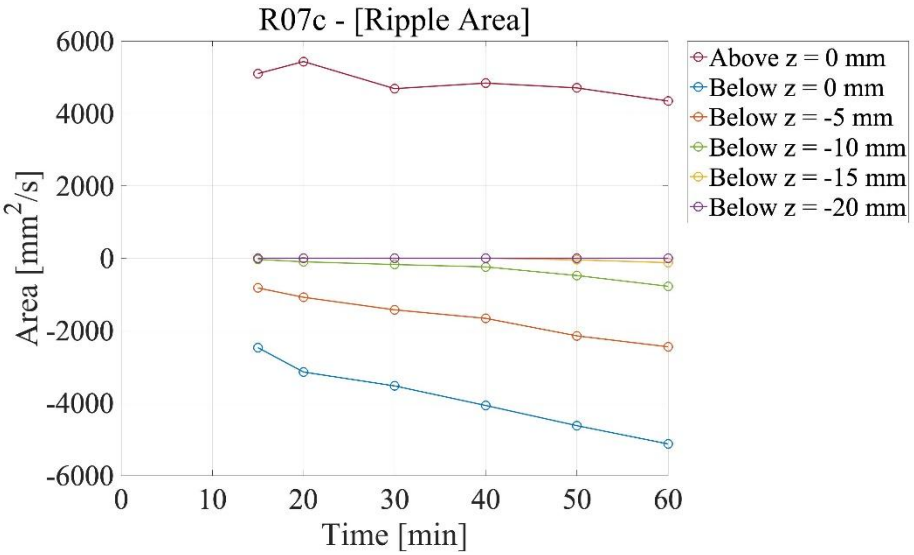
R07c - [Ripple Area]
6000
4000
2000
0
-2000
-4000
-6000
Area [mm^2/s]
0
10
20
30
40
50
60
Time [min]
Above z = 0 mm
Below z = 0 mm
Below z = -5 mm
Below z = -10 mm
Below z = -15 mm
Below z = -20 mm

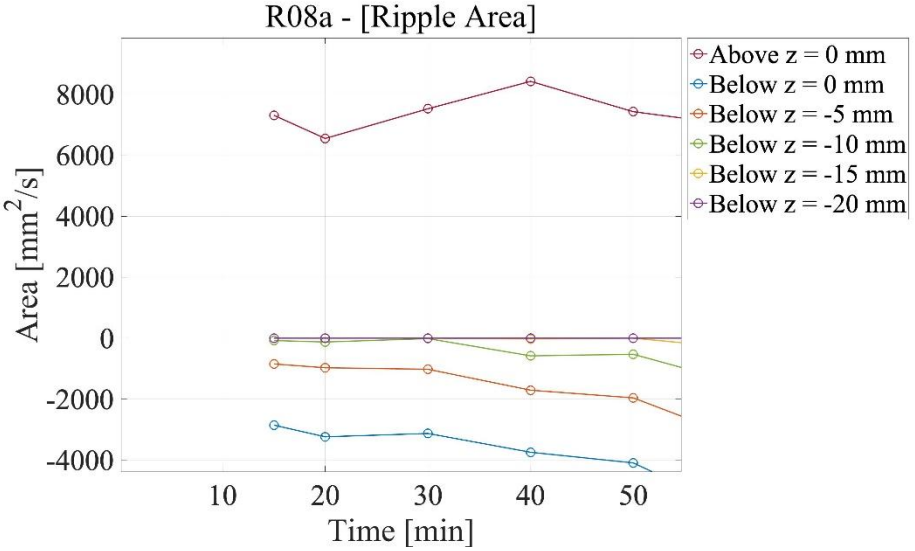
R08a - [Ripple Area]
Area [mm²/s]
Time [min]
Above z = 0 mm
Below z = 0 mm
Below z = -5 mm
Below z = -10 mm
Below z = -15 mm
Below z = -20 mm

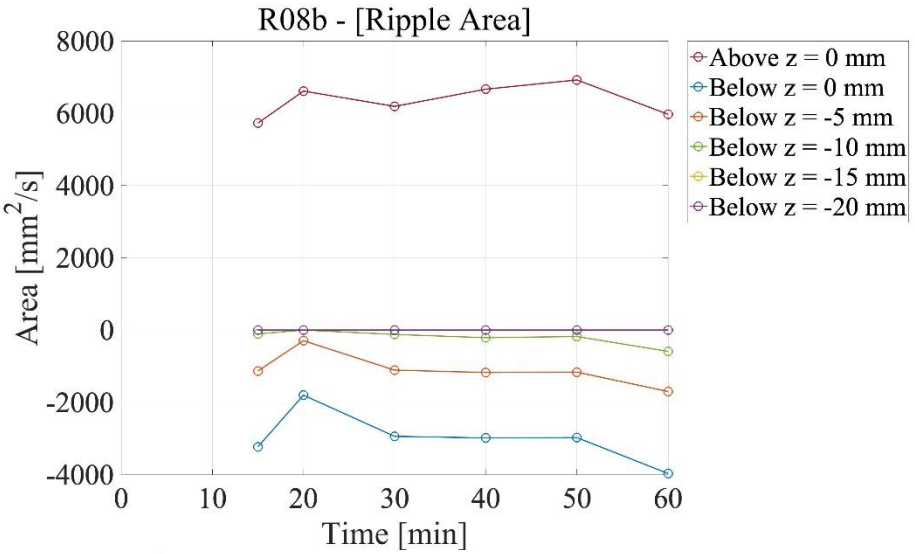
R08b - [Ripple Area]
Area [mm²/s]
Time [min]
Above z = 0 mm
Below z = 0 mm
Below z = -5 mm
Below z = -10 mm
Below z = -15 mm
Below z = -20 mm

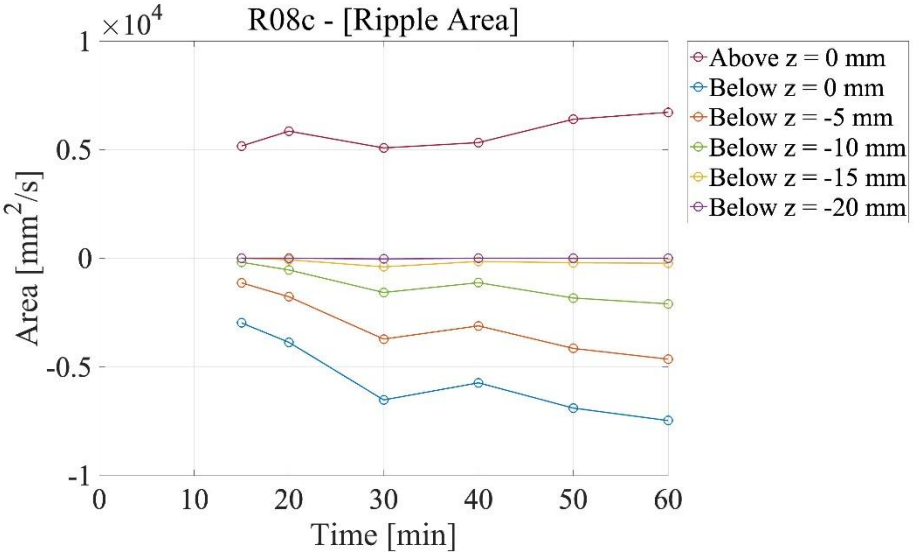
R08c - [Ripple Area]
×10⁴
Area [mm²/s]
Time [min]
Above z = 0 mm
Below z = 0 mm
Below z = -5 mm
Below z = -10 mm
Below z = -15 mm
Below z = -20 mm

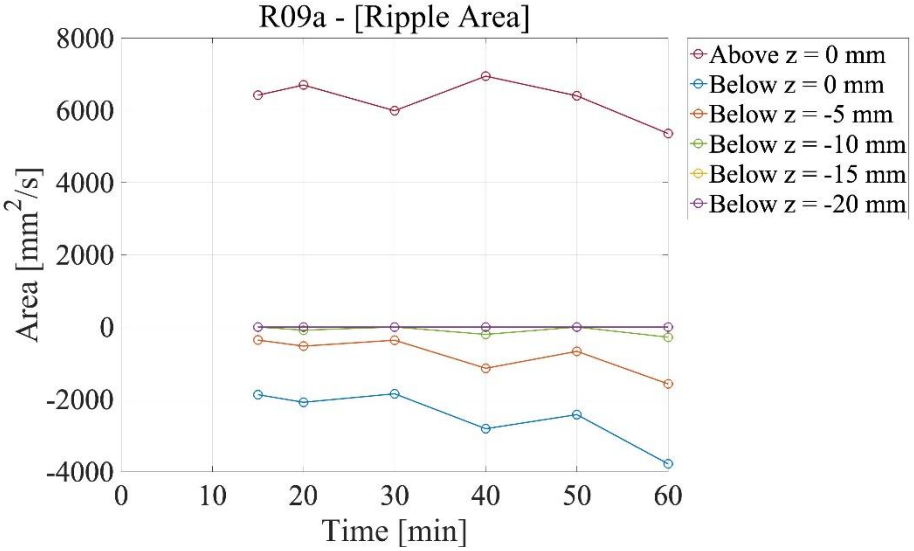
R09a - [Ripple Area]
Area [mm²/s]
Time [min]
Above z = 0 mm
Below z = 0 mm
Below z = -5 mm
Below z = -10 mm
Below z = -15 mm
Below z = -20 mm

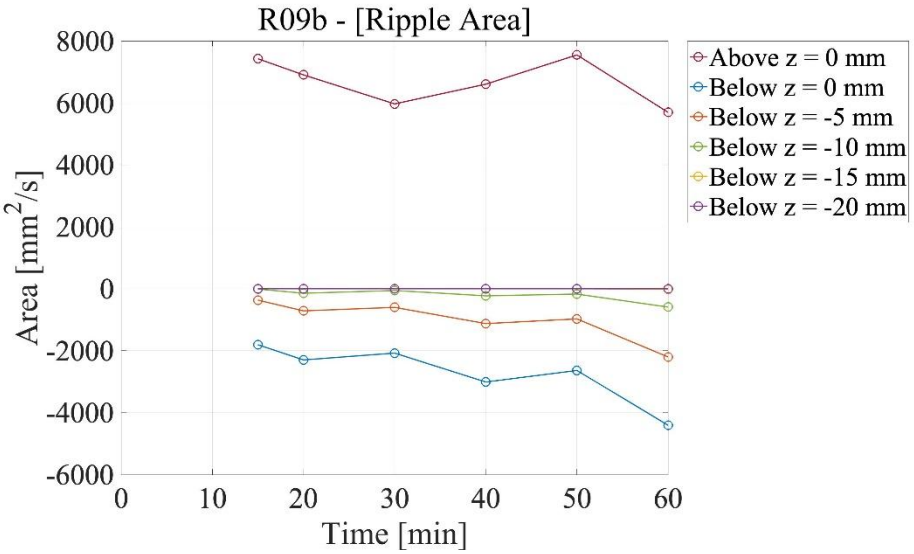
R09b - [Ripple Area]
Area [mm²/s]
Time [min]
Above z = 0 mm
Below z = 0 mm
Below z = -5 mm
Below z = -10 mm
Below z = -15 mm
Below z = -20 mm

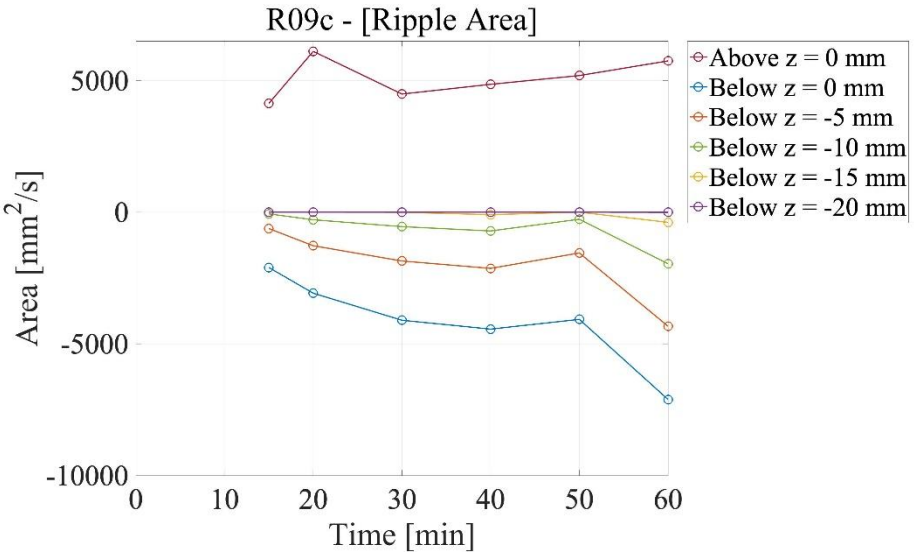
R09c - [Ripple Area]
Area [mm²/s]
Time [min]
Above z = 0 mm
Below z = 0 mm
Below z = -5 mm
Below z = -10 mm
Below z = -15 mm
Below z = -20 mm

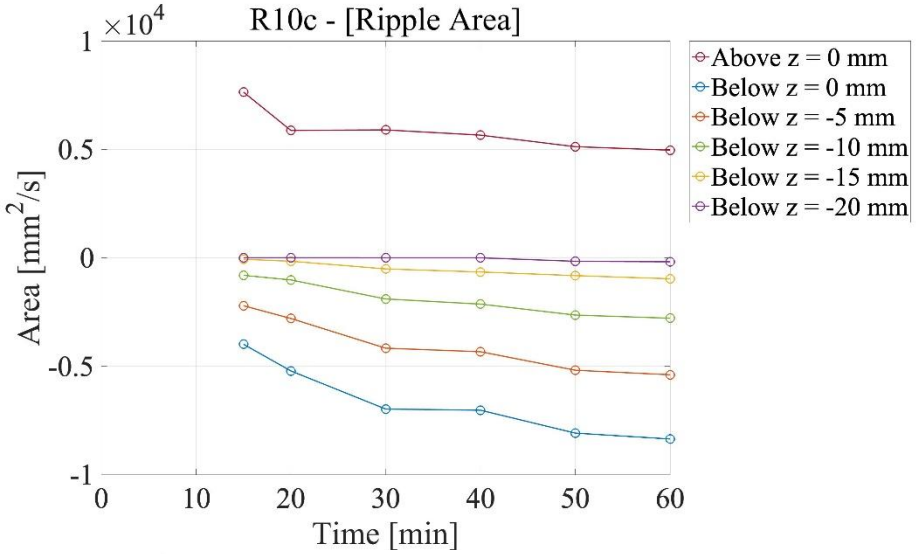
R10c - [Ripple Area]
×10^4
Area [mm^2/s]
Time [min]
Above z = 0 mm
Below z = 0 mm
Below z = -5 mm
Below z = -10 mm
Below z = -15 mm
Below z = -20 mm

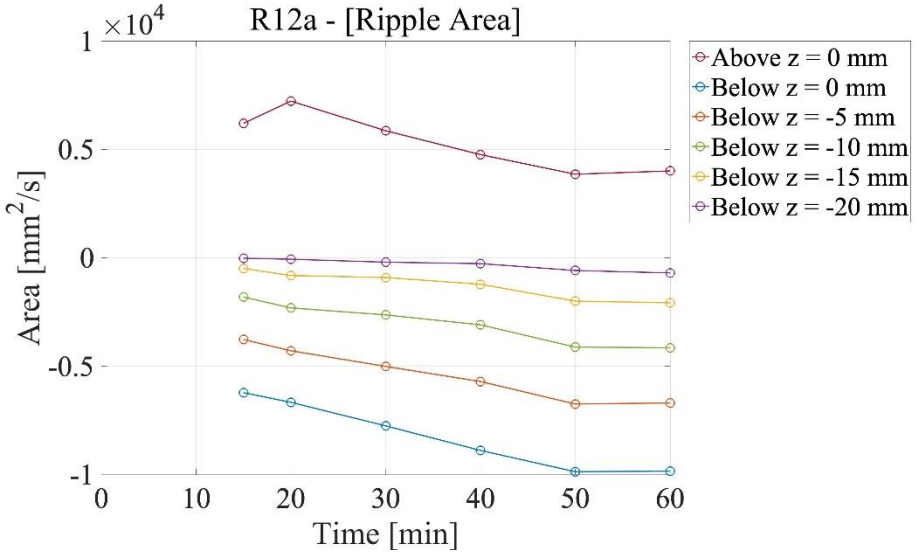
R12a - [Ripple Area]
×10^4
Area [mm^2/s]
Time [min]
Above z = 0 mm
Below z = 0 mm
Below z = -5 mm
Below z = -10 mm
Below z = -15 mm
Below z = -20 mm

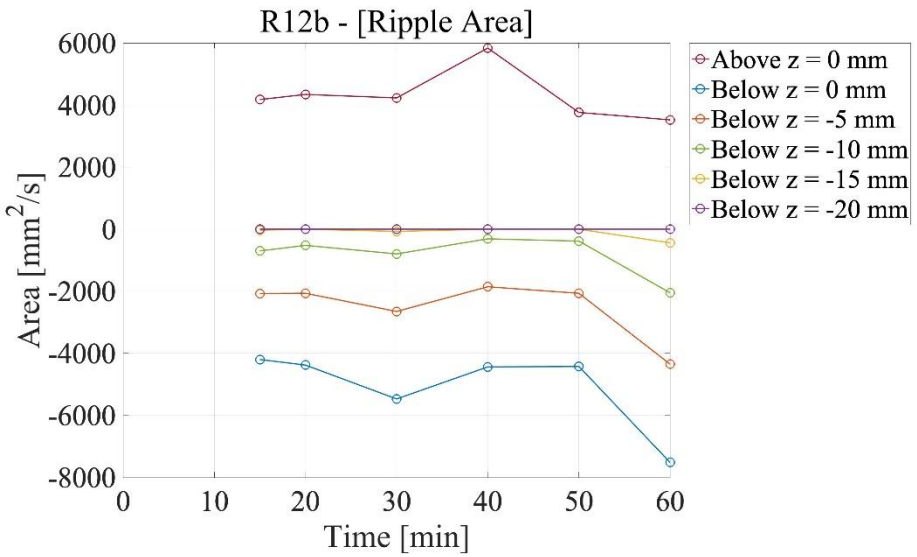
R12b - [Ripple Area]
Area [mm^2/s]
Time [min]
Above z = 0 mm
Below z = 0 mm
Below z = -5 mm
Below z = -10 mm
Below z = -15 mm
Below z = -20 mm

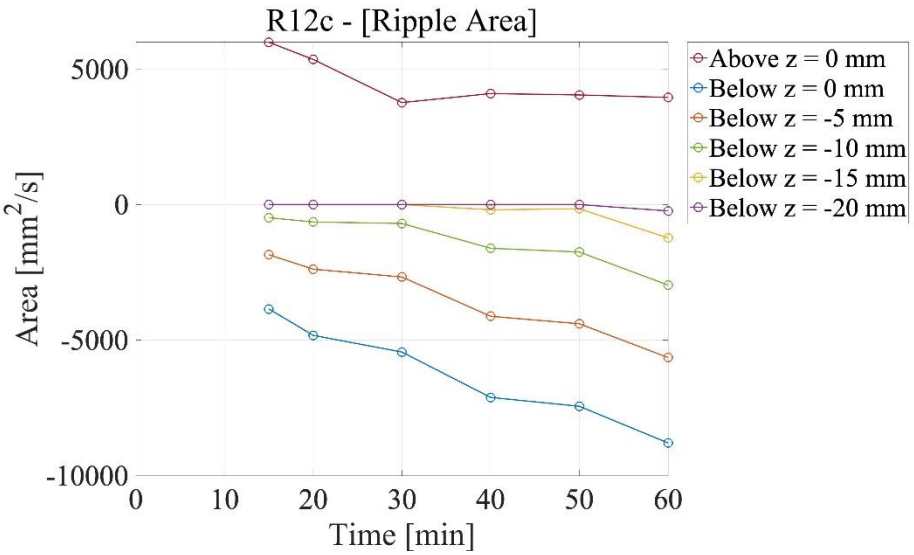
R12c - [Ripple Area]
Area [mm^2/s]
Time [min]
Above z = 0 mm
Below z = 0 mm
Below z = -5 mm
Below z = -10 mm
Below z = -15 mm
Below z = -20 mm

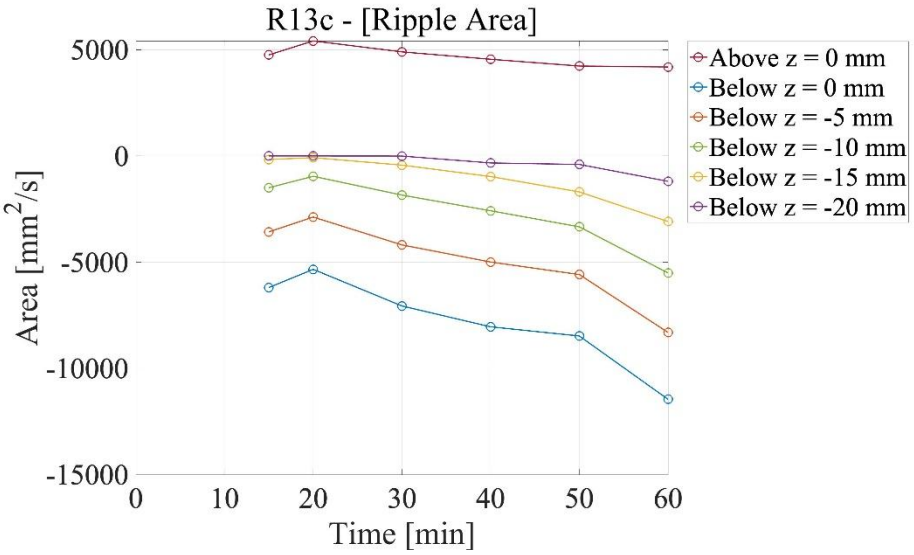
R13c - [Ripple Area]
Area [mm^2/s]
Time [min]
Above z = 0 mm
Below z = 0 mm
Below z = -5 mm
Below z = -10 mm
Below z = -15 mm
Below z = -20 mm

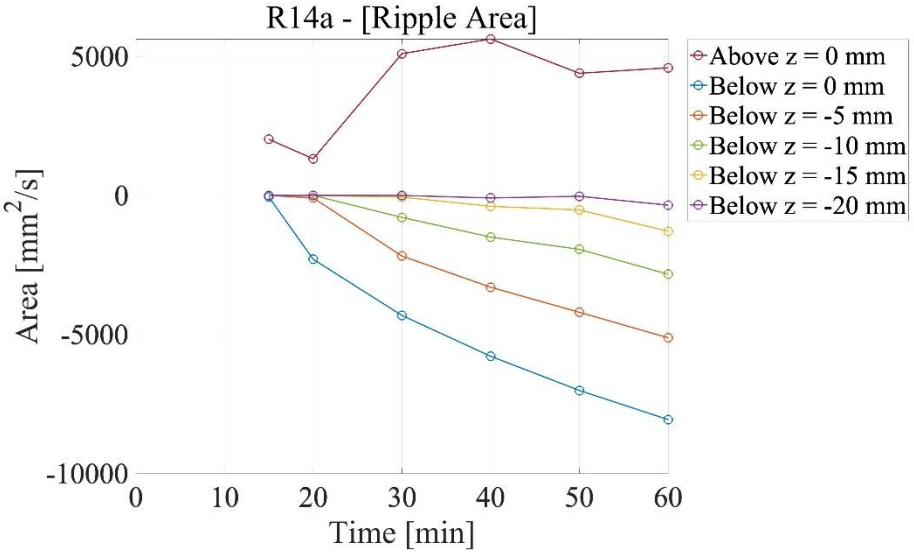
R14a - [Ripple Area]
Area [mm^2/s]
Time [min]
Above z = 0 mm
Below z = 0 mm
Below z = -5 mm
Below z = -10 mm
Below z = -15 mm
Below z = -20 mm

국문 초록

해안 유사에서 수체로의 플라스틱 입자 방출에 관한 실험적 연구

서울대학교 공과대학원

건설환경공학부

황 동 욱

1970년대 이후로 급증한 플라스틱 사용량은 플라스틱 환경 오염을 가속화하였으며, 이로 인한 해안·해양 환경으로의 플라스틱 유출이 지속적으로 발생하고 있다. 이 환경 오염 심각성은 전세계 곳곳에서 발견되고 있는 플라스틱으로 인해 2000년 후반부터 인지되고 많은 관심을 받으며 현재 많은 연구가 이루어지고 있다. 육지에서 배출된 대부분의 플라스틱 폐기물은 해안 환경으로 유입되어 장기간 체류하게 된다. 그 과정에서 플라스틱들은 다양한 요인과의 상호작용을 통하여 물리적·화학적 반응을 하게 된다. 이러한 반응은 플라스틱 폐기물을 더 작아지게 만들고, 작아진 플라스틱 조각들은 해안에 퇴적되거나 해양으로 유출됨으로써 관리 및 처리함에 있어 많은 어려움을 야기한다. 해안 지역에서 발생하는 여러 요인들과 플라스틱 간 상호작용의 이해가 중요함에도 불구하

고, 현재 이루어지고 있는 해안·해양 환경 내 플라스틱 관련 연구는 얼마나 플라스틱으로 인해 해양이 오염됐는지를 보여주는 오염도 보고 연구가 대부분의 비중을 차지하고 있다. 더불어, 환경 내 플라스틱의 물리적 거동과 관련된 기초 연구가 필요하다. 이에 따라, 이러한 연구 배경 및 필요성을 가지고 본 연구는 해안 환경 내 플라스틱의 거동을 파악하고자 진행되었다. 특히, 해안 유사 내부에 분포되어 있는 플라스틱 입자가 수체로 방출되어지는 과정에서 드러나게 되는 특성을 실험을 통하여 알아보고자 하였다. 해당 연구의 목적을 달성하기 위하여 해안 왕복흐름과 유사 이동을 실험실 규모에서 구현하기 위하여 왕복흐름발생장치를 설계 및 구축하였으며, 이렇게 구현한 흐름의 레이놀즈 수와 플라스틱 입자의 크기를 매개변수로 하여 이에 따른 입자의 방출 특성을 분석하였다.

왕복흐름발생장치는 서울대학교 해안공학연구실에 구축되었으며, 또한 설계한 실험 모두 수행되었다. 그 결과, 흐름이 유사에 전달하는 에너지로 인하여 발생하게 되는 하상 변화가 플라스틱 입자 방출에 가장 큰 역할을 한다는 것을 알 수 있었다. 따라서, 하상 변화에 관한 임계값과 입자의 방출에 관한 임계값은 동일하게 보고, 본 실험 조건 하에 산정된 값은 대략 $Re_{cr} = 5.5 \times 10^4$, $\psi_{cr} = 7.25$, 또는 $Fr_{cr} = 2.69$이다. 즉, 해당 임계값을 초과하는 조건에서 하상이 변화하게 될 것이고, 그에 따라 유사 내부에 있는 플라스틱 입자가 수체로 방출될 것이다. 흐름 레이놀즈 수가 커질수록 하상 변화가 더욱 적극적으로 발생하게 되고 그에 따른 입자 방출 또한 많이 발생하게 되는 것을 실험을 통해 관찰하였다.

더불어, 입자의 크기와 플라스틱 입자의 방출 간의 인과관계를 찾을 수 있었다. 실험에서 사용된 입자의 크기는 3 mm, 6 mm, 8 mm로 총 세 가지이며, 입자의 크기가 작을수록 큰 입자의 비하여 방출에 있어서 더 유리하다는 것을 알 수 있었다. 이와 같이, 실험을 통하여 플라스틱 입자의 방출되는 과정에서 알 수 있는 특성들을 파악 및 분석하였다. 이렇게 밝혀진 해안 내 플라스틱 입자의 거동 특성은 해안·해양 플라스틱 오염 문제와 관련된 기초 연구로써 해당 문제 해결에 기여될 수 있을 것이다.

주요어 : 실험적 연구, 플라스틱 오염, 플라스틱 입자의 방출, 유사 이동, 왕복흐름발생장치

학 번 : 2020-26707